Crystal Growth of Bi-based Cuprate Whiskers and Their Superconducting Properties

Ichiro Matsubara

1994

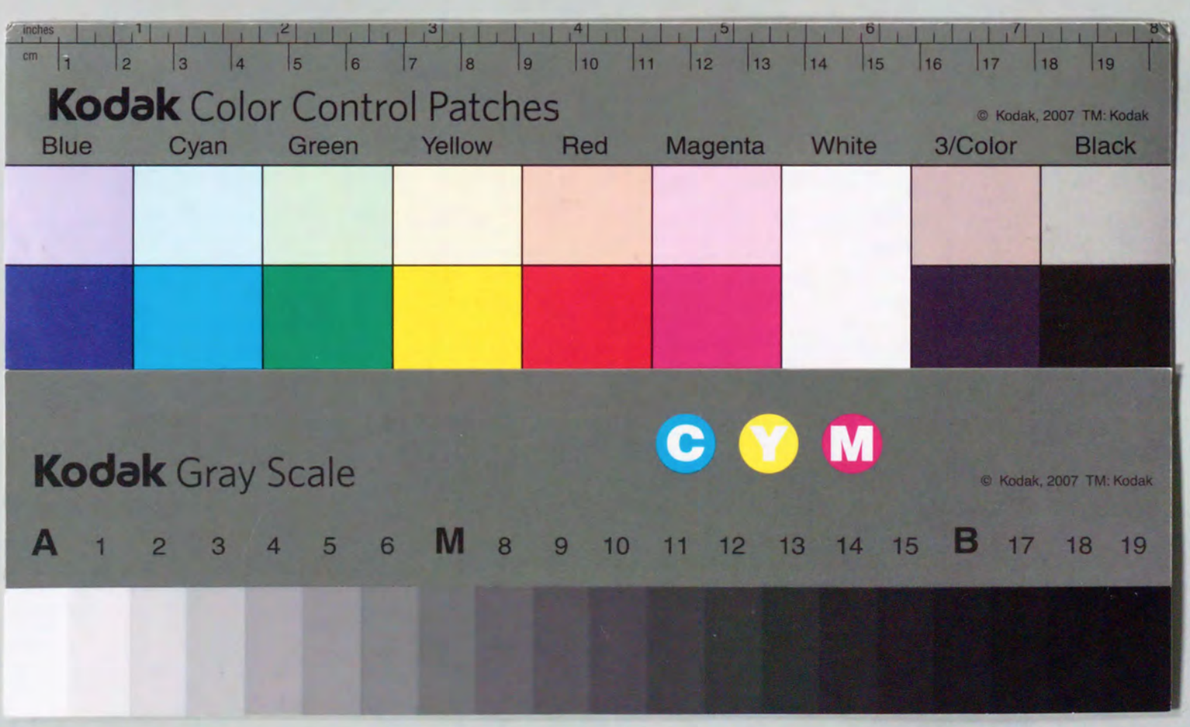

Crystal Growth of Bi-based Cuprate Whiskers and Their Superconducting Properties

Ichiro Matsubara

1994

Acknowledgments

The studies presented in this thesis have been carried out at Osaka National Research Institute during 1988–1993.

The author wishes to express his sincerest gratitude to Professor Tomoji Kawai of Osaka University for his continuing interest, guidance and encouragement in this work. The author is greatly indebted to Professor Fumikazu Kanamaru and Professor Michio Sorai of Osaka University for their helpful discussions and comments.

The author's grateful thanks are also due to Dr. Hiroshi Yamashita of Osaka National Research Institute for his guide to this research, insightful discussions and hearty encouragement.

The author also wishes to express his gratitude to Professor Masanori Hangyo of Osaka University for the collaborations in the Raman experiment. He also thanks Dr. Masahiro Setoguchi of Osaka National Research Institute for measurement of Weissenberg photographs, and to Mr. Toru Ogura of Osaka National Research Institute for measurement of TG–DTA.

It is also a pleasure to acknowledge the hospitality, collaboration and helpful advice of the members of his laboratory. Sincere thanks are due to Mrs. Machiko Otani for her nice assistance.

Finally, the author sincerely thanks his family and parents for their affectionate encouragement throughout this work.

Ichiro Matsubara

1994

Contents

Chapter 1

General Introduction

Large and high-quality single crystals are essential for investigating their physical properties which lead us to a further understanding of the fundamental properties of the material. In particular, this is also the case in the field of the high temperature superconductors. Since the discovery of high temperature superconductivity in copper-oxide-based superconductors in 1986 [1], a lot of studies on these materials has been conducted. As a result, the superconducting cuprates having the critical temperature (T_c) higher than the liquid nitrogen temperature have been synthesized in Y-Ba-Cu-O [2], Bi-Sr-Ca-Cu-O [3], and Tl-Ba-Ca-Cu-O [4] systems. These compounds have attracted much attention because of their potential usefulness in practical applications and the basic theory with respect to the mechanism of the superconductivity. Concerning the mechanism, although a number of models have already been proposed, the origin of the superconductivity has not been authenticated unambiguously. One of limiting factors for the progress in such the basic study is the difficulty in preparing high-quality crystals. The growth of single crystals of the superconducting cuprates is a challenging and an essential work for the progress of superconductors.

All of the cuprate superconductors contain the square network of the planes composed of copper and oxygen, and the high-T_c superconductivity is believed to come from the CuO_2 plane doped with carriers. As for the Bi-Sr-Ca-Cu-O system, three isostructual compounds with different numbers of CuO_2 planes in a unit formula are known (fig. 1-1), $Bi_2Sr_2Ca_{n-1}Cu_nO_x$ (n = 1, 2, 3). Hereafter, the n=1, 2, 3 materials are denoted as 2201, 2212, and 2223, respectively. These compounds have layered crystal structures based on the stacking of Bi_2O_2-SrO-CuO_2-$(Ca-CuO_2)_{n-1}$-SrO-Bi_2O_2 [5, 6]. The T_c value of these phases are around 20 [7], 80 [3], and 110 K [3], respectively. For these phases, it is interesting to investigate the change of the basic superconducting parameters such as coherence length, critical field, and penetration depth in order to clear how the

number of CuO_2 plane is related to T_c.

One important feature of the high-T_c oxide superconductors is the degree of anisotropy of the superconducting properties derived from their layered crystal structure. For the understanding of the physical properties of these compounds, it is essential to reveal what the significant factors for determining the anisotropy are. The Bi-system is considered to be a good model to examine the correlation between the degree of anisotropy and the number of CuO_2 planes. The evaluation of anisotropy for the cuprate superconductors has been made by upper critical field (H_{c2}), critical current density, resistivity, thermopower, fluctuation effects in conductivity, specific heat, and electronic structure, and others. Among these, the H_{c2} is intrinsic to the superconductor because the H_{c2} is associated with microscopic currents on a length scale given by the vortex size [8].

To measure the superconducting parameters and evaluate the degree of anisotropy in the Bi-system, the single crystals are needed. Several studies have been made on the crystal growth of the 2201 and the 2212 phases by the self-flux method [9-12], the alkali-halides flux method [13,14], the floating zone method [15,16], the laser pedestal method [17], and the traveling solvent floating zone (TSFZ) method [18]. However, it has been difficult to achieve the controlled growth of the high-quality 2212 single crystals without the intergrowth of the 2201 or the 2223 phase, since the 2212 phase shows the incongruent melting and consists of five kinds of element including oxygen.

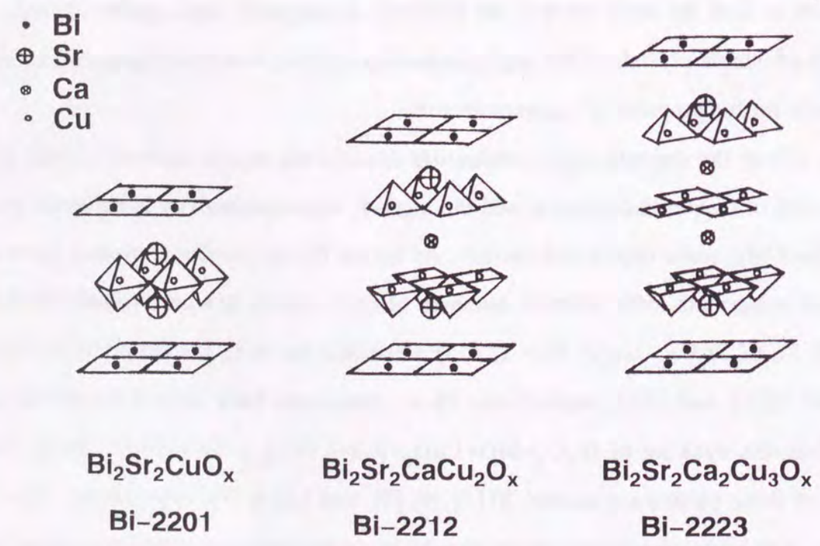

FIG. 1-1. Crystal structure of Bi-system superconductors.

As for the 2223 phase, as this material is so delicate to synthesize the 2223 samples have been limited to a powder, sintered bodies, or thin films. Large crystals have not been previously obtained, although the 2223 compound has attracted much attention because of its high-T_c over 100K with non-toxic combination of the elements compared with the Tl system. Although the phase relation is not clear in the Bi-system, Shigematsu *et al.* have claimed that the 2223 phase is not neighboring with a liquid phase in their pseudo-binary system between $Bi_2(Sr,Ca)O_4$ and $(Sr,Ca)CuO_2$ [19]. On the other hand, Komatsu *et al.* have reported the pseudo-binary phase diagram of $Bi_2(Sr,Ca)_{n+1}Cu_nO_x$ where the 2223 phase coexists with a liquid phase [20], although they have not obtained the 2223 single crystals. Therefore, the 2223 crystals are hardly grown from a liquid phase, which means that the growth methods used for the 2201 or 2212 phase are not applicable to the growth of the 2223 crystals.

Even in the substitution experiment for the polycrystalline compound, only Pb doping has been proved to be effective to stabilize the 2223 phase [21], although no effect has been observed on the T_c value. That is, the improvement of T_c by the doping of other element has been unsuccessful. In general, it is well established that T_c strongly depends on the carrier concentration. By the doping of carrier to the CuO_2 plane, the system becomes superconducting from antiferromagnetic insulator. By increasing hole concentration further, it becomes similar to a normal metal, and superconductivity disappears. The substitution experiment is one of the most important methods to change the carrier concentration, hence to examine the behavior of T_c against the carrier concentration. Because of difficulty in the substitution experiment, the fundamental superconducting properties of the 2223 phase have not been sufficiently examined. This undeveloped

field is one of the most interesting themes for the understanding of high T_c superconductivity.

The Bi-system superconductors are also noted from the field of practical applications. Much research on the fabrication of wires has been undertaken by the powder in silver tube method using the 2212 and the 2223 phases. Various groups have reported achieving high critical current densities (J_c) in these materials [22-25]. Oxide superconductors are generally evaluated by their T_c, H_{c2}, and critical current density (J_c). It is preferred to have high values in these three parameters for practical applications. However, there is another important factor for practical usage of oxide superconductors. In some applications, superconducting wires are subjected to large stretching stresses in making coils and Lorentz force due to high magnetic fields. Under the high stresses, a generation of small cracks in the high current will cause a fatal damage or destruction of the coil. Therefore, the evaluation of mechanical properties of superconductors is an important work for the practical applications. The data on mechanical properties of Bi-based superconductors have been limited to the polycrystalline state [26-28], so that grain boundaries, pours, and probably micro cracks in the samples could obscure the mechanical data. So, the measurements of mechanical strength and the effects of bending strain on the superconductivity using single crystals have been desired.

In this way, there are many undeveloped subjects with respect to the fundamental properties concerning the mechanism of superconductivity as well as practical application due to the lack of high-quality crystals. On these points of view, this study has been undertaken with the purpose of i) the development of a new method for preparing the large and high-quality single crystals in the Bi-system, 2201, 2212, and 2223 phases, ii) clarifying the crystal growth mechanism, iii) revealing the physical properties from the measurements of superconductivity, degree of anisotropy, and mechanical property using the crystals, iv) carrying out the substitution experiment especially for the 2223 compound.

In chapter 2, preparation and properties of 2212 whiskers [29] are described. The

2212 whiskers have been successfully prepared by annealing a melt-quenched glass plate in a stream of O_2 gas. Each whisker with the dimensions of 2-10 μm thick, 10-500 μm wide and ~20 mm long is composed of several plate-like single crystals which are stacked in a layered structure. The 2212 whiskers are flexible and are elastically bent up to a curvature of radius of 0.2 mm corresponding to a bending strain of 0.5%. The details of the preparation condition, growth mechanism, crystal structure, superconducting properties, and mechanical properties for the 2212 whiskers have been investigated.

In chapter 3, preparation and properties of 2201 whiskers are described. The 2201 whiskers are grown by the same method as that for the 2212 whiskers by changing the annealing temperature and the composition of the glass precursors. The growing phase (2201 or 2212 phase) of the whiskers can be controlled by changing the initial composition and annealing temperature.

In chapter 4, preparation and properties of 2223 whiskers are described. A new approach giving the 2223 whiskers to be called as Conversion by Annealing in Powder method (CAP method) is shown. The 2223 whiskers are obtained by annealing the 2212 whiskers in a Ca- and Cu-rich Bi-Sr-Ca-Cu-Pb-O calcined powder with retaining the outline of the form in the original whiskers. The detail preparation method, the phase conversion mechanism from the 2212 to the 2223 phase, and superconducting properties of the 2223 whiskers are described. The CAP method is also applied to the 2212 sheet crystals, resulting 2223 sheet crystals as large as $1mm^2$ in area.

In chapter 5, the effects of Li-doping on the superconductivity of the 2212 and 2223 whiskers are described. The Li-doped 2212 whiskers and the Li-doped 2223 whiskers have been prepared by the glass annealing method and the CAP method, respectively. The enhancement of T_c by the Li-doping has been confirmed for both the whiskers. The enhancement mechanism of T_c by Li-doping is discussed from the compositional analysis, measurement of the *c*-axis lattice parameter, and the annealing experiment under a reduced pressure to change the oxygen content, i.e. hole concentration in the whiskers.

References

[1] J.G.Bedonorz and K.A.Müller, Z.Phys., **B64**, 189 (1986).

[2] M.K.Wu, J.R.Ashburn, C.J.Torng, P.H.Hor, R.L.Meng, L.Gao, Z.J.Huang, Y.Q.Wang, and C.W.Chu, Phys.Rev.Lett., **58**, 908 (1987).

[3] H.Maeda, Y.Tanaka, M.Fukutomi, and T.Asano, Jpn.J.Appl.Phys., **27**, L209 (1988).

[4] Z.Z.Sheng and A.M.Hermann, Nature, **332**, 138 (1988).

[5] J.M.Tarascon, Y.Le Page, P.Barboux, B.G.Bagley, L.H.Greene, M.R.McKinnon, G.W.Hull, M.Giroud, and D.M.Hwang, Phys.Rev.B, **37**, 9382 (1988).

[6] M.A.Subramanian, C.C.Torardi, J.C.Calabrese, J.Gopalakrishnan, K.J.Morrissey, T.R.Askew, R.B.Flippen, U.Chowdhry, and A.W.Sleight, Science, **239**, 1015 (1988).

[7] C.Michel, M.Hervieu, M.M.Borel, A.Grandin, F.Deslandes, J.Provost, and B.Raveau, Z.Phys.B, **68**, 421 (1987).

[8] T.T.M.Palstra, B.Batlogg, L.F.Schneemeyer, and R.J.Cava, Phys.Rev. B **38**, 5102 (1988).

[9] Y.Hidaka, Y.Tanaka, M.Fukutomi, and T.Asano, Jpn.J.Appl.Phys., **27**, L209 (1988).

[10] J.J.Lin, E.L.Benitez, S.J.Poon, M.A.Subramanian, J.Gopalakrishnan, and A.W.Sleight, Phys.Rev.B, **38**, 5095 (1988).

[11] T.F.Ciszek, J.P.Goral, C.D.Evans, and H.Katayama-Yoshida, J.Cryst.Growth, **91**, 312 (1988).

[12] S.Kishida, H.Tokutake, S.Nakanishi, H.Fujimoto, K.Nishimori, N.Ishihara, Y.Watanabe, and W.Futo, J.Cryst.Growth, **99**, 937 (1990).

[13] L.F.Schneemeyer, R.V.van Dover, S.H.Clarum, S.A.Sunshine, R.M.Fleming, B.Batlogg, T.Siegrist, J.H.Marshall, J.V.Waszczak, and L.W.Rupp, Nature, **332**, 423 (1988).

[14] T.Shishido, D.Shindo, K.Ukei, T.Sasaki, N.Toyota, and T.Fukuda, Jpn.J.Appl.Phys., **28**, L791 (1989).

[15] Y.Kubo, K.Michisita, Y.Higashida, M.Mizuno, H.Yokoyama, N.Shimizu, E.Inukai, N.Kuroda, and H.Yoshida, Jpn.J.Appl.Phys., **28**, L606 (1989).

[16] S.Takekawa, H.Nozaki, A.Umezono, K.Ksuda, and H.Kobayashi, J.Cryst.Growth, **92**, 687 (1988).

[17] D.Gazit and R.S.Feigelson, J.Cryst.Growth **91**(1988)318.

[18] S.Takekawa, H.Nozaki, A.Umezono, K.Ksuda, and H.Kobayashi, J.Cryst.Growth, **92**, 687(1988).

[19] K.Shigematsu, H.Takei, I.Higashi, K.Hoshino, H.Yakahara, and M.Aono, J.Cryst.Growth, **100**, 661(1990).

[20] H.Komatsu, Y.Kato, S.Miyashita, T.Inoue, and S.Hayashi, Physica C, **190**, 14(1991).

[21] S.A.Sunshine, T.Siegrist, L.F.Schneemeyer, D.W.Murphy, R.J.Cava, B.Batlogg, R.B.VanDover, R.M.Fleming, S.H.Glarum, S.Nakahara, R.Farrow, J.J.Krajewski, S.M.Zahurak, J.V.Waszczak, J.H.Marshall, P.Marsh, L.W.Rupp,Jr., and W.F.Peck, Phys.Rev. B, **38**, 893 (1988).

[22] K.Sato, T.Mikata, H.Mukai, M.Ueyama, T.Kato, T.Masuda, M.Nagata, K.Iwata, and T.Misui, IEEE Trans.Magn., **27**, 1231 (1991).

[23] Y.Yamada, B.Obst, and R.Flukiger, Supercond.Sci.Technol., **4**, 165 (1991).

[24] L.R.Motowidlo, E.Gregory, P.Haldar, J.A.Rice, and R.D.Blaugher, Appl.Phys.Lett., **59**, 736 (1991).

[25] K.Chen, L.Homg, H.S.Koo, C.Y.Shei, L.P.Wang, C.Chiang, T.J.Yang, W.H.Lee, and P.T.Wu, Appl.Phys.Lett., **59**, 1635 (1991).

[26] T.Goto, Jpn.J.Appl.Phys., **28**, L1402 (1989).

[27] D.W.Johnson Jr., and W.W.Rhodes, J.Am.Ceram.Soc., **72**, 2346 (1989).

[28] M.Shoyama, H.Nasu, and K.Kamiya, Jpn.J.Appl.Phys., **30**, 950 (1991).

[29] "Whisker" is defined as a single crystal of any material in an elongated form such that it has a minimum length to a maximum average transverse dimension of 10:1, a maximum cross-sectional area of $5x10^{-8}m^2$, and a transverse dimension of $2.5x10^{-4}m$.
Whisker technology, ed. A.P.Levitt, (Wiley-Interscience, New York, 1970) p. 1.

Chapter 2

Preparation and Properties of $Bi_2Sr_2CaCu_2O_x$ Whiskers

2-1. Introduction

Since the discovery of the high temperature superconductors of the Bi-Sr-Ca-Cu-O system [1], a lot of works on this system have been reported. There are several superconducting phases in the Bi-Sr-Ca-Cu-O system. Two of them have critical temperature (T_c) higher than liquid nitrogen temperature: $Bi_2Sr_2CaCu_2O_x$ (2212) phase with T_c=80 K and $Bi_2Sr_2Ca_2Cu_3O_x$ (2223) phase with T_c=110 K. Although the phase relation in the Bi-Sr-Ca-Cu-O system is not well known due to its large number of constitutional element, the growth of single crystals of the 2212 phase has been intensively carried out. The slow cooling method using an excess of CuO as a self-flax [2-8] or alkali-halides as an additive flux [9-11], the floating zone method [12], traveling solvent floating zone method [13, 14], the directional solidification [15, 16], the top-seeded solution growth method [17], the laser pedestal method [18], as well as the use of a $SrCaCu_4O_6$ sealed cavity [19] have been used. In spite of these methods, pure 2212 single crystals cannot easily be made for the following reasons: i) $Bi_2Sr_2CuO_x$ (2201) phase appear to intergrow. ii) They tend to be mixed with other phases, especially Ca and Sr cuprates. iii) A contamination from crucible materials easily occurs. iv) The phase relation is not clear. v) There is a remarkable anisotropy in the growth rate. Therefore, it is desired to develop a new method for preparing the large and high-quality single crystals of the 2212 phase.

For the production of bulk superconducting oxides, there are mainly three methods, i.e. the solid state, the liquid phase and the melting methods. The solid state reaction method, in which powders of oxides and/or carbonates are mixed and heated under the melting point, is a simple and standard method for preparing polycrystalline superconductor. Sol-gel method [20], coprecipitation and pyrolysis of a metal salt solution belong to

the liquid phase method which is expected to give homogeneous and fine starting materials. In addition, the direct synthesis using an alkaline metal hydroxide solution has been reported in the La–system [21]. The melting method has some advantages compared with the above two methods because the reduction of pores and control of the crystal orientation are readily attained. In the case of the Bi–system, glassy solid is easily obtained by quenching melt at a moderate speed such as using metal plates (cooling rates is about 10^3 ks^{-1}). Afterward, it is transformed into a polycrystalline superconductor by heating the glass at an appropriate temperature [22, 23].

In our studies on crystallization from a glassy state in the Bi–system, we have developed a method preparing flexible superconducting whiskers of the 2212 phase. The 2212 whiskers have been successfully prepared by annealing a melt–quenched glass plate in a stream of O_2 gas [24–26]. In this chapter, preparation and properties of the 2212 whiskers are described. Each whisker with the dimensions of 2–10 μm thick, 10–500 μm wide, and ~20 mm long is composed of several plate–like single crystals which are stacked in a layered structure. The noteworthy characteristic property of the 2212 whiskers is their bending property. A whisker can be elastically bent to a radius of curvature of 0.2 mm corresponding to a bending strain of 0.5%. The details of the preparation method, crystal structure, superconducting properties in a bending state, and mechanical properties for the 2212 whiskers have been investigated. For the whisker growth, the glass precursor, addition of Al to the glass, and a steady stream of O_2 gas are required. The growth mechanism is discussed in relation to these experimental conditions.

2–2. Preparation and Characterization

This section describes the preparation method and characterization of $Bi_2Sr_2CaCu_2O_x$ (2212) superconducting whiskers. A new method has been developed for preparing the 2212 whiskers. The 2212 whiskers have been prepared by annealing a melt–quenched glass plate in a stream of O_2 gas. The dimensions of the whiskers are 2–10 μm thick, 10–500 μm wide, and ~20 mm long. Characterization of the whiskers has been made by means of X–ray diffraction, Weissenberg photograph, polarized Raman spectra, transmittance electron microscope (TEM) observation, electron diffraction, and compositional analysis. The superconductivity has been evaluated by measuring the resistivity–temperature (R–T) behavior and magnetic susceptibility. Typically, the 2212 whiskers show two resistance drops in the R–T curve at 105 and 76 K, and the zero resistance temperature ($T_{c,zero}$) is 74–75 K. The volume fraction of the 2223 phase in the whiskers is estimated to be less than 1% from the susceptibility measurement. A maximum critical current density (J_c) of $7.3x10^4$ A/cm^2 (66 K, 0 T) is obtained by a four–probe method.

Experimental

The 2212 whiskers were prepared by annealing a melt–quenched glass plate in a stream of O_2 gas. The powders of Bi_2O_3, $SrCO_3$, $CaCO_3$, and CuO were mixed to the nominal composition of $BiSrCaCu_2O_x$ using a ball mill for 30 min. The mixture was melted in an alumina crucible at 1200°C for 30 min in air. A box type electric furnace with heating elements on the two side walls was used for the melting process. The melt was quenched to room temperature by pouring the melt on a copper plate and pressing with another copper plate. The cooling rate is estimated to be 10^3 ks^{-1} in this method [27]. The thickness of the quenched glassy plates was less than 1 mm. This process used to form the glass plates is the same as that used for fabricating a glass ceramic superconductor [22]. Pieces of this glass plates were then placed in an alumina boat and heated at

865°C for several days in a stream of O_2 (150 ml/min) using a tubular furnace. After heating, the samples were cooled to room temperature in the furnace. Whiskers with typical dimensions of 2–10 μm thick, 10–500 μm wide, and ~20 mm grew out from the surface of the crystallized glass plates.

Crystallographic lattice parameters and orientation were determined by means of X–ray diffraction (XRD), Weissenberg camera, and Raman spectra. The X–ray diffraction measurement was made using a RIGAKU diffactometer with Cu–Kα radiation. Well–grown whiskers were selected as the specimens for a Weissenberg camera with Cu–Kα radiation. Raman spectra were measured under the quasi–backscattering configuration using the 4880 Å line of an Ar^+ ion laser at room temperature. High resolution electron microscope observations were made by a Hitachi H–9000 UHR electron microscope operating at 300 kV. Specimens for high–resolution electron microscopy and electron diffraction were prepared by ion milling with argon ions for 30–50 h. The crystal morphology was characterized with a Hitachi scanning electron microscope (SEM) model S–2400. The compositional analysis was performed with a Horiba EMAX–5770 energy dispersive X–ray spectroscopy (EDX) system.

The temperature dependence of resistance was measured under a direct current of 0.1 mA, and J_c was measured in a zero magnetic field by a standard four–probe technique. The susceptibility was measured with a superconducting quantum interference device (SQUID: Quantum Design $MPMS_2$) magnetometer. This measurement was made under a magnetic field of several gauss.

Results and discussion

Figure 2–1 (a) shows the growth of the whiskers from a melt–quenched glass plate after heating at 865°C for 80 h under a stream of O_2 gas. The crystals are twiglike assemblies of whisker–shaped particles, each of which is 3–8 mm in length. The melt–quenched glass plate is curved after the heating because the temperature is in the range of partial melting of the glass plate. The dimensions of the whiskers are 2–10 μm thick,10–

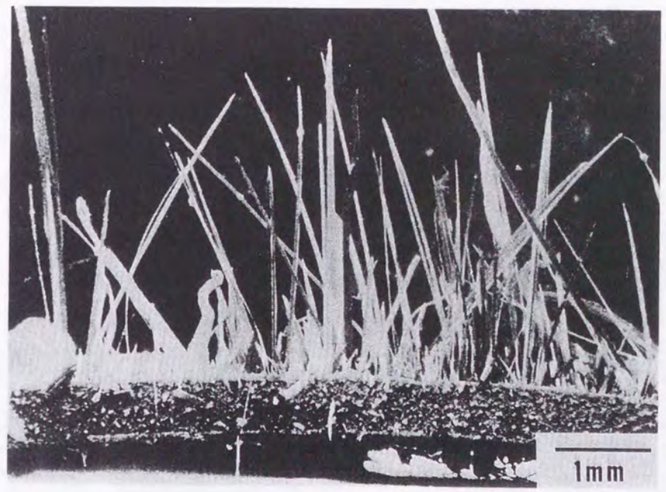

(a)

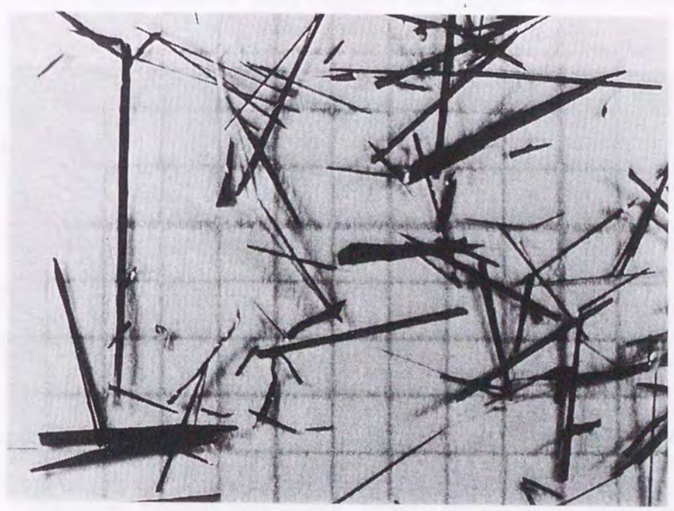

(b)

FIG. 2–1. (a) Growth of the 2212 whiskers by heating a melt–quenched glass plate in a stream of O_2 gas. (b) A typical example of the 2212 whiskers. Grid spacing is 1 mm.

500 μm, wide and several millimeters long. Typical example of whiskers is shown in fig. 2–1 (b). The whiskers grow in the long period of heating, reaching a maximum length of 20 mm (500 h).

Each whisker is composed of several platelike single crystals which are stacked in a layered structure along the direction of thickness. Figure 2–2 (a) shows the well–grown surface of the whisker. The whisker has a flat and smooth surface sometime with steps. The steps are always parallel to the whisker axis, growth direction. The side surface of the whisker clearly shows a layered structure (fig. 2–2 (b)). The thickness of this whisker is about 9 μm.

The bottom part of the whisker on the crystallized glass plate is shown in fig. 2–3. Grains several microns in diameter are observed on the surface of the crystallized glass plate, and the whisker grows outside the plate through the space between the grains. Almost all the whiskers are composed of several plate–like single crystals. However, a whisker which is made up only of one single crystal is sometimes observed as in this case.

Figure 2–4 shows the XRD pattern of the whiskers crushed into powder. It is found that all the diffraction peaks consist solely of the 2212 phase. No 2223 phase is observed in the XRD pattern.

Figure 2–5 shows a high resolution transmission electron microscope image with the incident electron beam along the [110] direction and the corresponding selected area electron diffraction pattern. Noticing the Bi–O double layers, the Bi atoms can be seen as dark dots as observed in the fig. 2–5 interposed by the remarkable bright dots. The lattice image clearly shows layers with a uniform spacing of 31 Å, which corresponds to the length of the *c*–axis of the 2212 phase. There is no stacking fault due to the 2201 and the 2223 phases in this area. The observation of wider area (0.36 μm x 0.47 μm) also shows no such the stacking fault, indicating that the whisker has a high homogeneity in the submicron scale. The electron diffraction pattern can be indexed with respect to the $(a^* + b^*) - c^*$ reciprocal lattice sections of the tetragonal subcell with a=b=5.4 and c=31 Å.

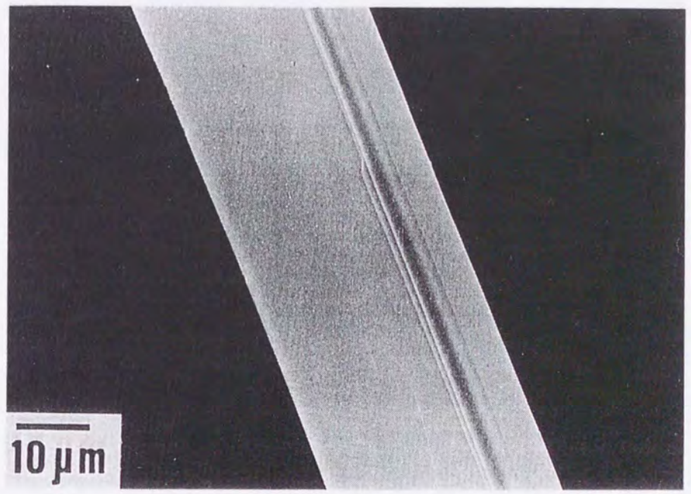

(a)

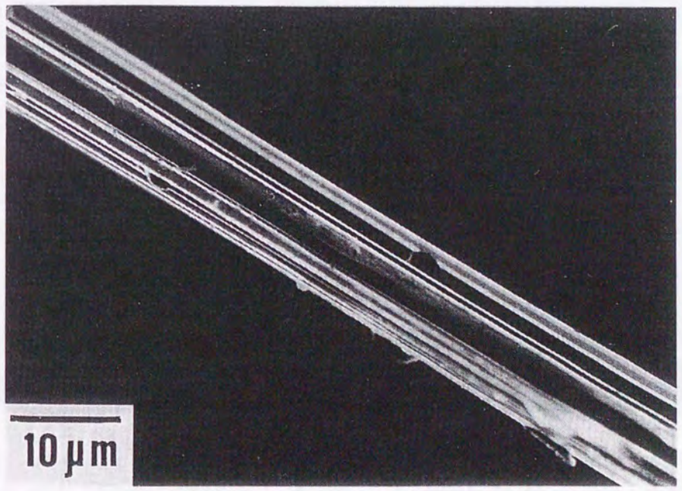

(b)

FIG. 2–2. Scanning electron micrograph of (a) the well–grown surface, and (b) the side surface of the 2212 whisker.

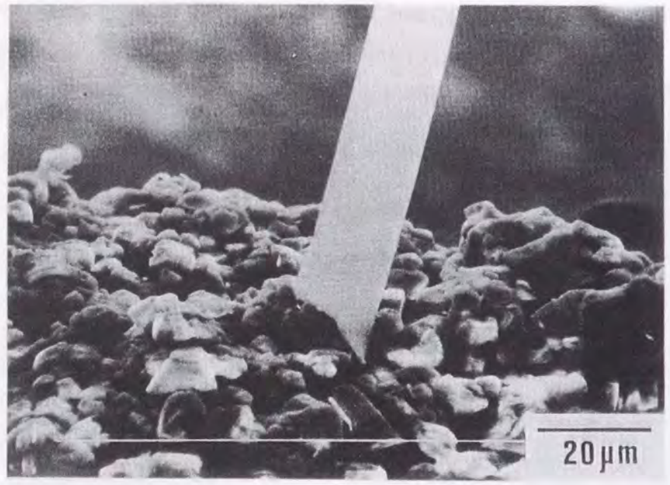

FIG. 2–3. Bottom view of the whisker grown on the surface of the crystallized glass plate.

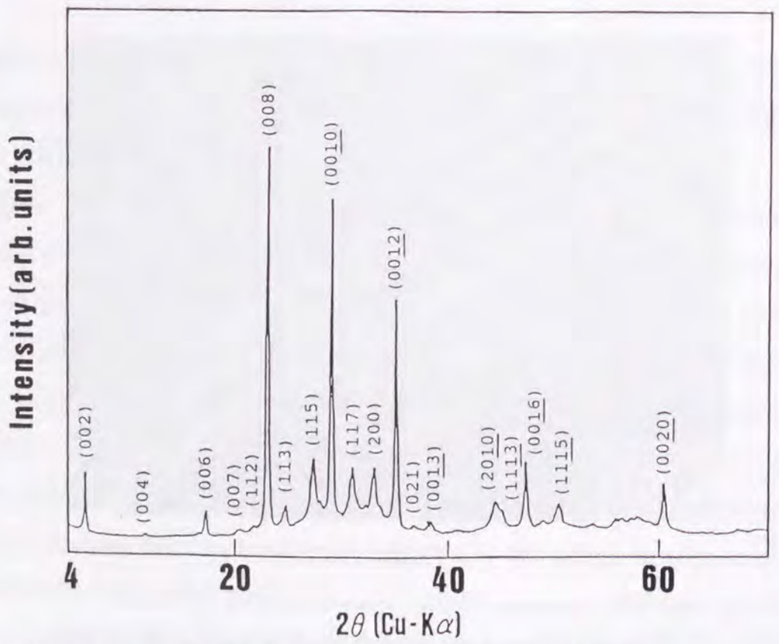

FIG. 2–4. X–ray powder diffraction pattern of the crushed whiskers.

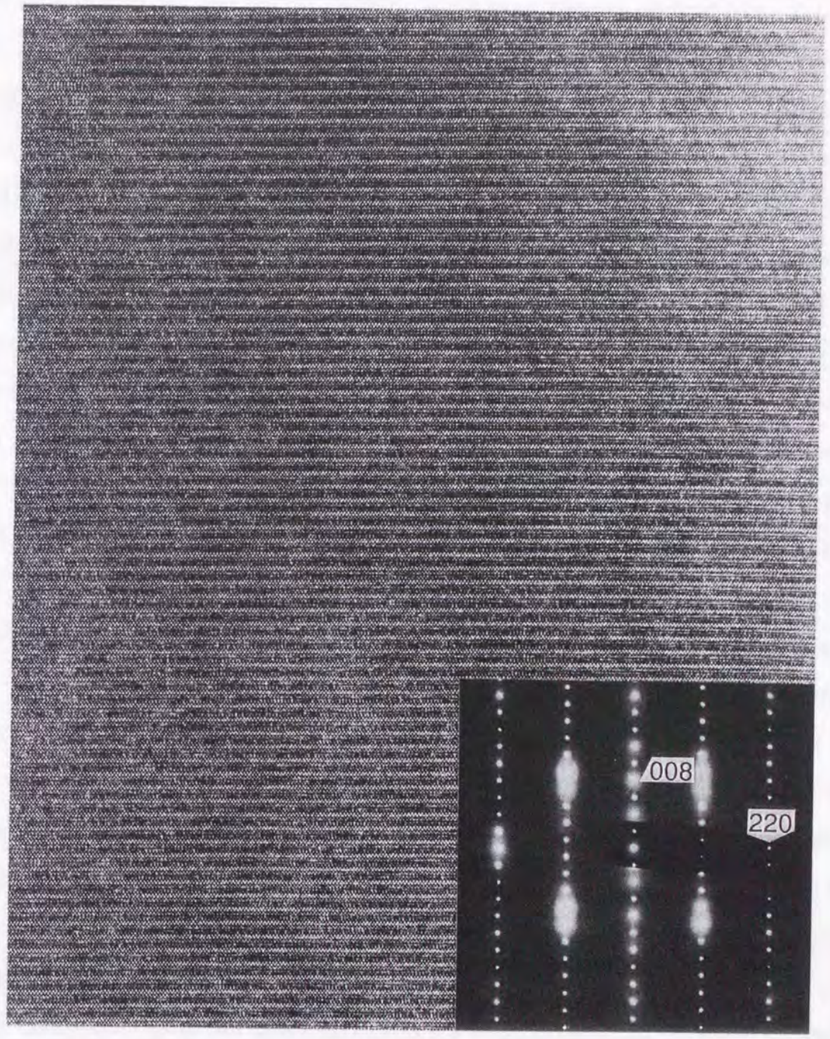

FIG. 2–5. A high resolution transmission electron microscope image with the incident electron beam along the [110] direction and the corresponding selected area electron diffraction pattern.

One of the most interesting structural features in the Bi–based superconducting oxides is the incommensurately modulated structure in the *b* direction of the tetragonal subcell [28–33]. Several models have been proposed to explain the modulation [34]. Neutron diffraction study on powder and single crystals suggests the presence of extra oxygen in the BiO double layer [35]. Figure 2–6 shows a high–resolution transmission electron microscope image with the incident electron beam along the [100] direction and the corresponding electron diffraction pattern. As shown firstly by Matsui *et al.* [31], a characteristic feature of the modulated structure can be directly imaged along this direction of beam incidence. It can be seen in fig. 2–6 that 6–8 pairs of dark dots are aligned along the [010] direction to form a dark region and such dark regions are accompanied with less–dark dots. The dark dots correspond to the Bi–rich atomic rows composed of Bi–concentrated bands, while the less–dark dots correspond to the Bi–poor atomic rows making Bi–deficient bands [31]. The spacing between the layers in the [001] direction is 31 Å. The average 'wavelength' of the Bi–concentrated band is 25 Å. Therefore, this fluctuation of the Bi–concentrated band gives the incommensurate period of $b=4.6b_0$ (b_0 is the *b*–axis lattice parameter of the tetragonal subcell), which is comparable to the previously reported value [28–33].

The crystallographic orientation of the 2212 whiskers has been determined by means of X–ray diffraction, Weissenberg photograph, and polarized Raman spectra. From the X–ray diffraction pattern, the well–grown plane of the whisker corresponds to the *ab* plane, so that the *c*–axis is perpendicular to the well–grown plane. In order to determine the *a*– and *b*–axis, we have taken the Weissenberg photograph and Raman spectra. Figure 2–7 shows the Weissenberg photograph obtained by rotating the whisker along the long axis of the whisker (growing axis). Other than the sharp main spots, satellite spots due to the modulated structure are observed. So, this reciprocal plane corresponds to (b^*–c^*). On the other hand, no satellite spots are observed on the Weissenberg photograph obtained by rotating the whisker along the axis parallel to the well–grown plane and perpendicular to the growing axis (fig. 2–8). The reciprocal plane corresponds

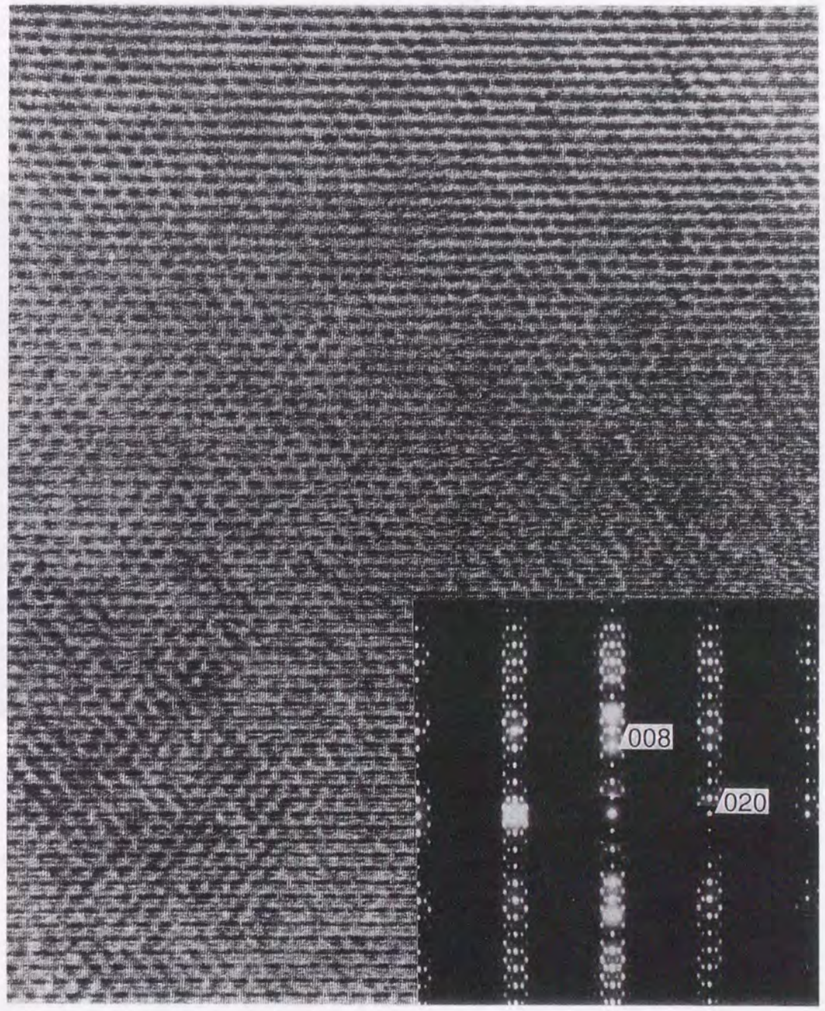

FIG. 2–6. A high resolution transmission electron microscope image with the incident electron beam along the [100] direction and the corresponding selected area electron diffraction pattern.

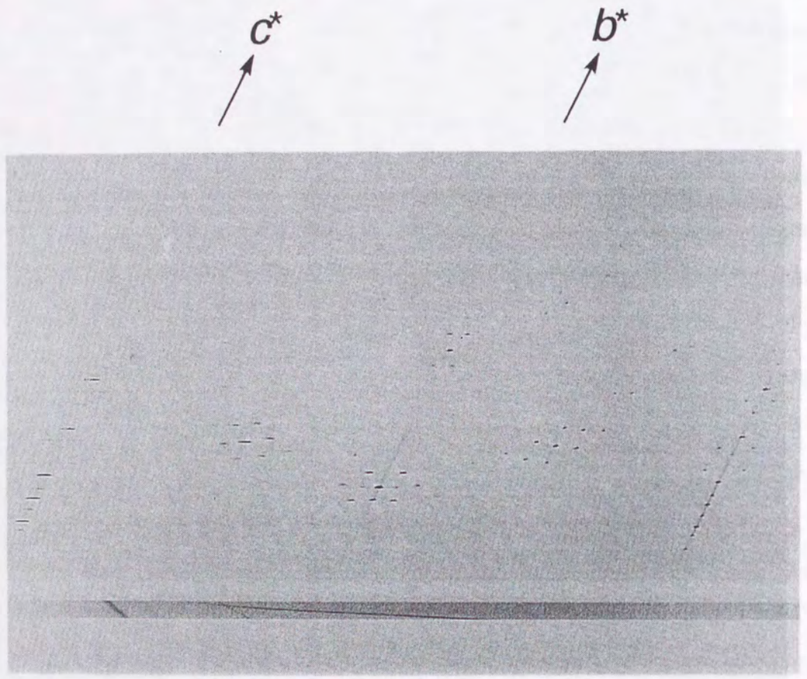

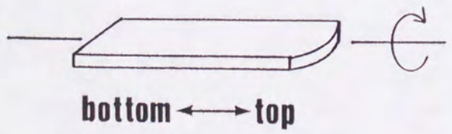

FIG. 2–7. Weissenberg photograph obtained by rotating the whisker along the long axis (growing axis) of the whisker.

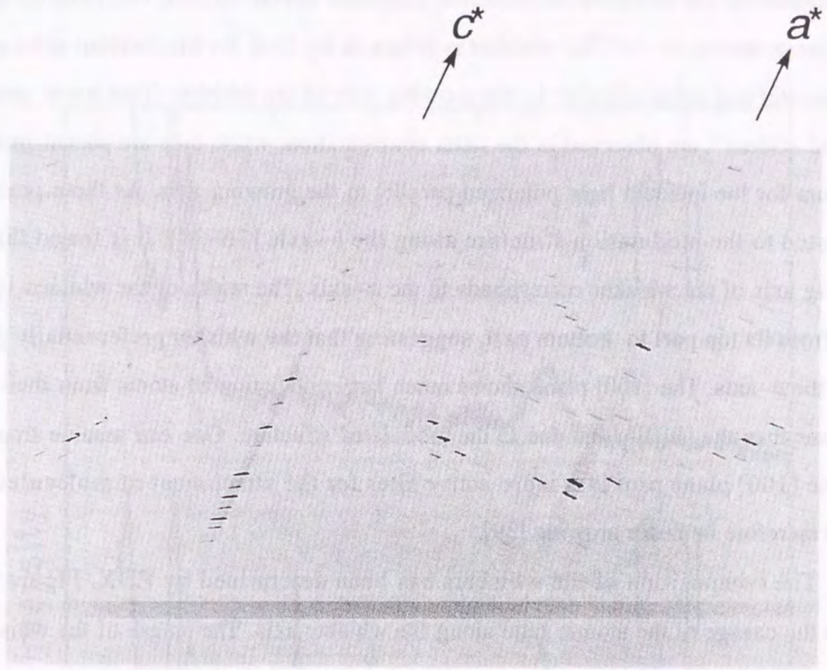

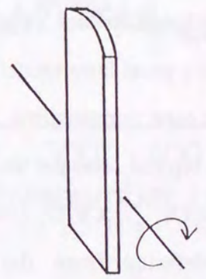

FIG. 2–8. Weissenberg photograph obtained by rotating the whisker along the axis parallel to the well–grown plane and perpendicular to the growing axis.

to (a^*–c^*) plane. The results therefore show that the growing axis of the whisker is the *a*–axis, the *b*–axis lies in the well–grown plane, and the *c*–axis is perpendicular to the plane. This orientation has also been confirmed by polarized Raman spectra. The room temperature Raman spectra of the 2212 whisker is shown in fig. 2–9, for the incident light polarized parallel and perpendicular to the growing axis of the whisker. Two broad peaks at 295 and 630cm^{-1} are observed in the latter configuration, while they are absent from the spectrum for the incident light polarized parallel to the growing axis. As these peaks are attributed to the modulation structure along the *b*–axis [36–38], it is found that the growing axis of the whisker corresponds to the *a*–axis. The width of the whisker is uniform from its top part to bottom part, suggesting that the whisker preferentially grows along the *a*–axis. The [100] plane shows much larger deviation of atoms from their ideal positions than the [010] plane due to the modulated structure. One can assume from this that the [100] plane provides more active sites for the attachment of molecules, and would therefore be faster growing [39].

The composition of the whiskers has been determined by EDX. Figure 2–10 shows the change of the atomic ratio along the whisker axis. The length of the whisker is 5.3 mm. The point analysis was made at 0.25 mm intervals from the bottom to the top of the whisker. Although the atomic ratio of Bi and Sr tend to increase and that of Cu and Ca tend to decrease, the whisker has a good homogeneity in the composition within about 1 mol% for each element. The average composition of this whisker is Bi:Sr:Ca:Cu = 31:17:19:33, which agrees with the typical ratio for the 2212 whiskers. The atomic ratios are written approximately in $Bi_2(Sr_zCa_{1-z})_{2.2}Cu_2O_x$ (z=0.47). It should be noted that the total amount of (Sr+Ca) is much deficient from the ideal stoichiometry, and the Ca content is larger than the Sr content. The sum of the Ca and Sr compositions is 2.2, corresponding to the occupancy ratio of 73%. Hong *et al.* have reported the solid solution range of the 2212 compound prepared by a conventional solid–state reaction method [40]. They have indicated that the solid solution range can be represented as $(Bi_xCu_{1-x})_{4+y}(Sr_zCa_{1-z})_{3-y}O_\delta$, $0.48<x<0.57$, $0.56<z<0.80$, $0<y<0.2$. They have summarized the

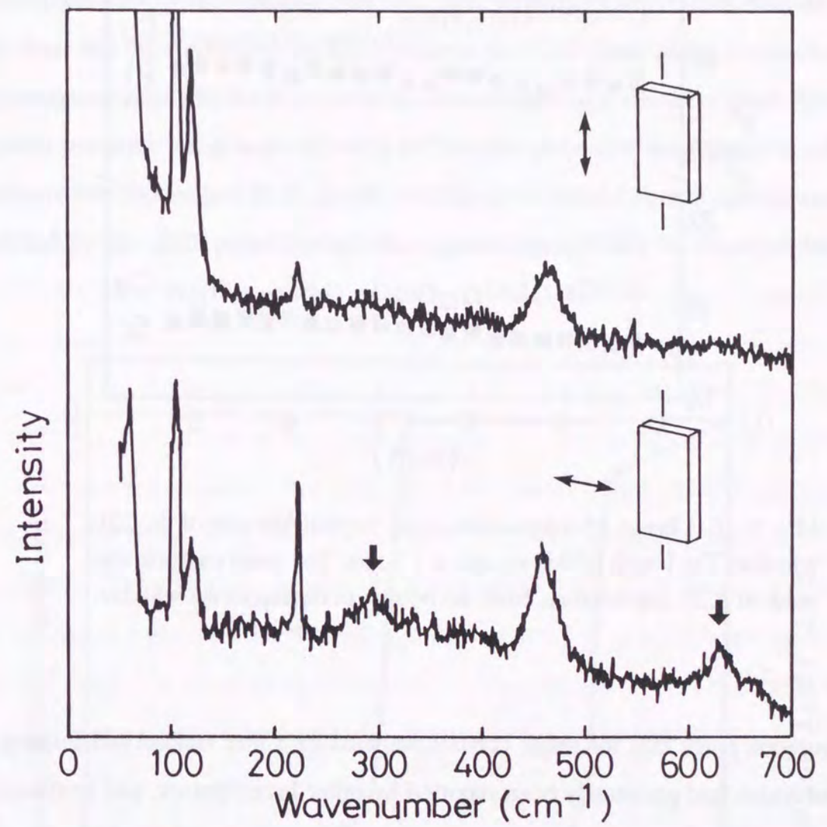

FIG. 2–9. Raman spectra of the 2212 whisker for the incident light polarized parallel (top) and perpendicular (bottom) to the growing axis of the whisker.

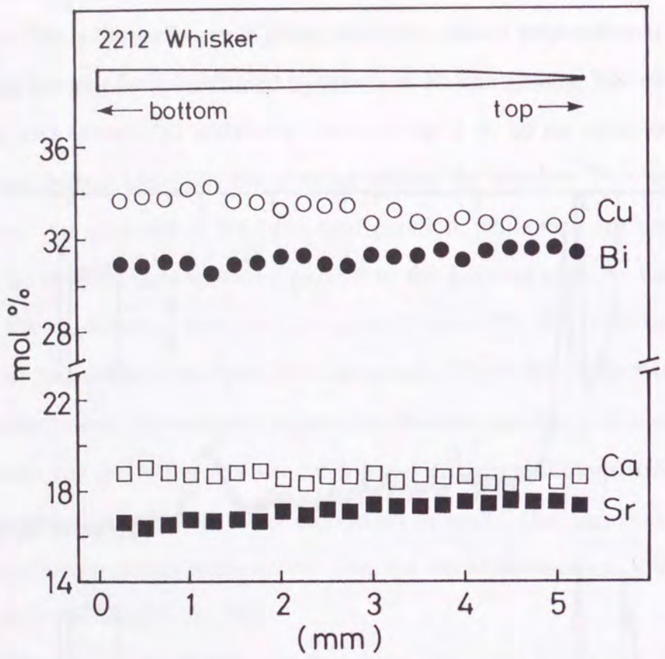

FIG. 2–10. Change of composition along the whisker axis of the 2212 whisker. The length of this sample is 5.3 mm. The point analysis was made at 0.25 mm intervals from the bottom to the top of the whisker.

solid solution range also for single crystals prepared by a flux method and floating zone method which had previously been reported by other investigators, and confirmed the consistency of the range for the powder samples. However, our 2212 whisker is outside of their range. The (Sr+Ca) deficiency is larger than their result and the Sr/Ca ratio of 0.9 is also out of the range to the direction of Ca–rich side. The 2212 whisker is characterized by the high (Sr+Ca) deficiency and the high Ca ratio.

Temperature dependence of resistance (R–T) and susceptibility for the 2212 whiskers are shown in fig. 2–11. A small change in growing condition can lead to variations in T_c and R–T behavior. However, the whiskers from every batch generally show

two steps in the R–T curve at around 105 and 76 K, and the zero resistance temperature at 74–75 K as shown in fig. 2–11. The whiskers show a sharp resistance drop, and the typical width of the transition is 2–3 K. The first resistance drop is due to the 2223 phase contained in the whiskers. The ratio between the height of the first and second resistance steps is dependent on the whisker. This ratio does not reflect the volume fraction of the 2223 phase but the fraction of the 2223 phase in the 2212 phase along a route between two voltage terminals in the four probe measurement. Some whiskers show the single resistance transition either near 105 or 75 K. The zero resistance temperature is achieved at temperature higher than 95 K in some whiskers, in which two voltage terminals are connected by the 2223 phase. A slight diamagnetic susceptibility is observed between

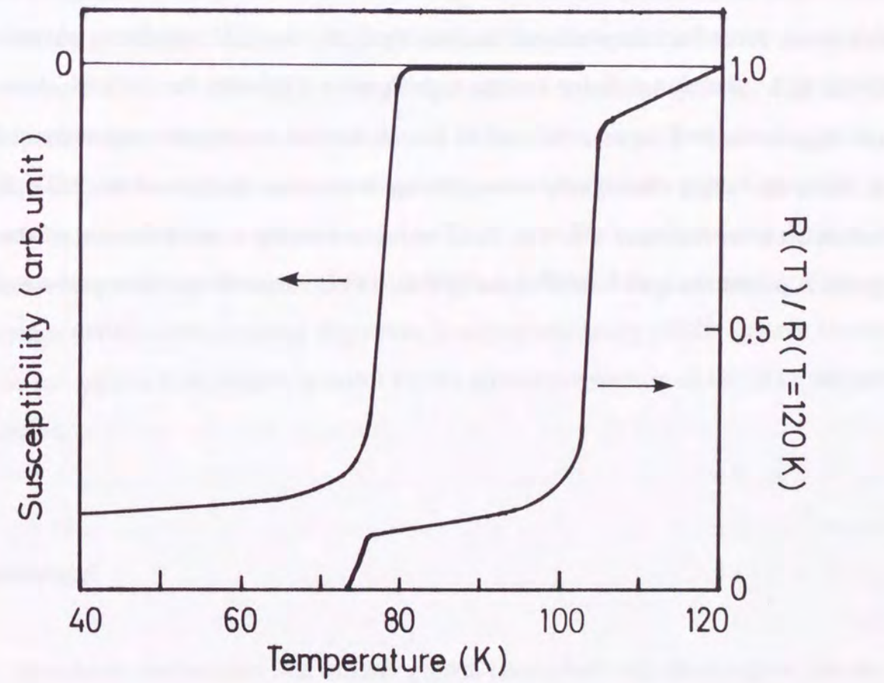

FIG. 2–11. Temperature dependence of normalized resistance and susceptibility for the 2212 whiskers.

104 and 80 K corresponding to the first resistance drop. From the susceptibility curve, the volume fraction of the 2223 phase is estimated to be less than 1%. The 2212 whiskers contain a small amount of the 2223 phase. A maximum J_c of 7.3×10^4 A/cm^2 (66 K, 0 T) is observed by a four-probe method.

In summary, a new method has been developed for preparing the 2212 whiskers of single crystals. The 2212 whiskers have been prepared by annealing a melt-quenched glass plate in a stream of O_2 gas. Each whisker with the dimensions of 2–10 μm thick, 10–500 μm wide, and ~20 mm long is composed of several platelike single crystals which are stacked in a layered structure. The crystallographic orientation of the 2212 whiskers has been determined by means of X-ray diffraction, Weissenberg photograph, and polarized Ramam spectra. The results show that the growing axis of the whisker is the *a*-axis, the *b*-axis lies in the well-grown plane, and the *c*-axis is perpendicular to this plane. From the compositional analysis by EDX, the 2212 whisker is characterized by the high (Sr+Ca) deficiency and the high Ca ratio. Typically, the 2212 whiskers show two steps in the R-T curve at 105 and 76 K with the zero resistance temperature at 74–75 K. From the slight diamagnetic susceptibility, the volume fraction of the 2223 phase is estimated to be less than 1%. The 2212 whiskers contain a small amount of the 2223 phase. A maximum J_c of 7.3×10^4 A/cm^2 (66 K, 0 T) is observed by a four-probe method.

2–3. Growth condition and mechanism

Elucidation of the growth condition and mechanism of the $Bi_2Sr_2CaCu_2O_x$ (2212) whiskers is important for producing them with the desired crystal shape on a large scale. This section describes the detailed conditions and growth mechanism of the 2212 whiskers. For the successful growth of the 2212 whiskers, there are three important factors in the growth conditions other than the appropriate heating temperature and starting composition. The first is the glass precursor [26] and the second is the presence of Al in the glass precursor [41]; although the 2212 whiskers contain no Al, the addition of Al to the glass precursor is found to greatly enhance the whisker growth. The appropriate amount of Al in the glass precursor is around 10 at.%. The third factor is a steady stream of O_2 gas (>100 ml/min) during annealing. These experimental conditions are thought to be related to the growth mechanism. The growth site of the whisker is the bottom part which is rooted several tens of micrometers deep in the crystallized glass substrate. It is therefore important that microstructural observation and analysis are performed near the surface of the crystallized glass substrate, especially around the bottom part of the whisker. This section describes the experimentally confirmed growing conditions and the results of a microstructural and compositional analysis carried out using a scanning electron microscope (SEM) with an energy dispersive X-ray spectroscopy (EDX) system. On the basis of the experimental results, a model for the growth mechanism of the 2212 whisker is proposed.

Experimental

In order to confirm that the whisker growth takes place only from a glass precursor, two kinds of samples were prepared. Powders of Bi_2O_3, $SrCO_3$, $CaCO_3$, and CuO were mixed at nominal composition of $BiSrCaCu_2O_x$. The mixture of 15 g was melted in

an alumina crucible at 1200°C for 30 min in air. The melt was quenched using copper plates, giving a glass precursor. The polycrystalline compound was prepared by slowly cooling the melt in the furnace. Both the glass and the polycrystalline samples were crushed to powder and formed into pellets, and then annealed at 865°C for 80 h in a stream of O_2 gas (150 ml/min).

Effects of Al addition into the glass precursor on the whisker growth were examined using the five glass precursors with differing Al contents. The starting materials were Bi_2O_3, $SrCO_3$, $CaCO_3$, CuO, and Al_2O_3. The powders were mixed at nominal compositions of $BiSrCaCu_2Al_xO_y$ (x=0, 0.25, 0.5, 0.75, 1.0) and were melted at 1150°C for 30 min using a Au–Pd alloy crucible. The melts were quenched using copper plates. The obtained melt–quenched samples were annealed at 859–874°C for 80 h in a stream of O_2 gas (150 ml/min) and then cooled to room temperature within the furnace.

The growth of the whiskers under different flow rates of O_2 gas was examined for the glass precursors prepared using an alumina crucible as described above. The glass plates were annealed at 865°C for 80 h in a stream of O_2 gas (0, 50, 100, 150, 200, 400, 700 ml/min) using a tubular furnace with a diameter of 50 mm and cooled to room temperature within the furnace.

Microstructural observation and analysis were performed on crystallized glass plates annealed variously at 500, 700, 800, and 865°C. The glass samples were prepared by using an alumina crucible to ensure sufficient Al content (~ 10 at.%). The annealed samples were quenched to air when the furnace temperature reached the appropriate temperature during the heating process. In addition, samples annealed at 865°C for various periods were also used for microstructural observation. Specimens were cut and polished for cross–sectional observation using a Hitachi SEM model S–2400 with a Horiba EMAX–5770 EDX system. Major phases in the crystallized glass plates were identified using a RIGAKU X–ray diffractometer with Cu–Kα radiation. The DTA curve was obtained by increasing the temperature from room temperature to 1000°C at a constant heating rate of 10°C/min.

Results and discussion

For the growth mechanism of whiskers, two typical mechanisms have been reported and both have been experimentally and theoretically confirmed and well characterized. The Vapor–Liquid–Solid (VLS) mechanism has been proposed by Wagner and Ellis for the Si whiskers [42]. The presence of a liquid droplet (VLS ball) at the tip of the growing crystal plays an important role. The surface of the liquid has a large accommodation coefficient and is therefore a preferred site for deposition. The VLS ball becomes supersaturated with material supplied from vapor, and crystal growth occurs by precipitation at the solid–liquid interface. Another is the spiral growth mechanism [43, 44]. Whisker growth takes place as a result of diffusion along the core of a screw dislocation. This mechanism is grouped into two types according to the growth site, either tip or base. In the former type, the grown whiskers have a single screw dislocation along their center axis, while in the latter type they have none. The first example of the latter type has been reported by Koonce and Arnold for tin whiskers [45]. Determination of the growth site is the first step in elucidating growth mechanism. When whiskers grow at the tip, growth proceeds by acquiring atomic species and accumulating them at that tip of the whiskers. The VLS mechanism belongs to this type. In the case of the base end growth, growth proceeds by pushing up the whiskers from below.

Figure 2–12 shows the top part of the 2212 whisker. In this case, the whisker has a round shaped tip, and shows a layered structure. There is no evidence of the VLS ball at the tip, indicating that the VLS mechanism is not likely for the growth of the 2212 whiskers. The 2212 whiskers are considered to grow at the bottom part. Figure 2–13 is one of the evidences for the base end growth. For growing the whiskers, the glass plate is set on an alumina plate. In this situation, one side of the plate is put in contact with the surface of the alumina plate, while another side is open to air. After the annealing, the whiskers grow on both the sides of the crystallized glass plate, and the plate is lifted up 3–5 mm high from the surface of the alumina plate supported by the growing whiskers

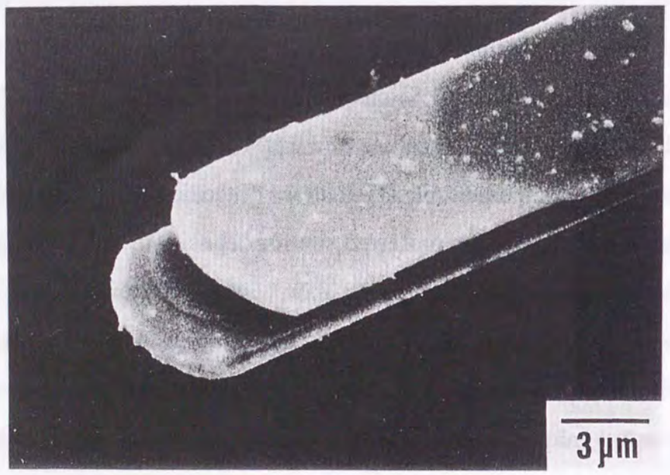

FIG. 2–12. Top view of the 2212 whisker.

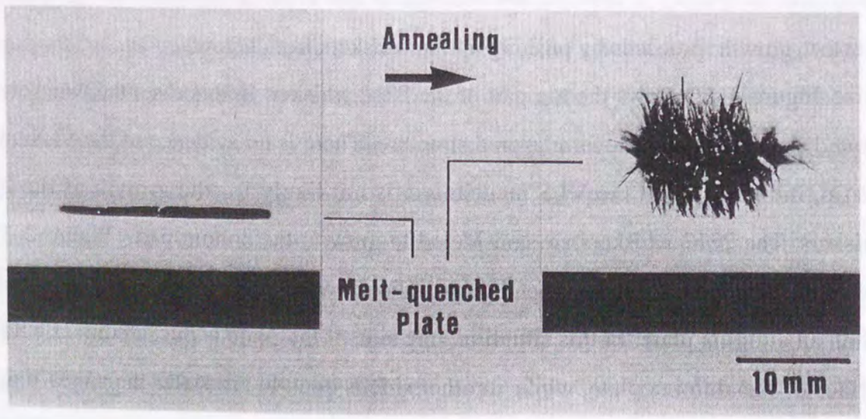

FIG. 2–13. Photograph of glass precursor before and after the whisker growth.

themselves. The length of the whiskers grown on the free side is nearly the same as that of the contacted side. If the whiskers grow at the tip, the length of the whiskers should be much influenced by contacting with the surface of the alumina. For the same situation, we sometimes observe a fact that the length of the whiskers at the contacted side is shorter than that of the free side. The shortening of the whisker length at the contacted side is due to the reaction between the alumina boat and the whiskers. Therefore, the 2212 whiskers are found to grow at their bottom part.

There are three important factors for the growth of the 2212 whiskers other than the appropriate annealing temperature and starting composition. The first factor is that the glass precursor is necessary for the growth of the 2212 whiskers [26]. In order to examine whether the glass is needed for the whisker growth or not, we have prepared two samples. One is the glass plate and the other is the polycrystalline one which are prepared by quenching and slowly cooling the melt, respectively. Each of them was crushed to powder and formed into pellets, and then annealed at 865°C for 80 h in a stream of O_2 gas (150 ml/min). These two samples are different only in the cooling process. The whiskers of 2–3 mm grow only from the glass sample after annealing (fig. 2–14). It becomes also apparent that the whisker growth takes place not only from a glass plate but also from a glass powder.

The second factor is the presence of Al in the glass precursor. This has been first reported by Abe *et al.* in the $BiSrCaCu_2Al_xO_y$ system [41]. In order to confirm the effectiveness of Al addition, five glass precursors with differing Al contents have been prepared, $BiSrCaCu_2Al_xO_y$ (x=0, 0.25, 0.5, 0.75, 1.0), using a Au–Pd alloy crucible so as not to dissolve extra Al from an Al_2O_3 crucible. The nominal content of Al in the glass precursors is calculated to be 0.0, 4.8, 9.1, 13.0, and 16.7 at.%, respectively. The glasses are free of crystalline phases except for the x=0.0 sample. The melt–quenched samples are annealed at 859–874°C for 80 h in a stream of O_2 gas (150 ml/min), then cooled to room temperature within the furnace. Figure 2–15 shows the results of the whisker growth at an annealing temperature of 868°C. The whisker growth is not observed for the

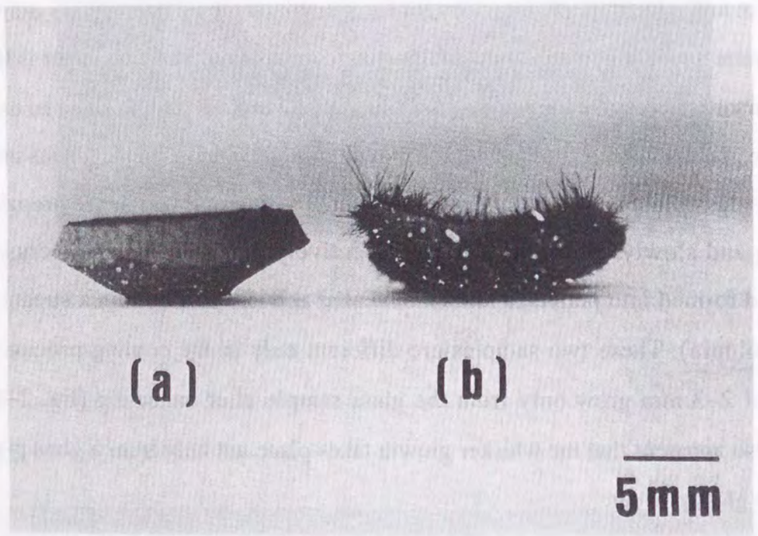

FIG. 2–14. Comparison of whisker growth between (a) polycrystalline precursor and (b) glass precursor.

glass precursor with a low content of Al, x=0.0 and x=0.25 samples. For the x=0.5 and x=1.0 samples, the growth of the whiskers is observed, whereas the length is less than 2 mm. The most appropriate one is x=0.75 sample which gives the whiskers with 3–6 mm in length.

The growth of the whiskers at different annealing temperatures is summarized in fig. 2–16. The star symbol means that no whiskers grow under the corresponding conditions. The horizontal line symbolizes the crystallized glass substrate. The length and the number of vertical lines indicate the length and the amount of the grown whiskers. The area surrounded by a circle is a favorable region for the whisker growth. It is obvious from fig. 2–16 that the addition of Al is effective for the whisker growth. The most favorable condition is 871°C for the x=0.75. The whisker growth has not been observed on the glass precursor in the absence of Al. The appropriate amount of Al in the glass precursor is around 10 at.%. EDX analysis shows that the annealed glass plate from which the whiskers grow actually contains about 10 at.% of Al. The annealing temperature most suitable for the whisker growth decreases with increasing Al content. This tendency is consistent with DTA analysis, in which decrease in the melting temperature is observed in response to increase in Al content. This suggests that the whisker growth occurs at just below the melting temperature of the glass precursor. When an alumina crucible is used for the glass preparation, the whiskers are obtained without extra addition of Al_2O_3 powder to the starting mixture as described in section 2–2. In this case, Al is derived from the alumina crucible during the melting process. The amount of Al dissolved in the melt depends on the melting temperature. A glass–fabricating temperature of 1150–1200°C is preferable when using an alumina crucible.

The third factor is a steady stream of oxygen gas during annealing. The growth of the whiskers is examined under various flow rates of O_2 gas using the glass precursors prepared using an alumina crucible. The glass plates are annealed at 865°C for 80 h in a stream of O_2 (0, 50, 100, 150, 200, 400, 700 ml/min) using a tubular furnace with a diameter of 50 mm. The whiskers grow in a stream of O_2 gas of 100–700 ml/min, but not

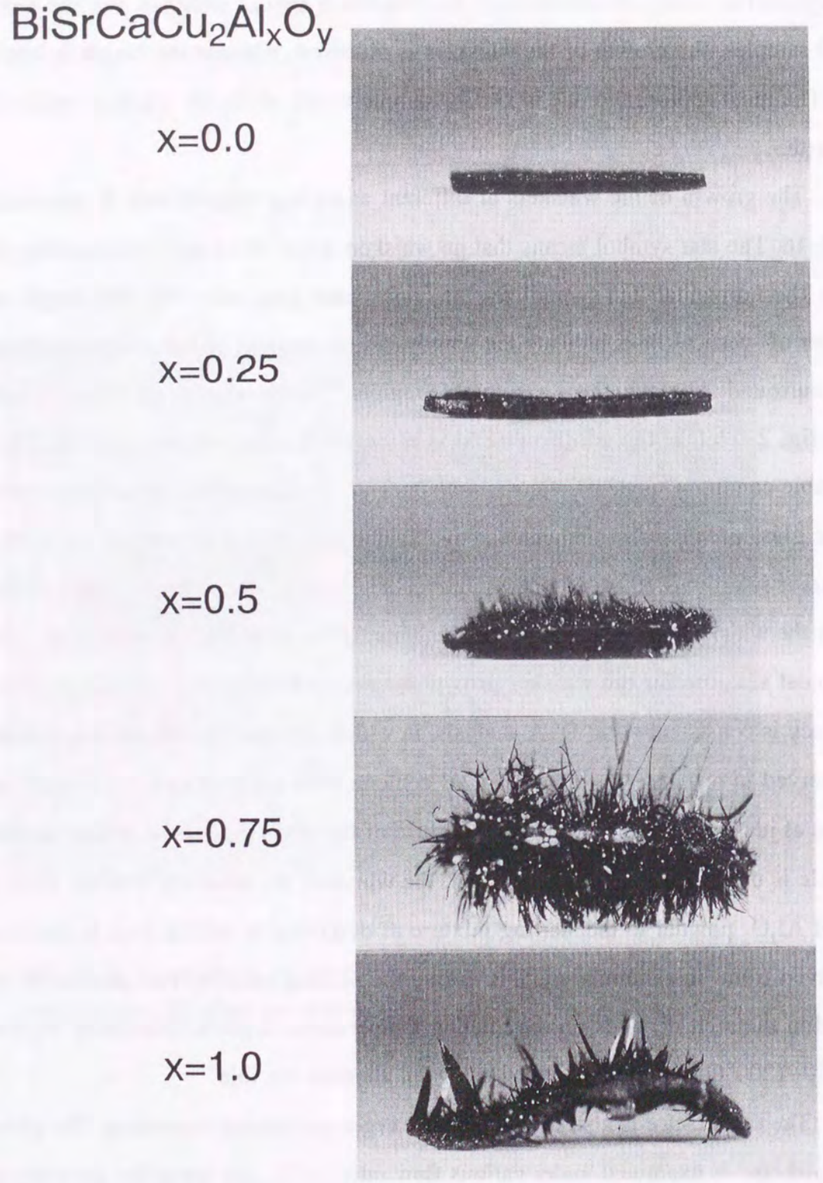

FIG. 2–15. Growth of the 2212 whiskers from glass precursors with different Al content, $BiSrCaCu_2Al_xO_y$ (x=0.0, 0.25, 0.5, 0.75,1.0), which are annealed at 868°C for 80 h in a stream of O_2 gas (150 ml/min).

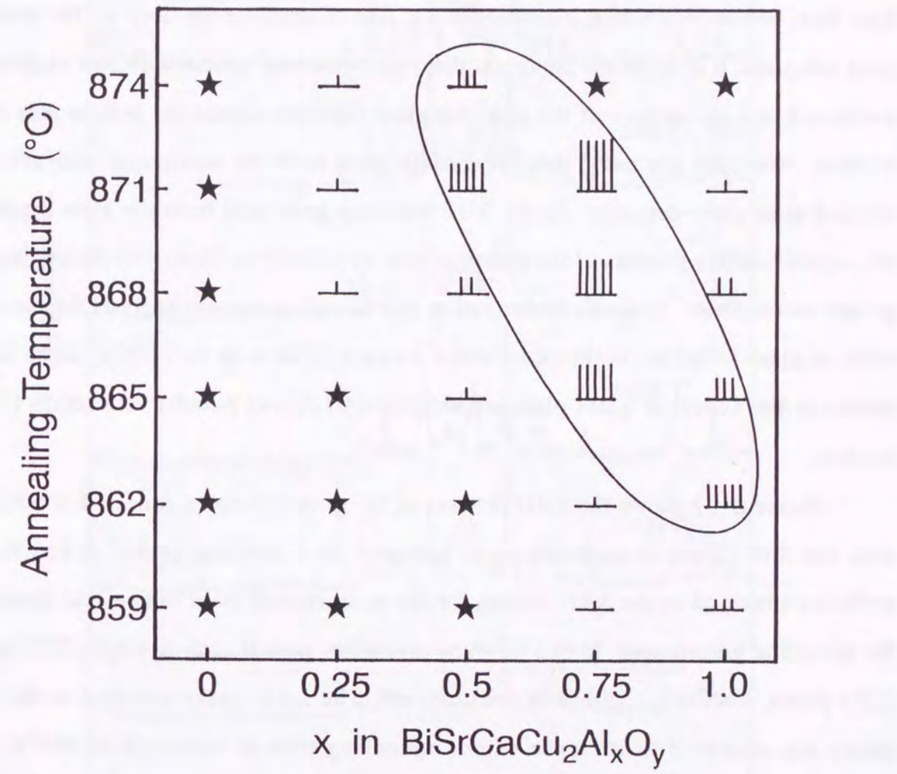

FIG. 2–16. Growth of the 2212 whiskers from glass precursors with different Al content, $BiSrCaCu_2Al_xO_y$ (x=0.0, 0.25, 0.5, 0.75,1.0), which are annealed at 859–874°C for 80 h in a stream of O_2 gas (150 ml/min).

grow in an oxygen flow less than 100 ml/min. The whisker growth is rather slow in low oxygen gas flows. O_2 gas flow of more than 100 ml/min is important for the successful growth of the 2212 whiskers.

The above three factors required for the whisker growth are thought to be explicable on the basis of the growth mechanism of the 2212 whiskers. The 2212 whiskers grow from their bottom part which is rooted several tens of micrometers deep in the annealed glass substrate. It is therefore important that microstructural observation and analysis are performed near the surface of the annealed glass substrate around the bottom part of the whisker. Materials processed through crystallization from the amorphous state are often referred to as glass-ceramics. As the 2212 whiskers grow only from the glass precursor, the crystallization process of the glass sample also gives an important insight into the growth mechanism. Structural observation and the compositional analysis for the crystallized glass substrate is thus conducted using a SEM with an EDX system. Major phases in the annealed glass plate are identified by X-ray powder diffraction (XRD) method.

Figure 2-17 shows the XRD patterns of the glass substrates annealed at 500, 700, 800, and 865°C, and of another sample annealed for a different period at 865°C. No peaks are observed in the XRD pattern for the as-quenched glass sample. As increasing the annealing temperature to 865°C, some crystalline phases such as Cu_2O, 2212 phase, 2201 phase, Ca_2CuO_3, and CuO are observed. The XRD peaks ascribed to the 2212 phase are observed to increase when annealing time is extended at 865°C. The $(Sr,Ca)_3Cu_5O_8$ phase appears in a sample annealed at 865°C over 10 h. A crystalline phase containing Al can be detected in the XRD patterns as indicated by the open triangular symbol. EDX analysis shows that this phase consisted of Bi-Sr-Ca-Al-O complex oxide. The Bi-Sr-Ca-Al-O phase is also confirmed in a sample independently prepared using the solid state reaction method. The compound is prepared by heating a mixture of Bi_2O_3, $SrCO_3$, $CaCO_3$, and Al_2O_3 powders (Bi:Sr:Ca:Al = 1:1:1:2) at 900°C for 12 h and displayer the same diffraction pattern as that shown in fig. 2-17 (open triangle). The

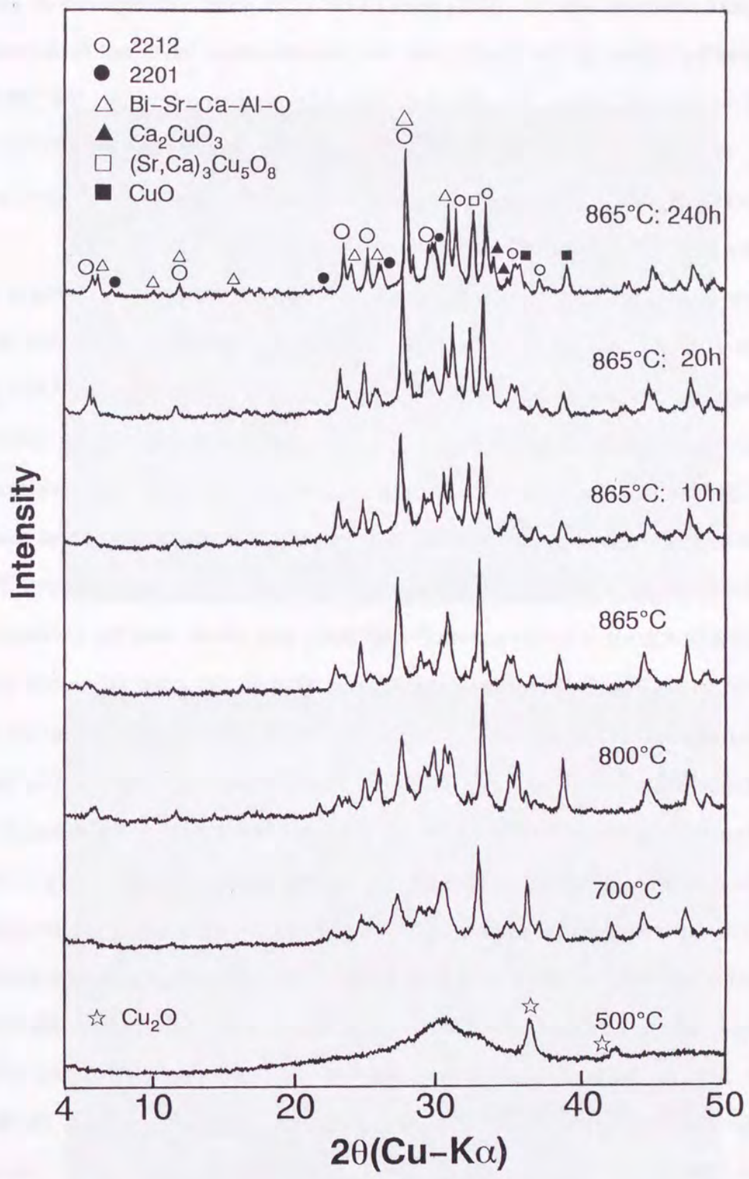

FIG. 2-17. X-ray diffraction patterns of the glass substrate annealed at 500, 700, 800, and 865°C, and for different period at 865°C.

diffraction peak observed near the (002) peak of the 2212 phase corresponds to 14.2 Å in the lattice spacing. Although the purification and identification have not been completed for the Bi–Sr–Ca–Al–O phase, it is found to have a layered structure like the 2212 phase or $Bi_4Ti_3O_{12}$ type structure [46]. The Al–containing phase is stable up to 1050°C. As the 2212 whiskers grow only from a glass precursor containing Al, the Bi–Sr–Ca–Al–O phase appears to play an important rule in the whisker growth.

Figure 2–18 shows cross–sectional views from a backscattered electron micrograph for the glass precursors annealed at 500 and 800°C. The sample annealed at 500°C appears featureless as seen in fig. 2–18 (a), while Cu_2O is detected in the XRD pattern. Crystallization has occurred in the glass substrate annealed at 800°C with needle–like crystals of $(Sr,Ca)_2CuO_3$ apparent in the middle layer of the plate. Observation of the surface portion at a higher magnification reveals small particles of CuO of less than 1 μm diameter. Generation of the 2212 whisker is not seen at this temperature. The as–quenched glass precursor is in oxygen–deficient state, and about half the Cu ions are reduced to Cu^+ [47]. Cu_2O therefore crystallizes first in the crystallization process. Thermogravimetry (TG) analysis in air indicates that a substantial amount of oxygen absorption takes place when the glass is heated. This is observed between near the glass transition temperature and 700°C. After the oxygen absorption, pronounced crystal growth starts as seen in the XRD pattern (fig. 2–17) and SEM observation (fig. 2–18).

A backscattered electron micrograph of a polished cross–section of the glass precursor annealed at 865°C for 20 h is shown in fig. 2–19. The large and dark needles are $(Sr,Ca)_3Cu_5O_8$ while the small black particles are CuO. Growth of the whiskers is observed only near the surface. It is clearly apparent that the bottom part of the whisker is buried in the annealed glass substrate several tens of micrometers deep. As the 2212 whiskers are thought to grow at the bottom part, detailed microstructural observation and analysis have been performed around this part of the whisker (fig. 2–19 (b)). The results of compositional analysis at the various points indicated in fig. 2–19 (b) are summarized in table 2–1. The atomic ratio of the whisker observed is Bi:Sr:Ca:Cu =

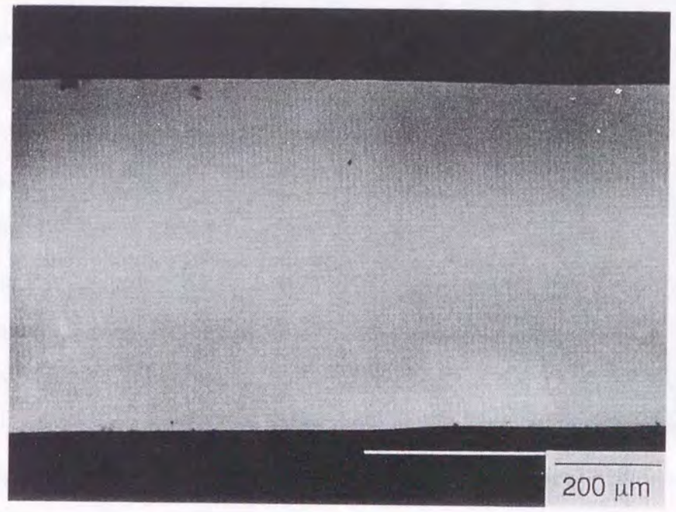

(a)

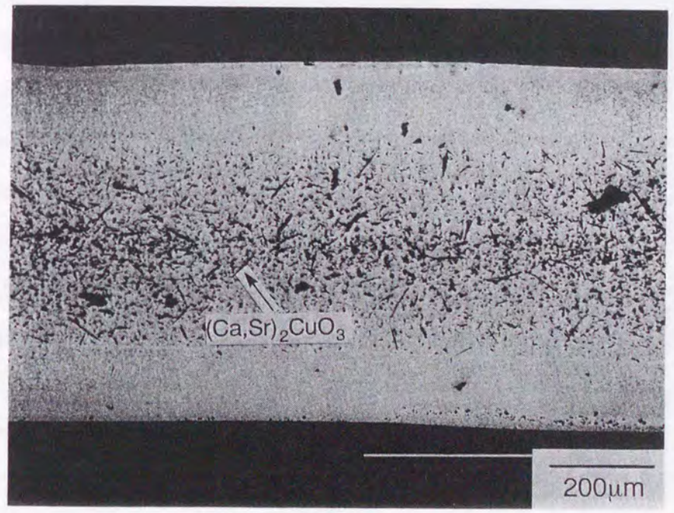

(b)

FIG. 2–18. Cross–sectional backscattered electron micrographs for the glass precursor annealed at (a) 500°C and (b) 800°C.

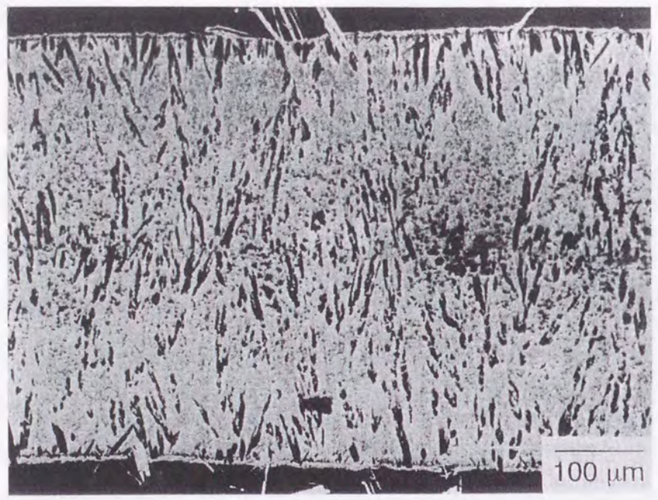

(a)

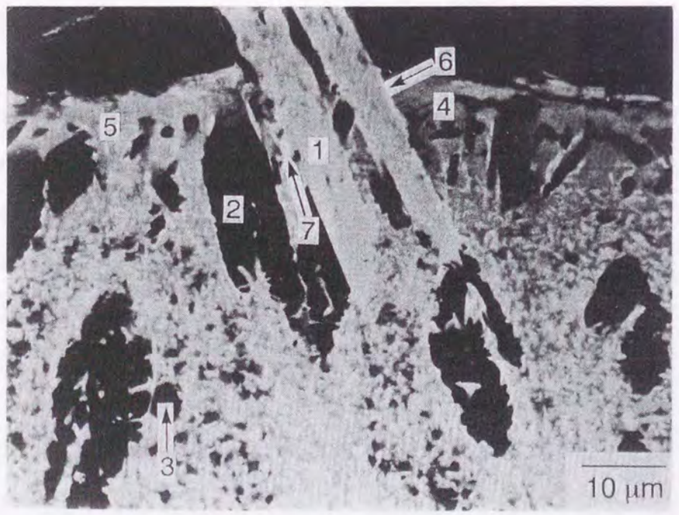

(b)

FIG. 2–19. (a) Cross–sectional backscattered electron micrograph for the glass precursor annealed at 865°C for 20h. (b) The magnified photograph of near the surface where a whisker is just observed.

33:19:18:30, which is a Bi–rich 2212 composition. The excess Bi is thought to occupy the Sr or Ca site. The large dark crystal (position 2) and small dark particle (position 3) are identified as $(Sr,Ca)_3Cu_5O_8$ and CuO, respectively. The Bi–Sr–Ca–Al–O phase is distributed near the surface (positions 4 and 5) and forms a layer of 20–30 μm in thickness. On the inner side of the Bi–Sr–Ca–Al–O layer, many small and white particles of the 2212 phase are observed. The most characteristic point in this microstructure is the existence of a Bi–rich phase observed along the 2212 whisker as a bright thin layer (positions 6 and 7). The thickness of this layer is about 1μm. The average atomic ratio of the Bi–rich phase is Bi:Sr:Ca:Cu:Al = 38:21:15:24:2. This composition should be in a liquid state at the annealing temperature (865°C). The bottom part of the whisker must therefore be surrounded by a thin liquid phase during the growth of the whiskers. This microstructure is not a special case, the same microstructures are also observed in other samples as shown in fig. 2–20. In fig. 2–20 (a), the Bi–Sr–Ca–Al–O phase distributes near the surface and the thin layer of the Bi–rich phase is observed along the bottom part of the 2212 whisker. The Bi–rich phase can be seen along the side surface of the whisker in fig. 2–20 (b). The thickness of the whisker is about 3 μm. The Bi–rich phase extends from the surface of the annealed glass substrate to the bottom end of the whisker.

Although phase stability among the 2201, 2212 and 2223 phases has been analyzed by many groups [48, 49], no precise phase relation has been determined yet. Shigematsu *et al.* have proposed a tentative phase relation in the pseudo–binary system between $Bi_2(Sr,Ca)O_4$ and $(Sr,Ca)CuO_2$ [50]. The important point is that the 2212 phase melts incongruently above 875°C in their phase relation. A hypothetical phase diagram for the incongruently melting compounds is shown in fig. 2–21. The incongruently melting compound (B) is equivalent to the 2212 phase, and compounds A and C correspond to $(Sr,Ca)CuO_2$ and $Bi_2(Sr,Ca)O_4$ each of which melts congruently. The 2212 phase is not in equilibrium with a melt of 2212 composition. When the melt of 2212 composition is cooled just below the liquidus temperature, the solid phase A will crystallize. It has in fact been reported that $(Sr, Ca)_3Cu_5O_8$ precipitates from the 2212 melt first

Table 2–1. Results of EDX analysis.

Position	atomic ratio (at.%)					Phase
	Bi	Sr	Ca	Cu	Al	
1	33	19	18	30	0	2212
2	1	12	24	63	0	$(Sr,Ca)_3Cu_5O_8$
3	1	1	1	97	0	CuO
4	25	24	16	5	30	Bi–Sr–Ca–Al–O
5	26	25	16	3	30	Bi–Sr–Ca–Al–O
6	39	22	14	21	4	Bi–rich
7	37	20	16	26	1	Bi–rich

[13]. The 2212 phase is equilibrated with a melt having the composition between P and E in fig. 2–21, a Bi–rich composition compared with the 2212 composition. The composition of this melt has been determined to be $Bi_{2.4}Sr_{1.5}Ca_{1.0}Cu_{1.8}O_x$ [13], which has an atomic ratio of Bi:Sr:Ca:Cu = 36:22:15:27. This composition agrees well with that of the thin layer seen surrounding the bottom part of the whisker in cross–sectional observation (figs. 2–19 and 2–20). The 2212 whiskers would therefore appear to grow through continuous precipitation from the Bi–rich melt surrounding the whiskers.

A model of the growth mechanism of the 2212 whiskers is devised based on microstructural observation and identification of the experimental conditions necessary for the whisker growth as shown in fig. 2–22. The 2212 whisker is buried several tens of micrometers deep in the annealed glass substrate. The Bi–Sr–Ca–Al–O compound is distributed near the surface. Between the 2212 whisker and the Bi–Sr–Ca–Al–O phase, the thin layer of the Bi–rich phase which is in a liquid state during annealing, surrounds

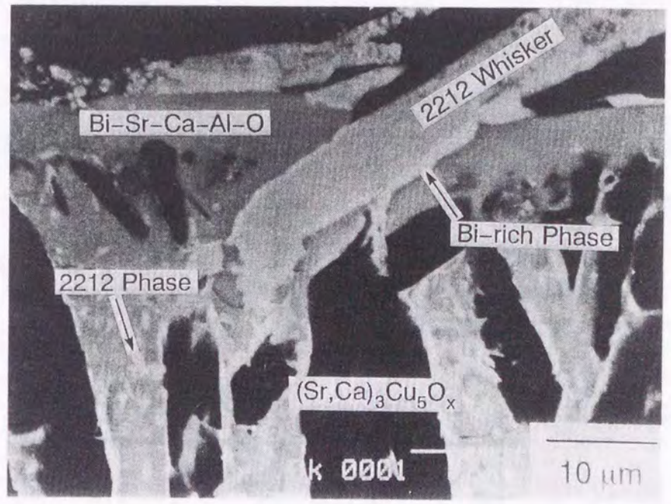

(a)

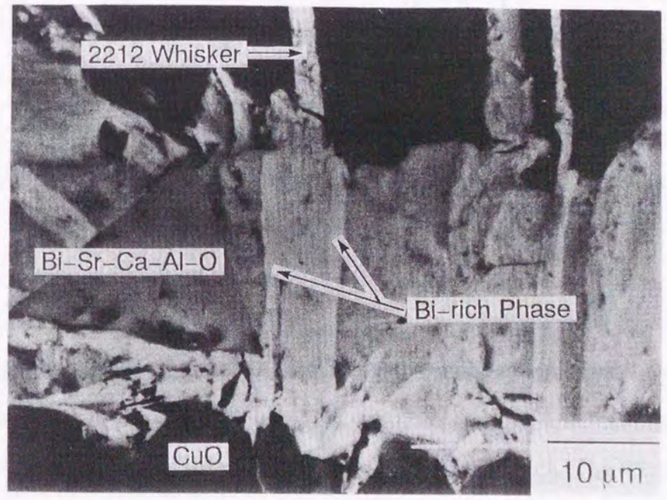

(b)

FIG. 2–20. Cross–sectional backscattered electron micrograph for the crystallized glass substrate from which the 2212 whiskers grow.

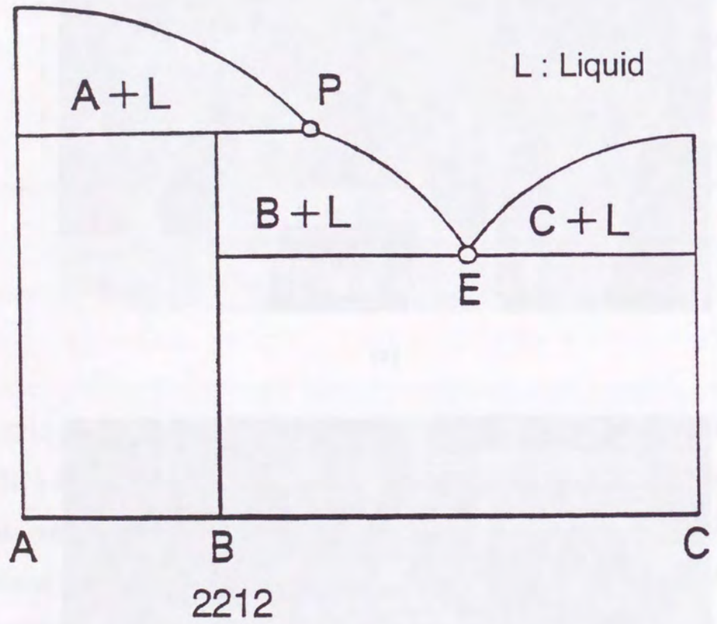

FIG. 2–21. Hypothetical phase diagram with an incongruently melting compound B.

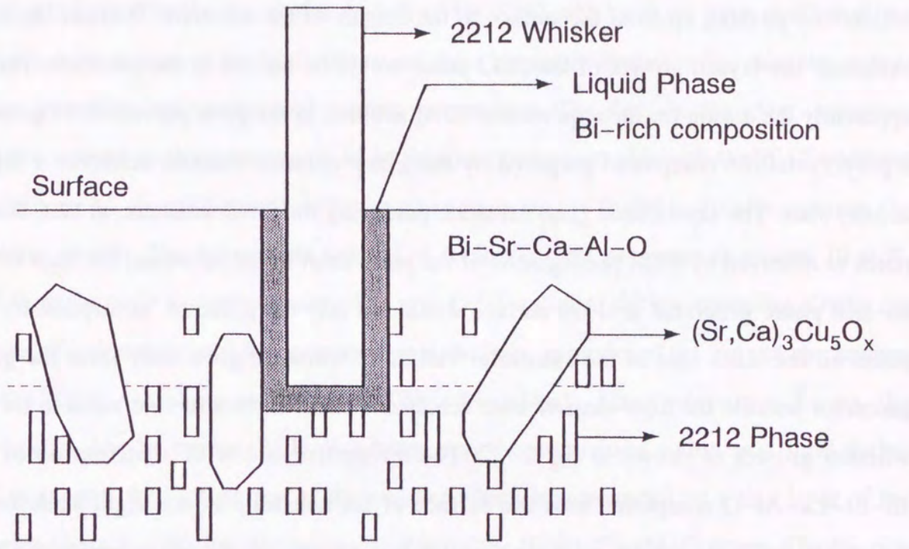

FIG. 2–22. A model for the growing mechanism of the 2212 whiskers.

the 2212 whisker. Large grains of $(Sr,Ca)_3Cu_5O_8$ are observed in the substrate, while no pores are observed in the crystallized glass substrate. Small particles of the 2212 phase are distributed on the inner side of the Bi–Sr–Ca–Al–O layer. The 2212 whiskers are thus found to grow through continuous precipitation of the 2212 phase from the melt of the Bi–rich phase. For the continuous growth of the whiskers, the composition and the volume of the Bi–rich liquid phase should be stable. The Bi–Sr–Ca–Al–O compound has

a higher melting temperature and is stable up to 1050°C, as described above. It would therefore act as a microcrucible to hold the 2212 whisker and the melt of the Bi-rich phase. The 2212 whisker and the surrounding liquid phase is supported by the 'rigid skeleton' of the Bi-Sr-Ca-Al-O complex oxide, which produces the growth of the whisker by pushing up from the surface to the outside of the substrate. Without the rigid skeleton, the crystal growth of the 2212 phase would be limited in the substrate. This is apparently the reason for the requirement of Al addition to the glass precursor. In general, a polycrystalline compound prepared by the glass-ceramic method achieves a high-density state. The crystallized glass substrate producing the 2212 whiskers, in fact, has no pores as observed by SEM photographs. If the pores exist in the substrate, the melt of the Bi-rich phase generated near the surface would not stay there due to absorption by the pores on the inner side of the substrate. The 2212 whiskers grow only from the glass precursor because the high-density state achieves a stable microstructure suitable for the whisker growth as shown in fig. 2-22. The microstructure with distribution of the Bi-Sr-Ca-Al-O compound near the surface of the substrate as the 'rigid skeleton' is thought to be achieved during the crystallization process of the glass precursor. This could also be a reason for the necessity of the glass precursor for the whisker growth.

The supplementation of the source materials to the melt at the bottom part of the whisker appears to proceed through diffusion of ions in the substrate. It is therefore predicted that the growth rate of the whiskers is determined by the diffusion process. A preliminary experiment on the kinetics of the whisker growth gives the result that the length of the whisker is proportional to the square root of time. This result is not inconsistent with the model, although more detailed experiments and analysis are required. While further investigations are required to clarify the necessity of the steady stream of O_2 gas, it can be speculated that the stream of O_2 gas makes a small gradient of temperature between the bottom part of the whiskers and the outside of the annealed glass substrate. Because the O_2 gas is supplied at room temperature, the outside of the substrate is at a temperature just lower than the bottom part of the whisker. This small gradient of

temperature is thought to be a driving force for the whisker growth.

In summary, the 2212 whiskers are the first example, to our knowledge, growing out from the surface of the crystallized glass substrate. The growth site of the whisker is not at the top part but the bottom part. Therefore, the VLS mechanism is unlikely for the 2212 whiskers. For the successful growth of the 2212 whiskers, we have confirmed the experimental conditions in detail. There are three important factors other than the appropriate annealing temperature and starting composition. The first is the glass precursor and the second is the presence of Al in the glass precursor; although the 2212 whiskers contain no Al, the addition of Al to the glass precursor is found to greatly enhance the whisker growth. The appropriate amount of Al in the glass precursor is around 10 at.%. The third factor is a steady stream of O_2 gas (>100 ml/min) during annealing. Using the results of microstructural and compositional analysis, a model of the growth mechanism of the 2212 whiskers is devised. The Al-added glass precursor forms the Bi-Sr-Ca-Al-O complex oxide distributed near the surface and acting as a 'rigid skeleton' to support the bottom part of the whisker which is surrounded by a thin layer of the Bi-rich phase and fits into the 'microcrucible' of the Bi-Sr-Ca-Al-O phase. The Bi-rich phase has the same composition as the liquid phase equilibrated with the 2212 phase and melts at the annealing temperature. The whisker growth takes place through the continuous precipitation of the 2212 phase from the melt at the base end of the whisker. This model can be called as a self-supporting micro-top-seeding mechanism.

2–4. Superconducting Properties in a Bending State

The noteworthy characteristic property of the $Bi_2Sr_2CaCu_2O_x$ (2212) whiskers is their bending property. A whisker can be elastically bent to a radius of curvature of 0.2 mm corresponding to a bending strain of 0.5%. Taking advantage of this property, we have measured the critical temperature (T_c) and critical current density (J_c) of the whiskers under such an extreme bending state. In the application of superconducting wires to a magnet, they receive bending strain in making coils. Therefore, it is important to study the relationship between the bending strain and superconductivity, T_c and J_c, using single crystals. The result gives the basic information for designing the superconducting magnet. This section describes the effects of bending strain on T_c and J_c [24].

Experimental

Pb–doped whiskers were used for the measurements of superconductivity in a bending state. The Pb–doped whiskers were prepared by annealing a glass plate with the starting composition of $Bi_2Sr_{1.9}Ca_{2.2}Cu_4Pb_{0.5}O_x$ at 840°C for 120 h in a stream of O_2 gas (150 ml/min). The zero resistance temperature of the whisker is 70 K. The temperature dependence of resistivity was measured using a direct current of 0.1 mA, and J_c was measured at 63 K, in pumped liquid nitrogen, in a zero magnetic field by a standard four–probe method. To measure T_c and J_c in a bending state, a whisker was set on an aluminum plate and it was bent to an appropriate curvature of radius (R) up to 2 mm. For $R \leq 1$ mm, a whisker was mounted on a MgO single crystal plate and was bent only between the voltage terminals by inserting a semi–cylindrical wire with an appropriate radius (fig. 2–23). At the bending strain of larger than 0.5%, the whiskers were often found to break or were unable to recover to their original shape, indicating that the outer surface of the crystals began to suffer from microcracks under the bending strain around 0.5%.

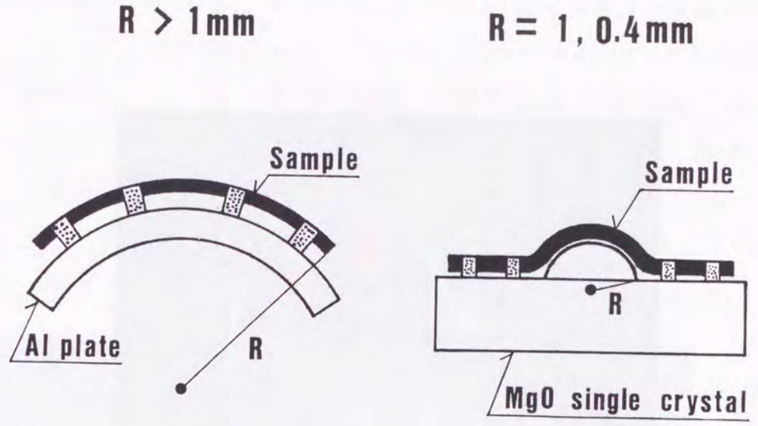

Fig. 2–23. Setting of a whisker to measure T_c and J_c in a bending state. For R>1mm, a whisker is set on an Al plate and bent it to an appropriate curvature. For $R \leq 1$mm, a whisker is mounted on a MgO single crystal plate and is bent only between the voltage terminals to the curvature by inserting a semi–cylindrical wire with an appropriate radius.

Results and Discussion

Figure 2–24 shows the photograph of the 2212 whisker in a bending state. The smallest curvature of radius (R) of this example is about 0.4 mm. This photograph is taken from a slightly oblique direction relative to the bending circle to show the circle clearly, so that the dark portion appears near the top of the hairpin curve as a result of the cross–sectional narrowing in the aspect of the curved whisker. A small coil can be made by winding a whisker onto a thin glass capillary (fig. 2–25). In this case, the diameter of the glass capillary is 0.5 mm.

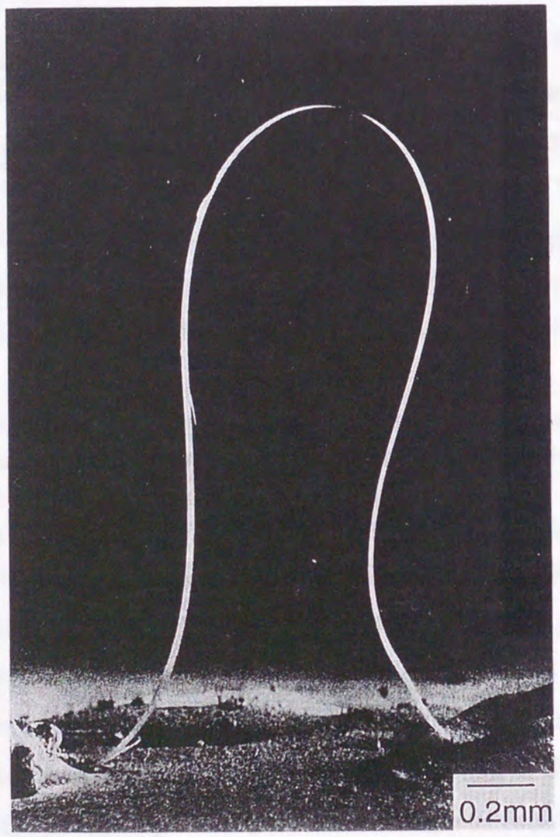

Fig. 2–24. Bi–2212 whisker in a bending state. This photograph is taken from a slightly oblique direction relative to the bending circle to show the circle clearly, so that the dark portion appears near the top of the hairpin curve as a result of the cross–sectional narrowing in the aspect of the curved whisker.

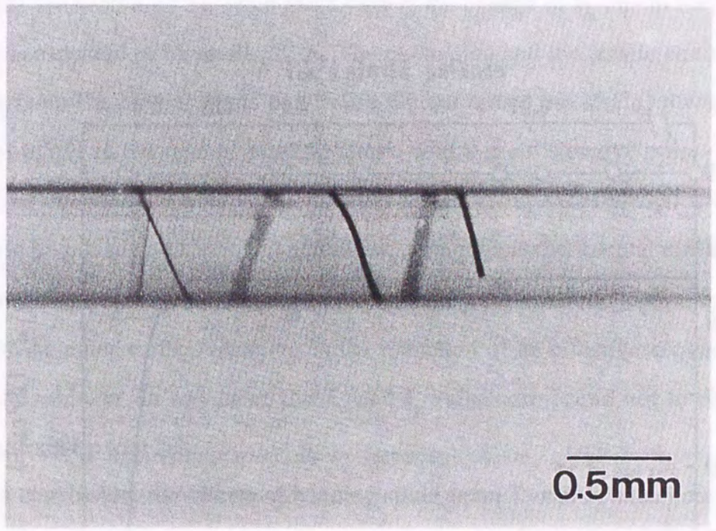

Fig. 2–25. A small coil made by winding the 2212 whisker onto a thin glass capillary.

The effect of bending upon T_c and J_c is shown in fig. 2–26. The T_c and J_c have been measured up to the R of 0.4 mm (bending strain 0.5% for 4 μm–thick whisker). The zero resistance temperature does not decrease and remains at a constant value (70 K). with decreasing the curvature to R=0.4 mm. The J_c value under the nonbending state is 6.7×10^4 A/cm^2 at 63 K in a zero magnetic field. For R≥1 mm (bending strain ≤ 0.2%), J_c surpasses 3.5×10^4 A/cm^2. For R=0.4 mm, however, it is lowered to 3.2×10^3 A/cm^2. The decreasing trend of J_c starts at 0.3–0.4% of the bending strain.

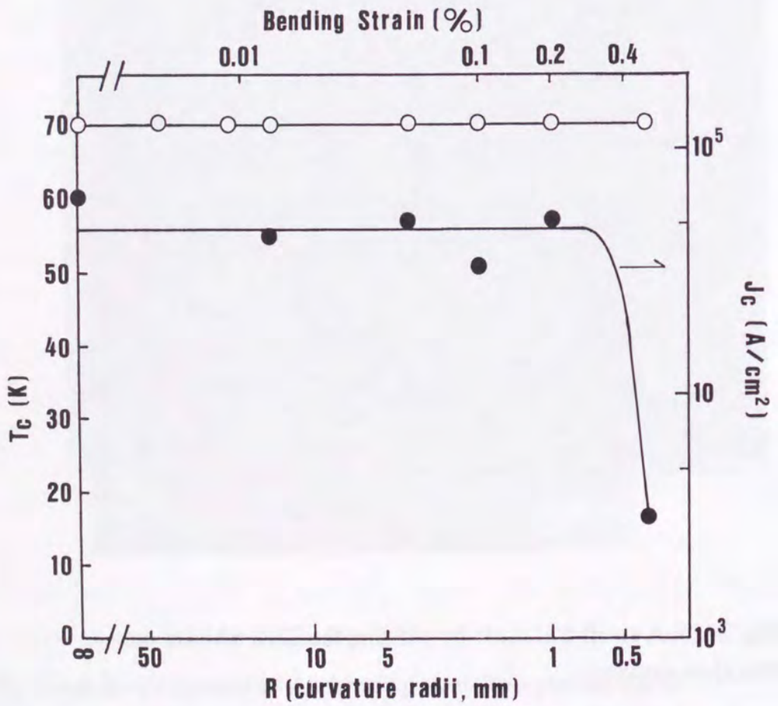

Fig. 2–26. The T_c (open circle) and J_c (closed circle) of the whiskers as a function of the radius of curvature (R). The J_c is measured at 63 K in a zero magnetic field. Bending strain is calculated for the thickness of 4 μm of the whisker.

For R=0.4 mm, although the central plane parallel to the curvature of the whisker does not receive the elongation strain, the inner plane receives about 0.5% of the compression stress along the direction of the *a*–axis. On the other hand, the outer plane receives the tensile strain, and there is a possibility that microcracks are present. The experimental results indicate that T_c does not increase or decrease under the bending strain applied here. The effect of hydrostatic pressure (P) on T_c of the 2212 compound has been reported to be $dT_c/d(-P) = -2$ K/GPa [51]. The bending strain of 0.5% corresponds to the pressure of ~100 MPa, assuming that the elastic modulus of the 2212 compound is 20–27 GPa ([52], see section 2–5). From these values, the change of T_c due to the bending strain of 0.5% is expected to be small, 0.2 K. The elongation and the tensile strain continuously increase from the central plane parallel to the curvature (no strain) toward the surface (strain of 0.5%) in the case of bending stress, which is a distinctive point compared with the case of uniaxial and hydrostatic stress. Therefore, our experimental results on T_c are thought to be not so surprising but acceptable within the experimental error. The decrease of J_c due to the bending strain could be explained by the possibility of microcracks introduced on the outer surface resulting in the reduction of an effective cross–sectional area across the whisker. In any case, the T_c and J_c values are found not to change under a bending strain up to 0.2%.

In conclusion, the effects of bending strain upon T_c and J_c have been studied using the Pb–doped 2212 whiskers. The whiskers can be elastically bent up to a bending strain of 0.5% without changing in T_c. This property is quite attractive for the twisting of wires in practical applications. The J_c value in a nonbending state (6.7×10^4 A/cm^2) is kept at the same level for the bending strain smaller than 0.2%.

2–5. Mechanical Properties

Oxide superconductors are generally evaluated by their critical temperature (T_c), critical current density (J_c), and critical field (H_c). It is preferred to have high values in these three parameters for practical applications. However, there is another important factor for practical usage of oxide superconductors. In some applications, superconducting wires are subjected to large mechanical stresses in making coils and Lorentz force due to high magnetic fields. Under the high stresses, a generation of small crack at the high current will cause a fatal damage or destruction of the coil. Therefore, the evaluation of mechanical properties of superconductors is an important work for the practical applications. Flexural strength [53], tensile strength [54, 55], microhardness [56], and elastic modulus [57–63] have been reported for Y–Ba–Ca–O compounds. On the other hand, there are few works on mechanical properties of Bi–based superconductors. Goto has reported a tensile strength of 55 MPa for the $Bi_2Sr_2Ca_2Cu_3O_x$ (2223) fiber prepared by Suspension Spinning method [64]. Johnson *et al.* have reported on a relationship between the bulk density and the bending strength of $Bi_2Sr_2CaCu_2O_x$ (2212) sintered bodies [65]. They have obtained the maximum value of 32 MPa when the sintering temperature is 910°C. Recently, Shoyama *et al.* have measured the tensile strength of the 2223 fiber prepared by the pyrolysis of organic acid salts and reported to be 18 MPa [66]. All of these data are obtained for polycrystalline compounds, so that grain boundaries, pours, and probably micro cracks in the samples could predominate these strength values.

This section describes the tensile strength and elastic modulus of 2212 whiskers of single crystals [67]. Almost all the whiskers are composed of several plate–like single crystals which are stacked in a layered structure. Transmittance electron microscopic (TEM) observation has revealed that they have no grain boundaries in the direction of whisker axis. Therefore, as long as tensile stress is applied in the direction of whisker axis, the strength may not be influenced by grain boundaries. Elastic modulus is calculated from the stress–strain curve and the cross sectional area of the whisker.

Experimental

Two kinds of whiskers were used for strength measurement. One is dopant–free 2212 (undoped) and the other is Li–doped 2212 (Li–doped) whiskers. The Li–doping is effective for improving T_c of the 2212 whiskers (chapter 5). Zero resistance temperatures ($T_{c,zero}$) of 77 K and 82 K are obtained for the undoped and Li–doped whiskers, respectively. These whiskers were prepared by annealing the melt–quenched glass plates at 830–865°C for several days, as described in section 2–2. The whiskers have the dimensions of 2–10 μm thick, 10–500 μm wide and ~20 mm long.

The tensile strength and elastic modulus of the whiskers were measured with a screw driven type autograph machine. One whisker with a length of several millimeters were fixed its both ends on MgO single crystals which were cramped and connected to a load cell (fig. 2–27). All tests were performed at room temperature with a crosshead speed of 0.1 mm/min. Tensile strength (σ) and elastic modulus (E) were calculated from a stress–strain curve as

$$\sigma = \frac{P_{max}}{S} \qquad (1)$$

$$E = \frac{P_{max} L}{S \Delta l} \qquad (2)$$

where P_{max} is the maximum fracture load, S whisker cross sectional area, L the sample length, Δl the elongation. The cross sectional area was determined from scanning electron microscopic (SEM) photograph for each whisker sample after the measurement.

Results and Discussion

Typical stress–strain curves and the corresponding fracture surfaces of the whisker are shown in fig. 2–28. One typical example (fig. 2–28 (a)) shows a load drop before the maximum fracture stress. Such the partial fracture could be attributed to the fracture of some layers composing the whisker. The SEM picture in fig. 2–28 (a) shows a step near the fracture surface, suggesting the two–step fracture. On the other hand, fig. 2–28 (b) shows another example in which the fracture occurs at once. A linear stress–strain relationship is observed before the maximum fracture load, indicating that the whisker has fractured at one instance. The latter case is adopted for evaluating the tensile strength and elastic modulus.

Figure 2–29 summarizes the results of the tensile strength for the undoped whiskers having various cross sectional areas. Although the observed tensile strengths are widely distributed from several tens of MPa to near 1000 MPa, It can be seen that the strength increases with decreasing in cross sectional area. The maximum tensile strength of 940 MPa is obtained for the whisker with smaller area. For the whiskers with larger area, both the maximum and average values decrease, and they are 300 MPa and 100 MPa, respectively (S=10^3 μm^2). The same tendency is observed common to the other whiskers [68]. Samples with a small cross sectional area have a large chance that no defects or cracks are contained. On the other hand, the probability of no defects decreases for the large area samples, if the defect density is supposed to be the same as in the small area samples. In the cross section containing the defect, stress concentration becomes so large at the defect that exceeds the maximum tensile stress leading to the fracture of the sample.

As described in the previous section (section 2–2), the whisker has a layered structure. The whiskers with a small cross sectional area are composed of fewer plate–like single crystals. In contrast, the whiskers with large cross sectional area are composed of many crystals. Therefore, smaller whisker is tend to be not influenced by defects, and

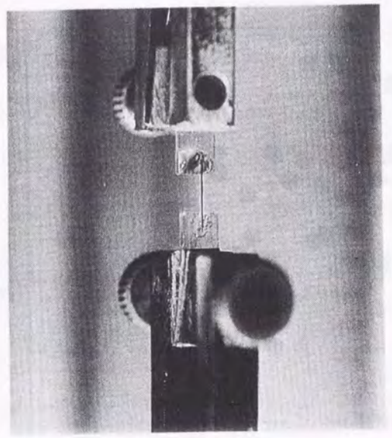

FIG. 2–27. Setting of a whisker sample for the tensile test.

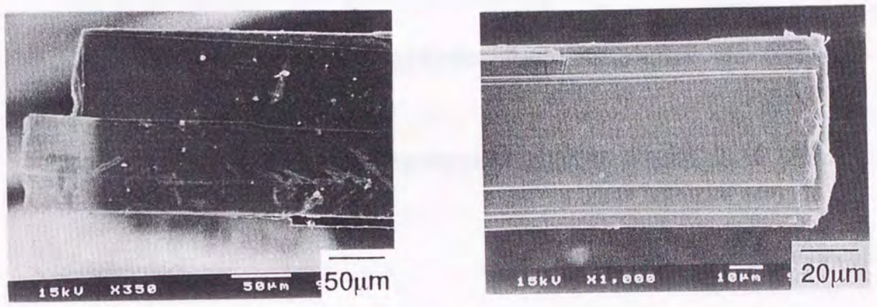

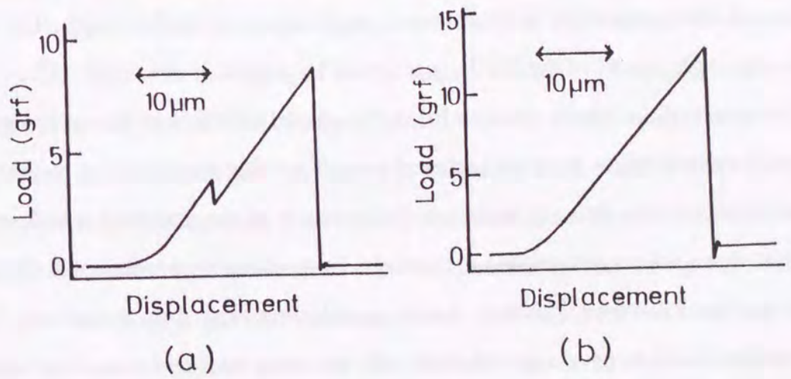

FIG. 2–28. Typical two kinds of stress–strain curves and SEM photographs at the fracture surface.

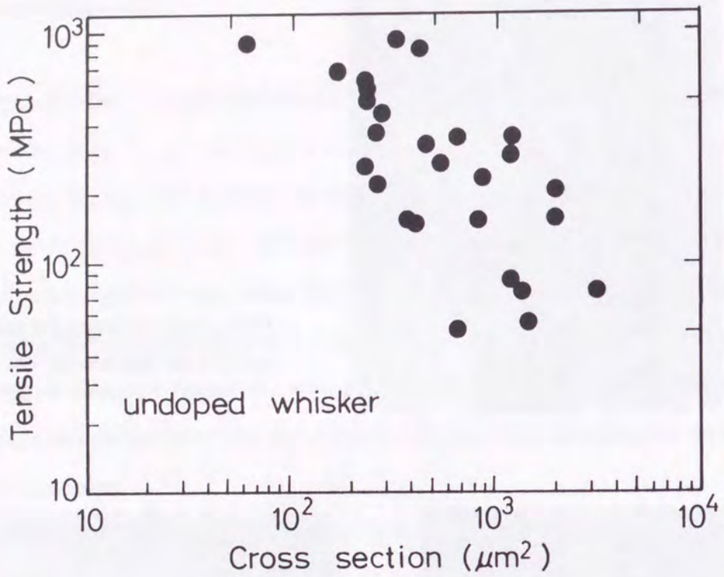

FIG. 2–29. Tensile strength of the undoped whiskers as a function of cross sectional area.

their strength being regarded to be or near to an intrinsic crystal strength. The tensile strength of a single crystal of the 2212 phase would be around or over 1000 MPa.

The result of the tensile strength for the Li–doped whiskers is shown in fig. 2–30. Although the distribution in cross sectional area is narrow compared with that of the undoped whiskers, the data reproduce well the result of the undoped whiskers. This means that there are no substantial differences in mechanical properties between the undoped and the Li–doped whiskers. As the samples are picked up at random, the Li–doped whisker looks to have a growth habit with the cross sectional area distributed in a narrower region than that of undoped whiskers.

The tensile strength and elastic modulus of the whiskers are summarized in table 2–2. The maximum tensile strength is 940 MPa which is about twenty times larger than

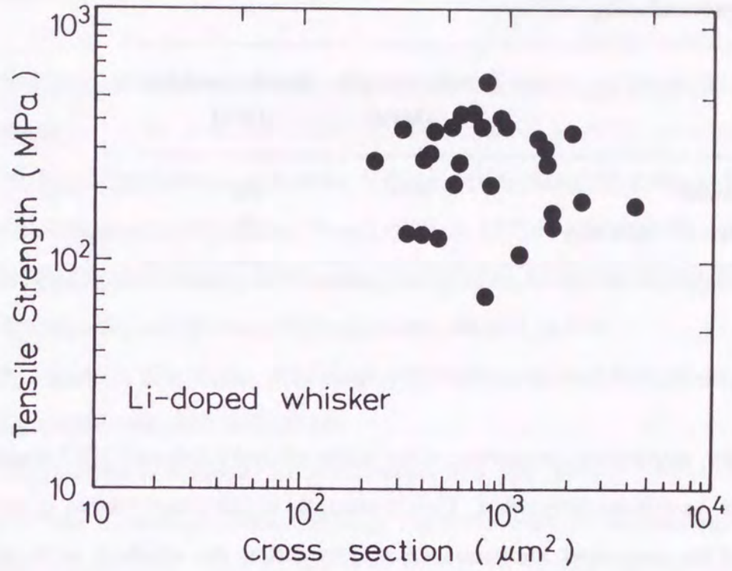

FIG. 2–30. Tensile strength of the Li–doped whiskers as a function cross sectional area.

that of the polycrystalline fibers previously reported [64]. The average tensile strength of 310 MPa is obtained for the undoped and Li–doped whiskers (53 samples). As the tensile strength of Ag or Cu metal is in a range of 200–250 MPa, the Bi–system superconductors are stronger than these metals unless grain boundaries are incorporated. Most of the oxide superconducting wires are made by Ag–sheath method. Present results indicate that the tensile strength of the Ag–sheathed wire is dependent on that of Ag wire without the oxide core. The average and the maximum elastic modulus are 27 GPa and 92 GPa, respectively. The maximum value of elastic modulus is comparable with that of Y–Ba–Cu–O compounds measured by acoustic, ultrasonic, and stress–strain methods [57–63]. In our preliminary experiment at liquid nitrogen temperature, the maximum and average strengths are almost the same as those at room temperature.

Table 2–2. Tensile strength and elastic modulus of the superconducting whiskers.

	Tensile strength (MPa)	Elastic modulus (GPa)
Maximum	940	92
Average (53samples)	310	27

In summary, mechanical properties of the undoped and Li–doped 2212 whiskers of single crystals have been determined. Tensile strength, which is assumed to be an intrinsic strength of the compound, has been measured by pulling the whiskers in the direction of *a*–axis corresponding to the whisker axis. There are no substantial differences in the mechanical properties between the undoped and the Li–doped whiskers. The maximum tensile strength and the elastic modulus determined from the stress–strain curve are 940 MPa and 92 GPa, respectively.

References

[1] H.Maeda, Y.Tanaka, M.Fukutomi, and T.Asano, Jpn.J.Appl.Phys., **27**, L209 (1988).

[2] J.Z.Liu, G.W.Grabtree, L.E.Rehn, V.Geiser, D.A.Young, W.K.Knok, P.M.Baldo, J.M.Williams, and D.J.Lam, Phys.Letters A, **127**, 444 (1988).

[3] S.Kishida, H.Tokutake, S.Nakanishi, H.Fujimoto, K.Nishimori, N.Ishihara, Y.Watanabe, and W.Futo, J.Cryst.Growth, **99**, 937 (1990).

[4] S.C.Gadkari, K.P.Muthe, K.D.Singh, S.C.Dabharwal, and M.K.Gupta, J.Cryst.Growth, **102**, 685 (1990).

[5] P.D.Han and D.A.Payne, J.Cryst.Growth, **104**, 201 (1990).

[6] P.D.Han, A.Asthana, Z.Xu, L.Chang, and D.A.Payne, J.Cryst.Growth, **104**, 201 (1990).

[7] T.F.Ciszik, and C.D.Evans, J.Cryst.Growth, **109**, 418 (1991).

[8] T.Fujii, Y.Nagano, and J.Shirafuji, J.Cryst.Growth, **110**, 994 (1991).

[9] L.F.Schneemeyer, R.V.van Dover, S.H.Clarum, S.A.Sunshine, R.M.Fleming, B.Batlogg, T.Siegrist, J.H.Marshall, J.V.Waszczak, and L.W.Rupp, Nature, **332**, 423 (1988).

[10] A.Katsui, Jpn.J.Appl.Phys., **27**, L844 (1988).

[11] T.Shishido, D.Shindo, K.Ukei, T.Sasaki, N.Toyota, and T.Fukuda, Jpn.J.Appl.Phys., **28**, L791 (1989).

[12] Y.Kubo, K.Michisita, Y.Higashida, M.Mizuno, H.Yokoyama, N.Shimizu, E.Inukai, N.Kuroda, and H.Yoshida, Jpn.J.Appl.Phys., **28**, L606 (1989).

[13] S.Takekawa, H.Nozaki, A.Umezono, K.Ksuda, and H.Kobayashi, J.Cryst.Growth, **92**, 687 (1988).

[14] I.Shigaki, K.Kitahama, K.Shibutani, S.Hayashi, R.Ogawa, Y.Kawate, T.Kawai, S.Kawai, M.Matsumoto, and J.Shirahuji, Jpn.J.Appl.Phys., **29**, L2013 (1990).

[15] D.B.Mitzi, L.W.Lombardo, A.Kapitulnik, S.S.Laderman, and R.D.Jacowitz, Phys.Rev.B, **41**, 6564 (1990).

[16] S.Pinol, J.Fontcuberta, and C.Miravitlles, J.Cryst.growth, **100**, 286 (1990).

[17] K.Shigematsu, H.Takei, I.Higashi, H.Hoshino, J.Takahara, and M.Aono, J.Cryst.Growth, **100**, 661 (1990).

[18] D.Gazit and R.S.Feigelson, J.Cryst.Growth **91**(1988)318.

[19] S.J.Guo, H.E.Easterling, S.X.Dou, and H.K.Liu, J.Cryst.Growth, **100**, 303 (1990).

[20] F.Uchikawa and J.D.Mackenzie, J.Mater.Res., **4**, 787 (1989).

[21] W.K.Ham, G.F.Holland, and A.M.Stacy, J.Am.Chem.Soc., **110**, 5214 (1988).

[22] T.Komatsu, K.Imai, R.Sato, K.Matsushita, and T.Yamashita, Jpn.J.Appl.Phys., **27**, L533 (1988).

[23] H.Zheng and J.D.Mackenzie, Phys.Rev.B, **38**, 7166 (1988).

[24] I.Matsubara, H.Kageyama, H.Tanigawa, T.Ogura, H.Yamashita, and T.Kawai, Jpn.J.Appl.Phys., **28**, L1121 (1989).

[25] I.Matsubara, H.Tanigawa, T.Ogura, H.Yamashita, M.Kinoshita, and T.Kawai, Jpn.J.Appl.Phys., **28**, L1358 (1989).

[26] I.Matsubara, H.Yamashita, and T.Kawai, J.Cryst.Growth, **128**, 719 (1993).

[27] R.Ota and N.Soga, Yogyo-Kyokai-Shi, **90**, 532 (1982).

[28] M.A.Subramanian, C.C.Toraradi, J.C.Calabresse, J.Gopalakrishnan, K.J.Morrissey, T.R.Askew, R.B.Flippen, U.Chowdhry, and A.W.Sleight, Science, **239**, 1015 (1988).

[29] H.Chen, D.J.Werder, S.H.Liou, H.S.Chen, and M.Hong, Phys.Rev.B, **37**, 9834 (1988).

[30] Y.Matsui, H.Maeda, Y.Tanaka, and S.Horiuchi, Jpn.J.Appl.Phys., **27**, L361 (1988).

[31] Y.Matsui, H.Maeda, Y.Tanaka, and S.Horiuchi, Jpn.J.Appl.Phys., **27**, L372 (1988).

[32] H.W.Zandergen, P.Groen, G.van Tendeloo, J.van Landuyt, and S.Amelinckx, Sodid State Commun., **66**, 397 (1988).

[33] T.M.Show, S.A.Shivashanker, S.J.LaPlaca, J.J.Cuomo, T.M.McGuire,R.A.Roy, K.H.Kelleher, and D.S.Yee, Phys.Rev.B, **37**, 9856 (1988).

[34] H.W.Zandergen, P.Groen, F.C.Mijlhoff, G.van Tendeloo, and S.Amelinckx, Physica C, **156**, 325 (1988).

[35] A.Yamamoto, M.Onoda, E.Takayama-Muromachi, F.Izumi, T.Ishigaki, and H.Asano, Phys.Rev.B, **42**, 4228 (1990).

[36] D.Kirillov, I.Bozovic, T.H.Geballe, A.Kapitulnik, and D.B.Mitzi, Phys.Rev.B, **38**, 11955 (1988).

[37] J.Saptiel, L.Pierre, D.Morin, J.C.Toledano, J.Schneck, H.Savary, J.Chavignon, J.Primot, C.Daguet, and J.Etrillard, Phys.Rev.B, **39**, 339 (1989).

[38] S.Martinez, A.Zwick, and M.A.Renucci, H.Noel, and M.Potel, Physica C, **200**, 307 (1992).

[39] J.Jung, J.P.Franck, S.C.Cheng, and S.S.Sheinin, Jpn.J.Appl.Phys., **28**, L1182 (1989).

[40] B.Hong and T.O.Mason, J.Am.Ceram.Soc., **74**, 1045 (1991).

[41] Y.Abe, K.Hirata, H.Hosono, and Y.Kubo, J.Mater.Res., **7**, 1599 (1992).

[42] R.S.Wagner and W.C.Ellis, Appl.Phys.Lett., **4**, 89 (1964).

[43] J.D.Eshelby, Phys.Rev., **91**, 755 (1953).

[44] F.C.Frank, Phil.Mag., **2**, 857 (1953).

[45] S.E.Koonce and S.M.Arnold, J.Appl.Phys., **24**, 365 (1953).

[46] B.Auriviellius, Arkiv.Kemi., **1**, 499 (1949).

[47] T.G.Holesinger, D.J.Miller, L.S.Chumbley, J.Mater.Res., **7**, 1658 (1992).

[48] J.M.Tarascon, Y.Le Page, P.Barboux, B.G.Bagley, L.H.Greence, W.R.MacKinnon, G.W.Hull, M.Giroud, and D.M.Hwang, Phys.Rev.B, **37**, 9382 (1988).

[49] H.Takei, M.Koike, H.Takeya, K.Suzuki, and M.Ichihara, Jpn.J.Appl.Phys., **28**, L1193 (1989).

[50] K.Shigematsu, H.Takei, I.Higashi, K.Hoshino, H.Takehara, and M.Aono, J.Cryst.Growth, **100**, 661 (1990).

[51] R.Kubiak, K.Westerholt, G.Pelka, and H.Bach, Physica C, **166**, 523 (1990).

[52] T.M.Tritt, M.Marone, X.F.Chen, M.J.Skove, G.X.Tessema, D.J.Gillespie, A.C.Ehrlich, J.P.Franck, and J.Jung, Physica C, **178**, 296 (1991).

[53] G.W.Crabtree, J.W.Downey, B.K.Flandermeyer, J.D.Jorgensen, T.E.Klippert, D.S.Kupperman, W.K.Kwok, D.J.Lam, A.W.Mitchell, A.G.McKale, M.V.Nevitt, L.J.Nowicki, A.P.Paulikas, R.B.Poeppel, S.J.Rothman, J.L.Routbort, J.P.Singh, C.H.Sowers, A.Umezawa, B.W.Veal, and J.E.Baker, Advanced Ceramic Materials, **2**, 444 (1987).

[54] T.Goto and M.Tsujihara, J.Mater.Sci.Lett., **7**, 283 (1988).

[55] H.Konishi, T.Takamura, H.Kaga, and K.Katsuse, Jpn.J.Appl.Phys., **28**, L241 (1989).

[56] M.K.Ihm, B.R.Powell, and R.L.Bloink, J.Mater.Sci., **25**, 1664 (1990).

[57] K.N.R.Taylor, G.L.Russell, B.Hunter, D.N.Matthews, A.Bailey, and J.Dunlop, J.Cryst.Growth, **85**, 656 (1987).

[58] R.E.Loehman, W.F.Hammetter, E.L.Venturini, R.H.Moore, and F.P.Gerstle Jr., J.Am.Ceram.Soc., **72**, 669 (1989).

[59] S.E.Dorris, M.T.Lanagan, D.M.Moffatt, H.J.Leu, C.A.Youngdahl, U.Balachandran, A.Cazzato, D.E.Bloomberg, and K.C.Goretta, Jpn.J.Appl.Phys., **28**, L1415 (1989).

[60] S.Block, G.L.Piermarini, R.G.Munro, and W.Wong-Ng, Advanced Ceramic Materials, **2**, 601 (1987).

[61] R.Round and B.Bridge, J.Mater.Sci.Lett., **6**, 1471 (1987).

[62] J.E.Blendell, C.K.Chiang, D.C.Cranmer, S.W.Freiman, E.F.Fuller,Jr., E.Drescher-Krasicka, W.L.Johnson, H.M.Ledbetter, L.H.Bennet, L.J.Swartzendruber, R.B.Marinenko, R.L.Myklebust, D.S.Bright, and D.E.Newbury, Advanced Ceramic Materials, **2**, 512 (1987).

[63] H.M.Ledbetter, M.W.Austin, S.A.Kim, and M.Lei, J.Mater.Res., **2**, 786 (1987).

[64] T.Goto, Jpn.J.Appl.Phys., **28**, L1402 (1989).

[65] D.W.Johnson Jr., and W.W.Rhodes, J.Am.Ceram.Soc., **72**, 2346 (1989).

[66] M.Shoyama, H.Nasu, and K.Kamiya, Jpn.J.Appl.Phys., **30**, 950 (1991).

[67] I.Matsubara, Y.Hashimoto, K.Atago, H.Yamashita, M.Kinoshita, and T.Kawai, Jpn.J.Appl.Phys., **31**, L14 (1992).

[68] *Whisker technology*, ed. A.P.Levitt, (Wiley-Interscience, New York, 1970) p. 159.

Chapter 3

Preparation and properties of $Bi_2Sr_2CuO_x$ Whiskers

Introduction

In the studies on crystallization from a glassy state in the Bi–system, we have found that flexible superconducting whiskers grow from the surface of a melt–quenched glass plate after annealing in a stream of O_2 gas (chapter 2). The whiskers are composed of several $Bi_2Sr_2CaCu_2O_x$ (2212 phase) plate–like single crystals which are stacked in a layered structure. The whiskers contain a small amount (<1%) of $Bi_2Sr_2Ca_2Cu_3O_x$ (2223) phase. In order to examine the possibility of the growth of the 2223 or $Bi_2Sr_2CuO_x$ (2201) whiskers by the same method, the composition of the glass precursor and annealing temperature have been changed. This chapter describes the influence of the composition of the glass precursor and annealing temperature on the growth of whiskers and resulting phase. The initial composition is widely changed in the Bi–Pb–Sr–Ca–Cu–O system. Heating temperature is changed from 810°C to 860°C. The 2201 whiskers grow at the lower annealing temperature (810–820°C), and the 2212 whiskers grow at the higher temperature (820–860°C). However, no whiskers of the 2223 single phase are obtained in the present results [1].

Experimental

The initial composition was changed in a triangular diagram, where $Bi_2Sr_2CuO_x$+CuO, $CaCuO_x$, and PbO are located at the vertices. Powders of Bi_2O_3, $SrCO_3$, $CaCO_3$, CuO, and PbO were mixed, and the mixture of 15g was melted in an alumina crucible at 1200°C for 30 min in air. The quenched specimens were obtained by pouring the melts on a copper plate and pressing with another copper plate. The cooling

rate is estimated to be 10^3 ks^{-1} in this method [2]. The quenched samples were placed in an alumina boat and heated in a stream of O_2 gas for 120 h. Annealing temperature was changed from 810 to 860°C. After annealing, the samples were cooled to room temperature in the furnace.

The growing phase was determined using a RIGAKU X–ray diffractometer equipped with a Cu–Kα tube and the morphology of crystals was observed with a Hitachi scanning electron microscope (SEM) model S–2400. Differential thermal analysis (DTA) was on a RIGAKU TAS100 equipment between a room temperature and 1000°C in a stream of O_2/Ar=1/4 gas with a heating rate of 10 K/min. The temperature dependence of the electrical resistance was measured by a standard four–probe method.

Results and discussion

Thirty five melt–quenched glass samples with different initial compositions, as indicated on the triangular diagram, have been prepared (fig. 3–1). The glass forming region of the $Bi_2Sr_2CuO_x$+CuO–$CaCuO_x$–PbO system is shown in fig. 3–1. In the $CaCuO_x$–rich and Bi–poor region (closed circles), the crystalline phases of CaO and Ca_2CuO_3 are observed in the X–ray diffraction pattern. Zheng *et al.* have reported that the glass forming condition is restricted in the range of 20 mol% < $BiO_{1.5}$, CuO, $Ca_{0.5}Sr_{0.5}O$ < 50 mol% for the Bi–Sr–Ca–Cu–O system [3]. It can be seen from the fig. 3–1 that the glass forming region becomes larger for the Bi–Pb–Sr–Ca–Cu–O system, 10 mol% < $BiO_{1.5}$+Pb, CuO, CaO+SrO < 50 mol%. The addition of Pb is effective in increasing the glass forming region.

The whisker growing region at the annealing temperature from 860°C to 840°C is shown in figs. 3–2 – 3–4. When the glass sample is annealed at 860°C, the whiskers are grown at the Pb–poor area (fig. 3–2). The specimens in the Pb–rich region are melted at this temperature, so that whiskers do not grow. The whisker growing region spreads out

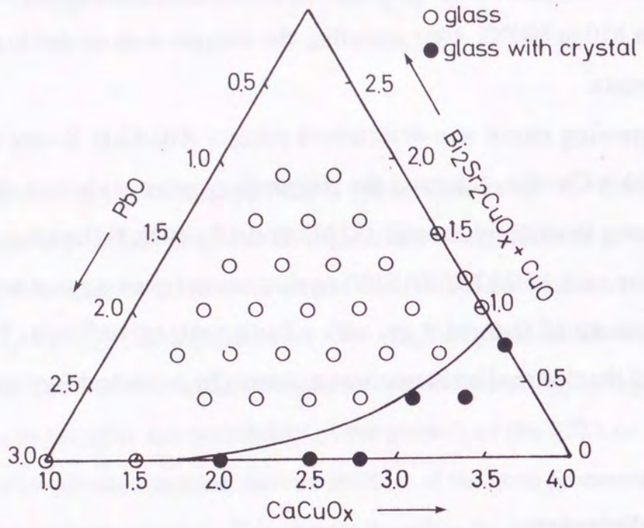

FIG. 3–1. The glass–forming range of $Bi_2Sr_2CaO_x$+CuO–$CaCuO_x$ –PbO system: (○) glass; (●) partially crystallized glass.

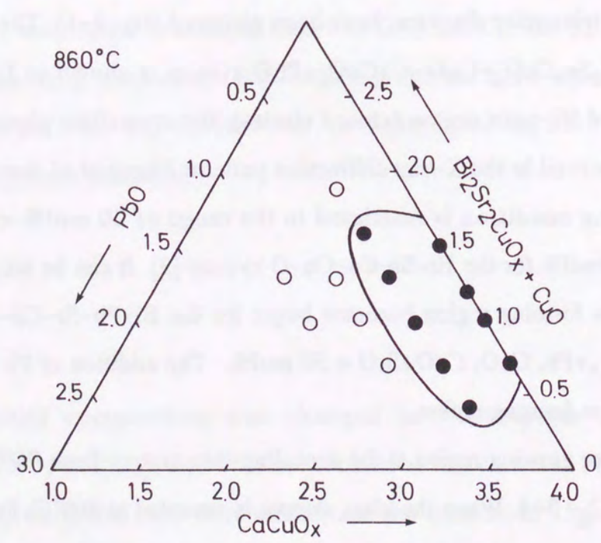

FIG. 3–2. The whisker growing region at 860°C for 120 h: (●) whiskers; (○) no whiskers.

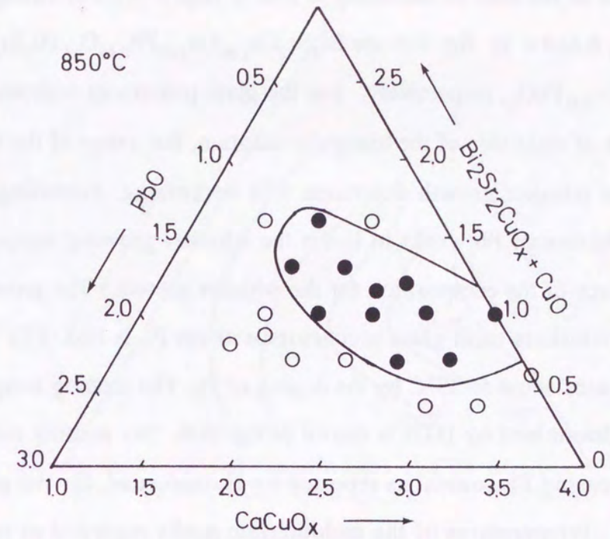

FIG. 3–3. The whisker growing region at 850°C for 120 h: (●) whiskers; (○) no whiskers.

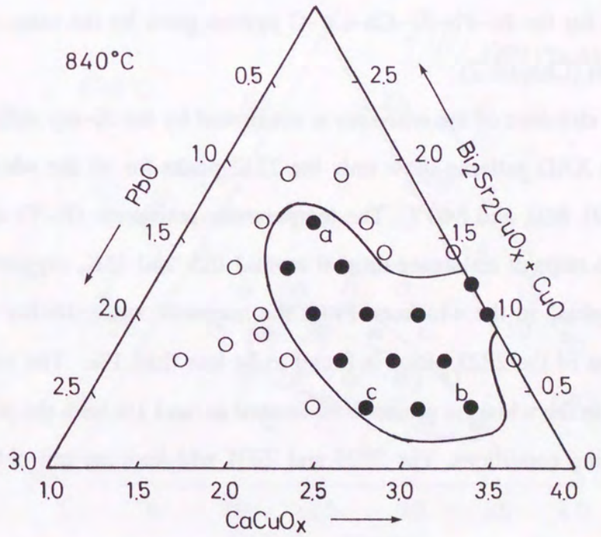

FIG. 3–4. The whisker growing region at 840°C for 120 h: (●) whiskers; (○) no whiskers.

toward the Pb–rich side at 850°C (fig. 3–3). The whiskers grow for the widest range of initial composition in the case of annealing at 840°C (fig. 3–4). For example, the initial compositions at a, b and c in fig. 3–4 are $Bi_2Sr_2Ca_{1.06}Cu_{3.06}Pb_{0.44}O_x$, $Bi_2Sr_2Ca_8Cu_{10}PbO_x$ and $Bi_2Sr_2Ca_{5.76}Cu_{7.76}PbO_x$, respectively. For the glass precursors without Pb which are located on the line of right side of the triangular diagram, the range of the initial composition suitable for whisker growth decreases with decreasing annealing temperature. Therefore, the addition of Pb works to lower the whisker growing temperature and to spread the allowance of the composition for the whisker growth. The growing temperature of the 2212 whiskers from glass precursors without Pb is 865–875°C, so that the temperature decreases about 5–35°C by the doping of Pb. The melting temperature of the glass precursors determined by DTA is shown in fig. 3–5. The melting temperature decreases with increasing Pb content as reported by Hatano *et al.* for the polycrystalline bulk samples [4]. Temperatures of the endothermic peaks regarded as partial melting decrease in the same manner as that of the melting temperature. The growing temperature of the 2212 whiskers corresponds to the partial melting temperature region. Therefore, the 2212 whiskers for the Bi–Pb–Sr–Ca–Cu–O system grow by the same mechanism as the undoped system (Chapter 2).

The crystal structure of the whiskers is confirmed by the X–ray diffraction (XRD) measurement. The XRD patterns show only the 2212 peaks for all the whiskers obtained by annealing at 860, 850, and 840°C. The temperature–resistance (R–T) curves of these whiskers show two steps of resistance drop at around 105 and 75K, suggesting the existence of the 2223 phase in the whiskers. From the magnetic susceptibility measurement, the volume fraction of the 2223 phase is found to be less than 1%. The volume fraction of the 2223 phase in the whiskers seems to be limited around 1% with the present compositions and annealing conditions. The 2223 and 2201 whiskers are not obtained in these conditions.

Figure 3–6 shows the whisker growing region at 820°C. The region is reduced and shifted to the Pb–rich area as compared with the case at higher temperatures. The whisk

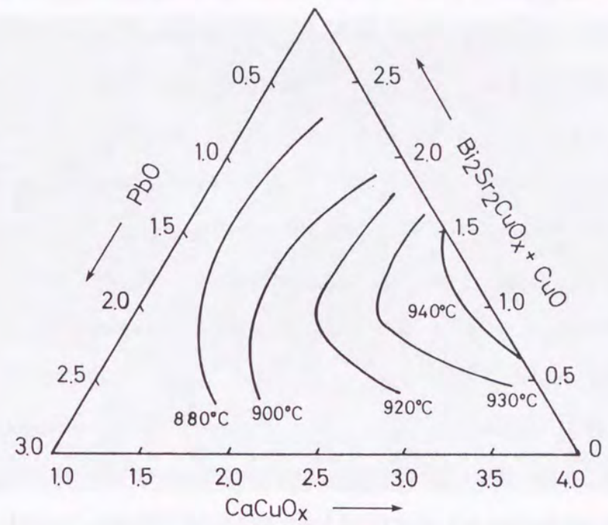

FIG. 3–5. Isotherms of melting temperature determined by DTA.

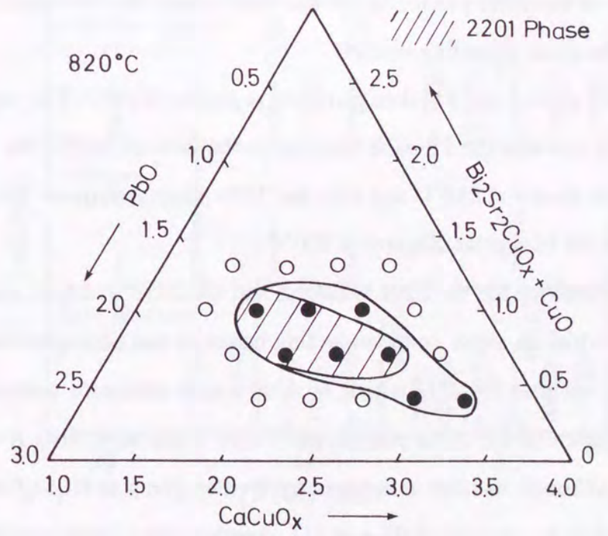

FIG. 3–6. The whisker growing region at 820°C for 120 h: (●) whiskers; (○) no whiskers.

ers are not grown from the glass precursors without Pb. The whiskers grown at 820°C exhibit two interesting points. One is related to the growing phase. Two kinds of whiskers having the 2201 and 2212 structures have been obtained separately in the different growing region. The 2201 whiskers grow in the obliquely lined area in fig. 3–6, and the 2212 ones grow from the region located in the $CaCuO_x$–rich side of the 2201 region. The 2212 structure appears in the $CaCuO_x$ –rich side because it has one more Ca and CuO_2 layers than the 2201 structure. In this way, the growing phase of whiskers can be controlled by the initial composition. The glass annealing method is similar to solid state reaction in that the 2201 phase is dominant at the lower annealing temperatures and the 2212 phase is at the higher temperatures and in the $CaCuO_x$–rich area. Another interesting point is related to the shape of the growing crystals. In the growth region of the 2201 whiskers at 820°C, scale–like crystals with the dimensions of several hundred μm in area and a few μm in thickness are observed together with fibrous crystals (whiskers) as shown in fig. 3–7. Figure 3–8 shows the XRD patterns of the scale–like and fibrous crystals compared with the 2212 whiskers. Both the scale–like and fibrous crystals show the diffraction peaks of the 2201 phase. As for the 2201 phase, the two types of the crystals are obtained by the glass annealing method.

Figure 3–9 shows the whisker growing region at 810°C. The region becomes smaller and shifts towards the Pb–rich area. As in the case of 820°C, the scale–like and fibrous crystals are grown at 810°C and only the 2201 phase is formed. No whiskers have been observed on the triangular diagram at 800°C.

The R–T behavior for the 2201 whiskers and the 2212 whiskers are shown in fig. 3–10. The 2201 whiskers show semiconducting behavior and no superconducting transition above 4.2 K, whereas the 2212 whiskers show a zero resistance temperature at 70 K. There are two phases in the 2201 compound. One is the so–called R–phase with T_c around 7 K [5]. Although its ideal stoichiometry is often given as $Bi_2Sr_2CuO_x$, in practice it is usually found to be somewhat Bi–rich [6]. Another phase, with stoichiometry much closer to $Bi_2Sr_2CuO_x$, exist but is not superconducting [6]. The two phases are distin–

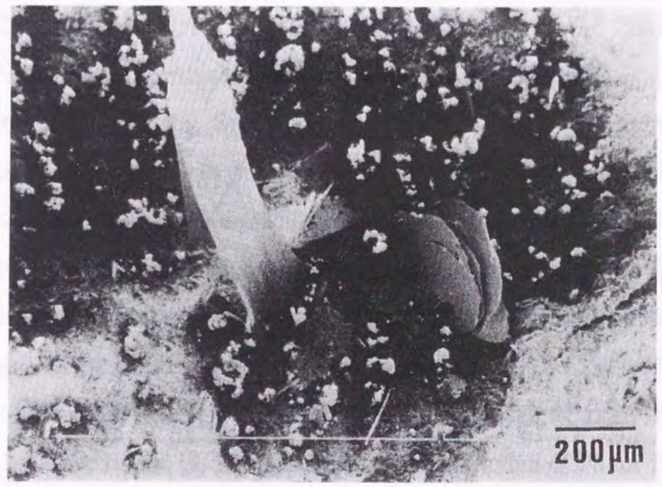

FIG. 3–7. Scanning electron micrograph of scale–like and fibrous crystals grown from the 2201 region at 820°C.

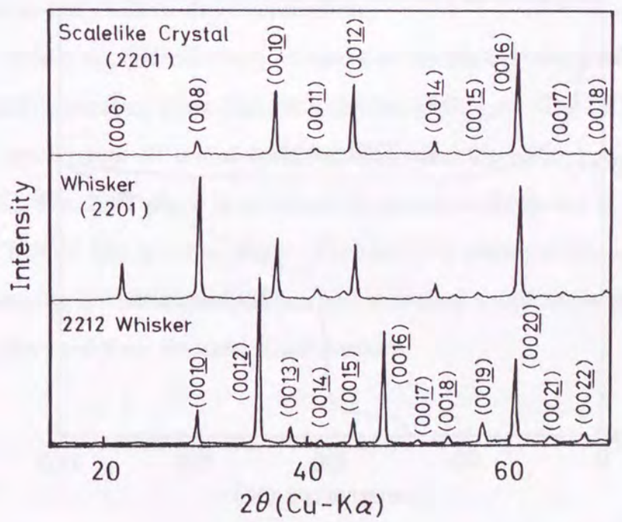

FIG. 3–8. X–ray diffraction patterns of the scale–like and fibrous crystals grown at 820°C compared with the 2212 whiskers.

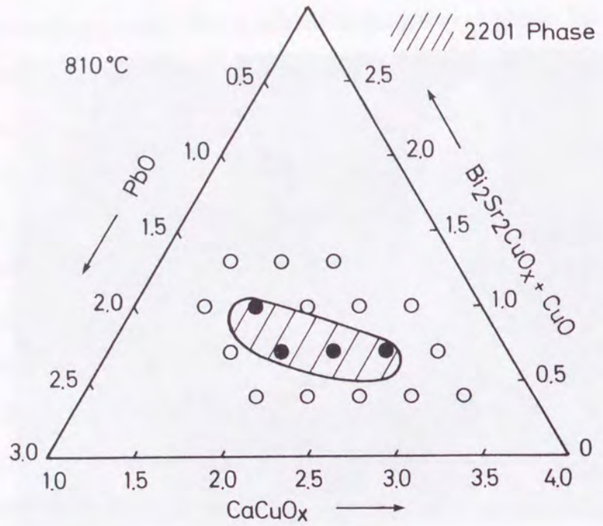

FIG. 3–9. The whisker growing region at 810°C for 120h: (●) whiskers; (○) no whiskers.

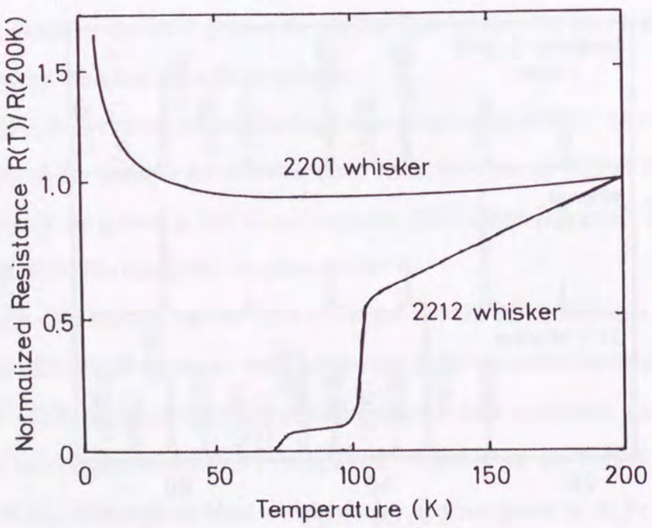

FIG. 3–10. Temperature dependence of the normalized resistance for the 2201 whisker and the 2212 whiskers.

guished by the *c*–axis of lattice parameter. The R–phase has a *c*–axis of lattice parameter of 24.6–24.8 Å, whereas the compound with stoichiometry much closer to $Bi_2Sr_2CuO_x$ has that of 23.4–23.6 Å [7]. As the *c*–axis lattice parameter of the 2201 whiskers obtained here is 24.5 Å, the whiskers are the R–phase. The R–phase is a solid solution phase of general formula $Bi_{2+x}Sr_{2-x}CuO_y$. Sinclair *et al.* have reported that the *c*–axis lattice parameter decreases with increasing x in the formula [8]. The 2201 whiskers are estimated to have x=0.3 – 0.4 from their result. Although the R–phase is a superconducting phase, the 2201 whiskers show no superconducting transition in the R–T curve. Assuming that the nonstoichiometry of oxygen is invariable for elemental substitution, the substitution of Bi for Sr reduces the hole concentration. The 2201 whiskers contain Pb, which is detected by energy dispersive X–ray spectroscopic analysis. It is thought that Pb occupy at the Bi site [9, 10]. Therefore, the substitution of Pb for Bi increases the hole concentration assuming that Pb become a divalent cation in this material. In this way, as for the cation substitution there are two competitive factors in the 2201 whiskers. The results of the resistivity measurement imply that the 2201 whiskers have a less hole concentration than that to show superconductivity.

In conclusion, superconducting whiskers of the Bi–system have been grown by annealing a melt–quenched glass plate in a stream of O_2 gas. The 2212 whiskers are grown from a wide range of initial compositions when the melt–quenched plates are heated at 840°C. The 2201 phase is dominant in the whiskers grown at lower temperatures, 820 and 810°C. The growing phase (2212 or 2201 phase) of the whiskers is controllable by changing the initial composition and annealing temperature, whereas the pure 2223 whiskers have not been obtained in this method.

References

[1] I.Matsubara, T. Ogura, H.Tanigawa, H.Yamashita, M.Kinoshita, and T.Kawai, J.Cryst.Growth, **110**, 973 (1991).

[2] R.Ota and N.Soga, Yogyo-Kyokai-Shi, **90**, 532 (1982).

[3] H.Zheng, R.Xu and J.D.Mackenzie, J.Mater.Res., **4**, 911 (1989).

[4] T.Hatano, K.Aota, S.Ikeda, K.Nakamura, and K.Ogawa, Jpn.J.Appl.Phys., **27**, L2055 (1988).

[5] C.Michel, M.Hervieu, M.M.Borel, A.Grandin, F.Deslandes, J.Provost, and B.Raveau, Z.Phys. B **68**, 421 (1987).

[6] J.A.Saggio, K.Sujata, J.Hahn, S.J.Hwu, K.R.Poeppelmeier, and T.O.Mason, J.Am.Ceram.Soc., **72**, 849 (1989).

[7] R.S.Roth, C.J.Rawn, and L.A.Bendersky, J.Mater.Res., **5**, 46 (1990).

[8] D.C.Sinclair, J.T.Irvine, and A.R.West, Jpn.J.Appl.Phys., **29**, L2002 (1990).

[9] Y.Takemura, M.Hongo, and S.Yamazaki, Jpn.J.Appl.Phys., **28**, L916 (1989).

[10] A.Maeda, Y.Kato, T.Shibauchi, Y.Nakajima, H.Watanabe, and K.Uchinokura, Jpn.J.Appl.Phys., **28**, L1549 (1989).

Chapter 4

Preparation and Properties of $Bi_2Sr_2Ca_2Cu_3O_x$ Whiskers

4-1. Introduction

For the Bi-Sr-Ca-Cu-O system, three types of superconducting phase are known: $Bi_2Sr_2CuO_x$ (2201) [1, 2], $Bi_2Sr_2CaCu_2O_x$ (2212) [3, 4], and $Bi_2Sr_2Ca_2Cu_3O_x$ (2223) [3, 4] with superconducting transition temperatures (T_c) around <20 K, 80 K and 110 K, respectively. Of these phases, the 2223 compound has attracted much attention in the field of superconductivity research because of its high-T_c over 100 K with non-toxic combination of the elements compared with the Tl-system. However, it is relatively harder to prepare the single 2223 compound in bulk form as compared to the single 2201 and 2212 compounds. There are a number of constraints in fabricating the single 2223 phase. Several starting compositions have been attempted to prepare the single 2223 phase material, leading to multiphase compound in general. The heating condition and environment have been found to play an important role for the growth of the 2223 phase. Annealing of the Bi-Sr-Ca-Cu-O material near its melting temperature for a long duration is necessary for growing a substantial amount of the 2223 phase [5, 6]. Sintering under a low oxygen partial pressure has been found to enhance the formation of the 2223 phase [7]. It has also been shown that the addition of extra Ca and Cu to the ideal 2223 composition is effective [8]. The partial substitution of Bi by Pb has been found to favor the development of the 2223 phase [9, 10]. The addition of Pb lowers the melting temperature of the composition and helps the diffusion of constituents for the growth of the 2223 phase. In this way, the strictly controlled initial composition and the heating conditions are necessary for preparing the 2223 compound even in a polycrystalline bulk form, so that much more difficult for single crystals.

The crystal growth of the 2201 phase and the 2212 phase has been studied by the self-flux method [11-14], the alkali-halides flux method [15, 16], the floating zone

method [17], the laser pedestal method [18,19], and the traveling solvent floating zone (TSFZ) method [20]. On the other hand, large crystals of the 2223 phase have not been previously obtained in spite of their great importance in determining the physical properties and in revealing the fundamental properties of this phase. Although the detail of phase relation is not clear in the Bi-system, Shigematsu *et al.* have claimed that the 2223 phase does not neighbor with a liquid phase in the pseudo-binary system between $Bi_2(Sr,Ca)O_4$ and $(Sr,Ca)CuO_2$ [21]. On the other hand, Komatsu *et al.* have reported the pseudo-binary phase diagram of $Bi_2(Sr,Ca)_{n+1}Cu_nO_x$ where the 2223 phase coexists with a liquid phase [22]. However, they have not obtained pure 2223 single crystals. Therefore, the 2223 single crystals are hardly grown from a liquid phase, indicating that the growth methods used for the 2201 or 2212 phase are not applicable to the growth of the 2223 single crystals. We have developed a new method to prepare the 2223 crystals, that is, conversion by annealing in powder (CAP) method [23, 24].

In this chapter, the detail of the preparation method and properties of the 2223 whiskers are described. The 2223 whiskers are obtained by annealing the 2212 whiskers in a Ca- and Cu-rich Bi-Sr-Ca-Cu-Pb-O calcined powder (CAP method). This CAP method provides the 2223 whiskers with the dimensions of 1-5 μm thick, 10-300 μm wide, and ~4 mm long. The CAP method is also applied to 2212 sheet crystals grown by the self-flux method, resulting 2223 sheet crystals as large as 1 mm^2 in area while retaining the outline of the form in the original crystals. The study of the 2223 phase is one of the undeveloped fields in the oxide superconductors because of the lack of high quality single crystals large enough to measure the physical properties. To date, most of the basic superconducting parameters such as upper critical field (H_{c2}), lower critical field (H_{c1}), coherence length, and penetration depth have been measured using a polycrystalline material. The CAP-treated 2223 whiskers are thought to be useful for measuring these parameters in further details. The magnetic field dependence of the critical current density (J_c) and the anisotropy of H_{c2} are also described in this chapter.

4-2. Preparation and Characterization

This section describes the preparation method and characterization of $Bi_2Sr_2Ca_2Cu_3O_x$ (2223) superconducting whiskers. A new method has been developed for preparing the 2223 whiskers. The 2223 whiskers have been prepared by annealing $Bi_2Sr_2CaCu_2O_x$ (2212) whiskers in a $Bi_2Sr_2Ca_4Cu_6Pb_{0.5}O_x$ calcined powder (Conversion by Annealing in Powder method: CAP method). The completeness of the phase conversion has been confirmed by X-ray diffraction, compositional analysis, susceptibility measurement, and a high resolution electron microscope observations. The outline of the form in the original samples is retained even after the CAP treatment. The CAP method has been also applied to single crystal sheets of the 2212 phase. The 2212 single crystal sheets have been converted to the 2223 phase, resulting in 2223 sheet crystals as large as approximately 1 mm^2. The 2223 whiskers and crystals obtained here are of great importance for obtaining basic information on the physical properties of the 2223 phase.

Experimental

The starting materials of the 2212 whiskers were prepared by the method described in chapter 2. Schematic representation of the CAP treatment is shown in fig. 4-1. The 2212 whiskers were embedded into a calcined powder with the composition of $Bi_2Sr_2Ca_4Cu_6Pb_{0.5}O_x$ which had previously been calcined at 780°C for 20 h and 820°C for 20 h with an intermediate grinding. In preparing polycrystalline sample, the addition of a small amount of Pb has been reported to enhance the growth of the 2223 phase by promoting the nucleation of 2223 phase and by increasing the diffusivity of Ca and Cu [9, 10, 25]. A small amount of Pb was added to the calcined powder to take advantage of these properties. The powder containing the whiskers was set between two sintered pellets with the same composition as that of the calcined powder to prevent the reaction of

the calcined powder with an alumina boat (fig. 4–1). After annealing at 830–860°C for 150 h in air, the whiskers were removed mechanically from the powder.

The detailed procedure of the CAP method is shown in fig. 4–2. The $Bi_2Sr_2Ca_4Cu_6Pb_{0.5}O_x$ calcined powder was spread on a sintered pellet in a layer of 2–3 mm thick with the surface as flat as possible. Then, the 2212 whiskers were placed on the surface making sure they did not overlap each other. The whiskers were covered with another layer of the calcined powder. Finally, a sintered pellet was put on the top. After annealing, the sample was divided into two pieces along the whisker containing layer. The whiskers were carefully recovered from the powder by picking them up under a microscope. The layer structure enables us to recover the whiskers easily. If the whiskers and the powder are randomly mixed, the whiskers are hardly recovered from the calcined powder without any damage.

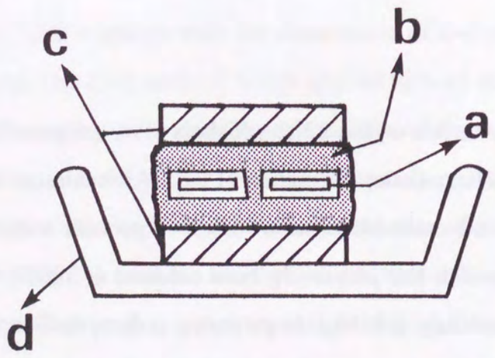

FIG. 4–1. Schematic representation of the CAP treatment. a: whiskers, b: calcined powder, c: sintered pellet, d: alumina boat.

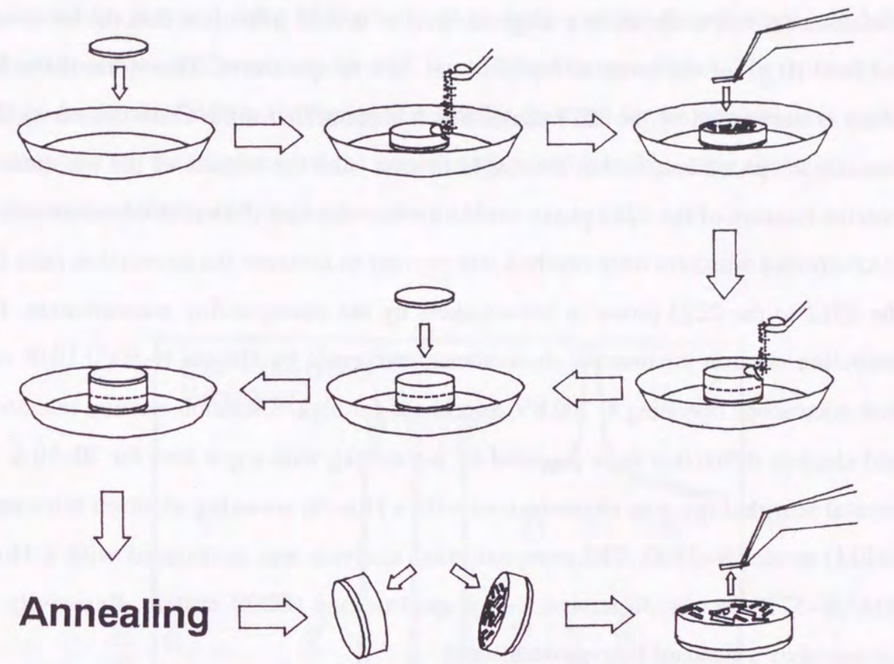

FIG. 4–2. Procedure of the CAP treatment.

Characterization of the CAP-treated whiskers was made by X-ray diffraction, compositional analysis, susceptibility measurement, and a high resolution electron microscope observations. X-ray diffraction measurement was made using a RIGAKU diffactometer with Cu-Kα radiation. The susceptibility was measured with a superconducting quantum interference device (SQUID: Quantum Design $MPMS_2$) magnetometer. This measurement was made under a magnetic field of several gauss less than the lower critical field (H_{c1}) of the samples especially at low temperatures. Therefore, if the 2212 phase is surrounded by the 2223 phase, which is plausible for the CAP-treated whiskers because the phase conversion is thought to start from the surface of the whiskers, the volume fraction of the 2223 phase could be overestimated. To avoid this situation, the CAP-treated whiskers were crushed into powder to measure the conversion ratio from the 2212 to the 2223 phase in the whiskers by the susceptibility measurement. High resolution electron microscope observations were made by Hitachi H-9000 UHR electron microscope operating at 300 kV. Specimens for high-resolution electron microscopy and electron diffraction were prepared by ion milling with argon ions for 30-50 h. The crystal morphology was characterized with a Hitachi scanning electron microscope (SEM) model S-2400. The compositional analysis was performed with a Horiba EMAX-5770 energy dispersive X-ray spectroscopy (EDX) system. Resistivity was measured by a standard four-prove method.

Results and discussion

X-ray diffraction (XRD) pattern of the well-grown surface of the whiskers CAP-treated at 855°C is shown in fig. 4-3, with that of the original 2212 whiskers for comparison. For the CAP-treated whiskers, several peaks corresponding to the (00*l*) indices of the 2223 phase are observed, although their intensity is somewhat smaller than that of the 2212 whiskers. The orientation of the *c*-axis is kept even after the CAP treatment. All

the lines observed in the CAP-treated samples can be assigned to those of the 2223 phase, indicating that the 2212 whisker was thoroughly converted to the 2223 phase after the CAP treatment. The *c*-axis lattice parameter calculated from the diffraction pattern using silicon powder as an internal standard is 37.07 Å, which is consistent with that of the 2223 phase. Diffraction pattern of CAP-treated whiskers crushed into powder also consist solely of peaks of the 2223 phase, which indicates that the whiskers are fully converted into the 2223 phase as far as X-ray diffraction can detect. The intensity of XRD peaks for the CAP-treated samples is smaller than that for the original ones and is probably due to the roughness of the crystal surface and possibly some slight inhomogenities induced during the phase conversion.

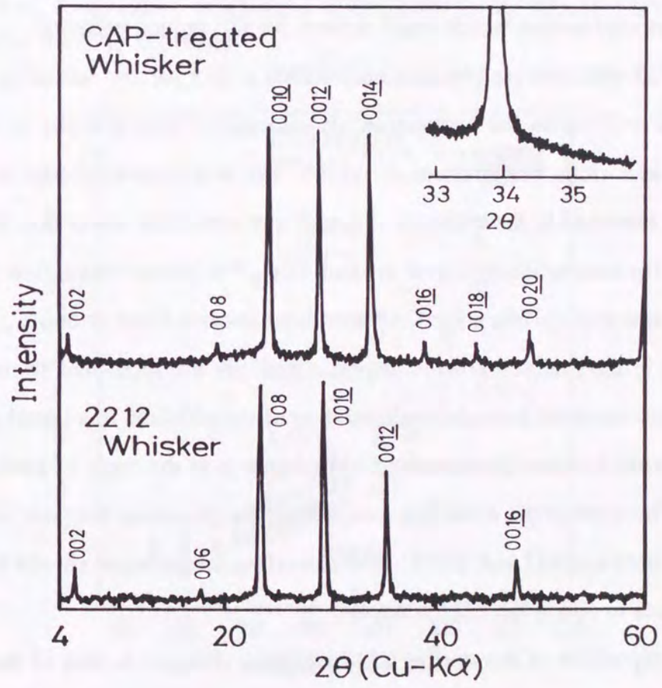

FIG. 4-3. X-ray diffraction patterns for the whiskers before and after the CAP treatment.

Figure 4–4 shows the temperature dependence of resistance (R–T) for the whisker CAP–treated using the $Bi_2Sr_2Ca_4Cu_6Pb_{0.5}O_x$ powder as compared with that of the starting 2212 whisker. The 2212 whisker shows two steps in the R–T curve at 105 and 75 K, since the whisker consists of the 2212 phase and a small amount of the 2223 phase (<1%, section 2–2). The zero–resistance temperature is 73 K. For the CAP–treated whisker, the resistance decreases steeply at 110 K, and the zero–resistance state is achieved at 107 K. The resistivity of the CAP–treated whisker is 550 μΩcm at room temperature and decreases linearly against temperature down to 130 K. In temperature region between 130 K and T_c, a wide shoulder is observed. This behavior is usually observed in oxide superconductors, and is attributed to the two–dimensional superconducting fluctuation resulting from a short coherence length [26]. In contrast, the R–T curve of the starting 2212 whisker persists to be linear until about 5 K above T_c. We are unaware of any explanation which could account for this unique behavior.

The 2223 whiskers are obtained only within a very narrow annealing temperature region. Figure 4–5 shows the temperature dependence of susceptibility of the whiskers CAP–treated at various temperatures for 150 h. The non–converted part of the original 2212 phase is observed in the whiskers annealed at temperature lower than 848°C, that is evident from the susceptibility signal around 75 K. The phase conversion is completed between 853 and 858°C. When the CAP treatment is carried out at 860°C, the whiskers are not found in the calcined powder anymore and are not recovered from the powder. This might have occurred through the dissolution of the whiskers in a liquid phase generated in the powder because the annealing temperature is in the range of partial melting of the powder. The appropriate annealing temperature for obtaining the pure 2223 whiskers is, therefore, between 853 and 858°C. The annealing temperature should be controlled within 5 degrees to obtain the 2223 whiskers.

The composition of the starting 2212 whiskers changes to that of the 2223 phase after the CAP treatment. The calcined powder contains Pb, whereas the starting 2212 whiskers do not contain it. In order to examine the existence of Pb in the CAP–treated

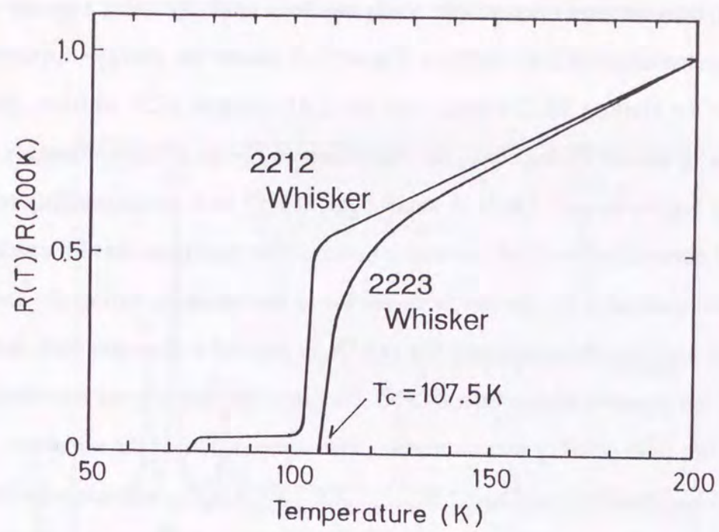

FIG. 4–4. Temperature dependence of resistance for the whiskers before and after the CAP treatment.

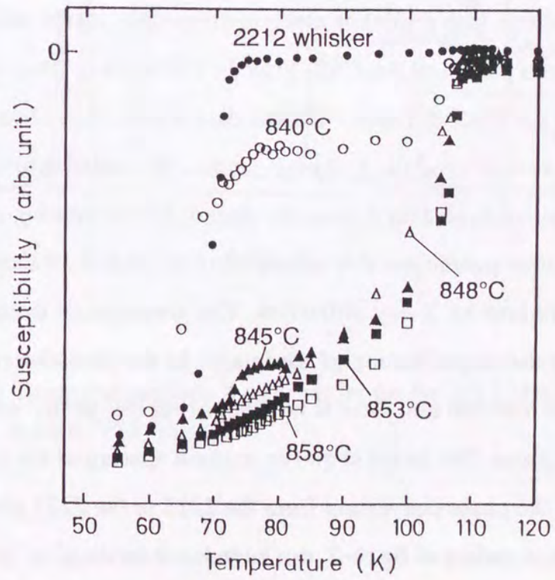

FIG. 4–5. Temperature dependence of susceptibility for the whiskers CAP–treated at various temperature for 150 h.

whiskers, analytical electron microscopic study has been made by using a energy dispersive X-ray spectroscopic (EDX) analyzer. Figure 4-6 shows the energy-dispersive X-ray spectra for the starting 2212 whisker and the CAP-treated 2223 whisker. Since the atomic number of Bi and Pb are close, the characteristic X-ray of these elements overlap at low energy region around 2 keV. A small peak at 10.5 keV corresponding to the Pb Lα-peak is observed for the CAP-treated whisker. This confirms that Pb exists in the 2223 phase. Pb diffuses from the calcined powder to the whiskers during the annealing. From the EDX analysis, the content of Cu and Ca is assured to increase with increasing the annealing temperature higher than 845°C. This increase has a good correlation with the results of the susceptibility measurements. The composition of the whiskers CAP-treated at 855°C is $Bi_{1.76\pm0.06}Pb_{0.3\pm0.1}Sr_{1.51\pm0.08}Ca_{1.69\pm0.08}Cu_3O_x$, when normalized to 3 copper atoms/formula unit. Although the 2223 whiskers are deficient in alkaline earth metal sites as in the case of the 2212 whiskers (section 2-2), the composition actually changes from the 2212 to the 2223 phase.

Figure 4-7 shows a high resolution electron microscope image and corresponding selected area diffraction pattern of the CAP-treated 2223 whisker taken with an incident electron beam along the [010] direction. Double dark dotted lines observed in fig. 4-7 correspond to the lock-salt type Bi_2O_2 double layers. The spacing between the Bi_2O_2 double layers is estimated to be 19.0 Å from the image. As this spacing corresponds to a half of the *c*-axis lattice parameter, it is estimated to be 38.0 Å, which is about 0.9 Å larger than that determined by X-ray diffraction. This discrepancy would be due to the error in determining the magnification of the image. In the area observed in fig. 4-7, which corresponds to 650x500 nm, there is no intergrowth due to the other phases such as the 2212 or 2201 phase. The image shows an uniform spacing of the layers, indicating the completeness of the phase conversion from the 2212 to the 2223 phase by the CAP method. The diffraction pattern of fig. 4-7 can be indexed on the a^*-c^* plane of the 2223 phase.

The CAP method has applied not only for the 2212 whiskers but also for 2212

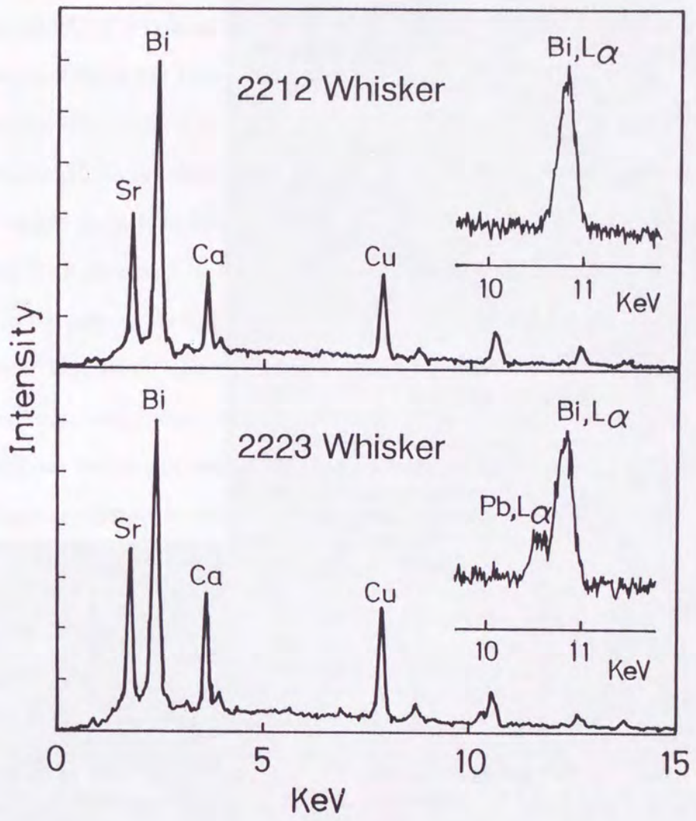

FIG. 4-6. Energy-dispersive X-ray spectra for the 2212 whisker and the CAP-treated 2223 whisker.

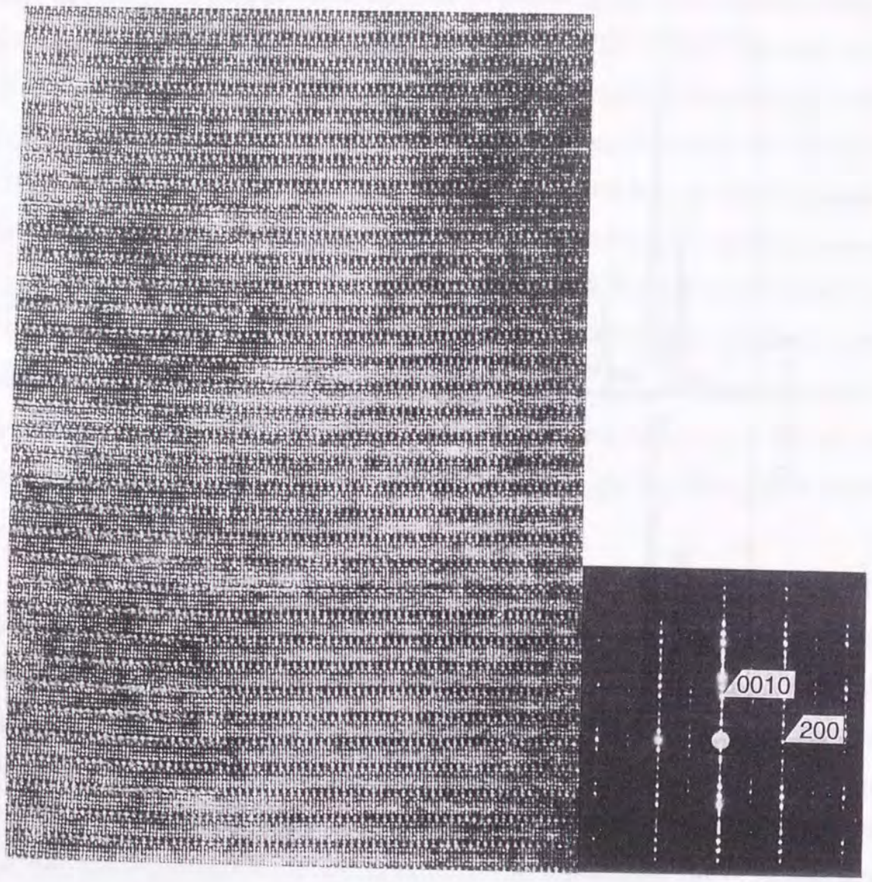

FIG. 4–7. A high resolution electron microscope image and corresponding selected area diffraction pattern of the CAP–treated 2223 whisker taken with an incident electron beam along the [010] direction.

single crystal sheets. The 2212 single crystals were prepared by the self–flux method. The mixture of oxide and carbonate powders with the composition of Bi:Sr:Ca:Cu = 2:1:1:2 were heated in an alumina crucible at 1000°C, held at this temperature for 10 h, cooled to 800°C at a rate of 5°C/h, cooled to 600°C at 40°C/h, and finally cooled to a room temperature in the furnace. After mechanical separation, the 2212 single crystals thus obtained were heated in the $Bi_2Sr_2Ca_4Cu_6Pb_{0.5}O_x$ calcined powder at 855°C for 180 h (CAP method). X–ray diffraction pattern and temperature dependence of resistance for the 2212 single crystals before and after the CAP treatment are shown in fig. 4–8. All the diffraction lines observed in the CAP–treated samples are assigned to those of the 2223 phase as in the case of the whiskers (fig. 4–8 (a)). The onset temperature and zero–resistance temperature of the starting 2212 single crystal are 80 and 66 K, respectively. The zero–resistance temperature is lower than the reported temperature for the 2212 phase. This would be not due to impurity phase but to the unoptimization of the hole concentration, because no impurity phase is observed in the XRD pattern of the starting 2212 single crystals as shown in fig. 4–8 (a). After the CAP treatment, zero–resistance temperature increases to 103 K. Susceptibility measurement and compositional analysis also confirm the phase conversion to the 2223 phase. Thus the CAP method is useful for the single crystals obtained by the flux method as well as for the whiskers, resulting the 2223 sheet crystals with 1 mm^2 in area. However, there is an upper–limit in the thickness of the starting 2212 crystals. When the thickness is thicker than 10 μm, the phase conversion is not completed, and the original 2212 phase remains in the crystals even after a long period of heating. This is not the problem for the whiskers because their thickness are less than 10 μm.

SEM appearances of the original 2212 whisker and the CAP–treated 2223 whisker and sheet crystal are shown in fig. 4–9. The original shape of the whisker is maintained even after the CAP treatment as shown in fig. 4–9 (a) and 4–9 (b). The 2223 samples that have been obtained previously by the solid state reaction method are polycrystals with the grain size smaller than 100 μm as shown in fig. 4–9 (d). In contrast, large

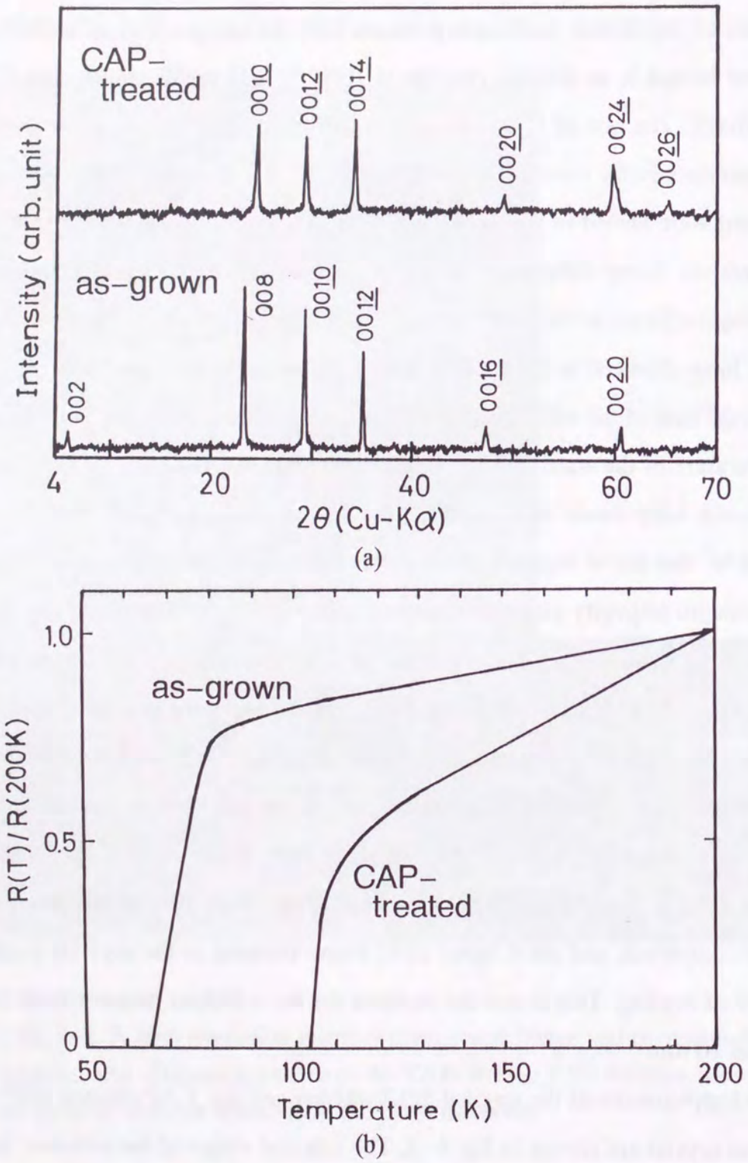

FIG. 4–8. X–ray diffraction patterns (a) and temperature dependence of resistance (b) for the single–crystal sheets before and after the CAP treatment.

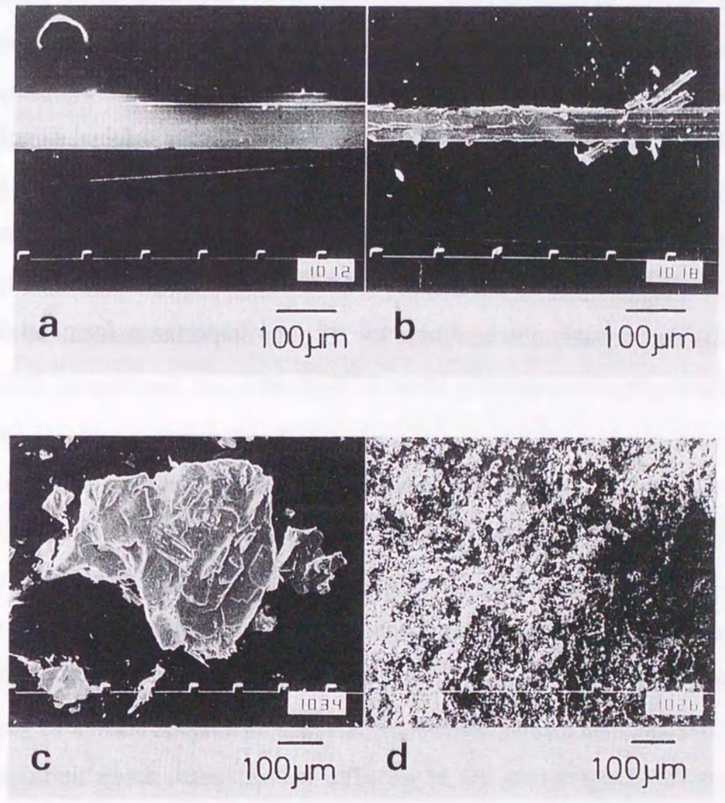

FIG. 4–9. SEM appearances of the (a) 2212 whisker, (b) CAP–treated 2223 whisker, (c) CAP–treated 2223 sheet crystal, (d) cross–section view for sintered pellet of the 2223 phase obtained by solid–state reaction method.

2223 whiskers and crystals are obtained with retaining the outline of the form in the original crystals by applying the CAP method.

In summary, a new method has been developed for preparing the 2223 whiskers. The 2223 whiskers have been prepared by annealing 2212 whiskers in a $Bi_2Sr_2Ca_4Cu_6Pb_{0.5}O_x$ calcined powder (Conversion by Annealing in Powder method: CAP method). The completeness of the phase conversion has been confirmed by X–ray diffraction, compositional analysis, susceptibility measurement, and a high resolution electron microscope observations. The outline of the form in the original samples is retained even after the CAP treatment. The CAP method has been also applied for single crystal sheets of the 2212 phase. The 2212 single crystal sheets have been converted to the 2223 phase, resulting in 2223 sheet crystals as large as approximately 1 mm^2. The 2223 whiskers and crystals obtained here are of great importance for obtaining basic information on the physical properties of the 2223 phase.

4–3. Phase Conversion Process of the $Bi_2Sr_2CaCu_2O_x$ Phase into the $Bi_2Sr_2Ca_2Cu_3O_x$ Phase

This section describes the phase conversion mechanism from the $Bi_2Sr_2CaCu_2O_x$ (2212) to the $Bi_2Sr_2Ca_2Cu_3O_x$ (2223) phase in the CAP method. An understanding of the formation mechanism and reaction kinetics is obviously important for the preparation of 2223 superconducting products with desired microstructure and properties. Several mechanisms have been proposed for the formation of the 2223 phase as follows. Nobumasa *et al.* [27] and Kijima *et al.* [28] have proposed a disproportionation reaction of the 2212 phase to form the 2223 and 2201 phases. Hatano *et al.* have reported that the 2223 phase are precipitated from a partially melted phase instead of through intergrowth of the phases or the disproportionation reaction [5]. A similar idea has been proposed for Pb–doped 2223 compounds, the 2223 phase is formed from the 2212 phase, CaO, and a liquid, the last two components arising from the decomposition of Ca_2PbO_4 [29, 30]. Morgan *et al.* have detected small Bi/Pb–rich liquid droplets that appeared to migrate over growing platelets, depositing ledges of product in their wake during equilibration [31]. From the experiments of the crystallization of 2223 glass, the 2223 phase forms at interface between the 2212 phase and Ca_2CuO_3 after certain amounts of Ca and Cu atoms have diffused into the 2212 phase [32]. Inserting process has also been reported [33, 34]. The supply of atomic species such as Ca, Sr, Cu, and O into the 2212 phase induces a edge dislocation which causes further diffusion of the atomic species to make the 2223 phase [33]. These mechanisms suggest that the 2223 phase is produced through the 2212 phase which acts as a precursor of the 2223 phase [35], and the other phases surrounding the 2212 compound such as a liquid phase, Ca_2CuO_3, or Ca_2PbO_4 are in crucial role for the 2223 phase formation. However, the microscopically detailed mechanism has not been authenticated yet. The CAP process is thought to give us a good method for revealing the formation mechanism of the 2223 phase because (i) the conversion process can be examined using high quality samples such as the 2212 whiskers without loosing its

shape in contrast to powders or polycrystalline bulk samples used in the previous reports, (ii) the whiskers and the surrounding powder can be separated, allowing us to know their composition and crystal structure individually.

In this section, two systematic experiments have been made. One is the effects of composition of the calcined powder used in the CAP method on the phase conversion of the 2212 whiskers. In the previous section, the $Bi_2Sr_2Ca_4Cu_6Pb_{0.5}O_x$ (defined as no.0) powder is used for the CAP method. Seven kinds of the calcined powder with different composition have been prepared, $Sr_2Ca_4Cu_6Pb_{0.5}O_x$ (no. 1), $Bi_2Ca_4Cu_6Pb_{0.5}O_x$ (no. 2), $Bi_2Sr_2Cu_6Pb_{0.5}O_x$ (no. 3), $Bi_2Sr_2Ca_4Pb_{0.5}O_x$ (no. 4), $Bi_2Sr_2Ca_4Cu_6O_x$ (no. 5), $Ca_4Cu_6Pb_{0.5}O_x$ (no. 6), and $Sr_2Ca_4Cu_6O_x$ (no. 7). These are lack of one (nos. 1–5) or two (nos. 6–7) elements compared with the no.0 powder. Using these powders, the CAP treatment has been done and the degree of the phase conversion has been evaluated. The other systematic experiment is kinetics of the phase conversion. A few kinetic study for the formation of the 2223 phase have been so far reported [36–38]. In these reports, the volume fraction between the 2212 phase and the 2223 phase was estimated from the intensity of the X–ray diffraction peak, which is thought to contain some inaccuracy because the intensity depends on orientation, crystallinity, and size of grain. On the other hand, susceptibility data have been used for determining the volume fraction in this study. Time dependence of the phase conversion in the CAP method using the no. 0 powder has been measured and analyzed by the Johnson–Mehl–Avrami relation. The phase conversion mechanism will be discussed with respect to the two experimental results of the effects of the composition in the calcined powder and the kinetics.

Experimental

The 2212 whiskers used for the CAP method were prepared as described in chapter 2. The CAP treatment was carried out using seven kinds of calcined powder. The

composition and calcining conditions are listed in table 4–1. The composition of the powder was chosen as that one (nos. 1–5) or two (nos. 6–7) elements were taken off from the $Bi_2Sr_2Ca_4Cu_6Pb_{0.5}O_x$ (no. 0) composition, keeping the ratio of the other cations. These powders were prepared by an ordinary solid–state reaction method. Source materials of oxides and carbonates powder of Bi_2O_3, $SrCO_3$, $CaCO_3$, CuO, and PbO were mixed and calcined at the condition listed in table 4–1 with an intermediate grinding. To prepare sintered pellets, the calcined powder was pressed and sintered at 850–860°C for 12 h in air. The calcined powders containing the 2212 whiskers were annealed at 830–875°C for 120 h in air. The whiskers were removed mechanically from the powder after the annealing. For the study on the kinetics of the phase conversion, the CAP treatment was carried out at 848, 851, 854, 857°C for 1.5–144 h by using the $Bi_2Sr_2Ca_4Cu_6Pb_{0.5}O_x$ (no. 0) powder.

Table 4–1. Composition and calcining condition of the powder used for the CAP method.

No.	Composition	calcining condition
0	$Bi_2Sr_2Ca_4Cu_6Pb_{0.5}O_x$	780°C 20 h and 820°C 20 h
1	$Sr_2Ca_4Cu_6Pb_{0.5}O_x$	820°C 20 h, 870°C 20 h, and 890°C 20 h
2	$Bi_2Ca_4Cu_6Pb_{0.5}O_x$	780°C 20 h and 820°C 20 h
3	$Bi_2Sr_2Cu_6Pb_{0.5}O_x$	780°C 20 h and 820°C 20 h
4	$Bi_2Sr_2Ca_4Pb_{0.5}O_x$	780°C 20 h and 820°C 20 h
5	$Bi_2Sr_2Ca_4Cu_6O_x$	780°C 20 h and 820°C 20 h
6	$Ca_4Cu_6Pb_{0.5}O_x$	780°C 20 h and 820°C 20 h
7	$Sr_2Ca_4Cu_6O_x$	820°C 20 h and 900°C 20 h

X–ray diffraction measurement was made using a RIGAKU diffactometer with Cu–Kα radiation. The fractional conversion of the 2223 phase was determined from the susceptibility measurements with a Quantum Design $MPMS_2$ superconducting quantum interference device (SQUID) magnetometer. The surface morphology was characterized with a Hitachi scanning electron microscope (SEM) model S–2400. The compositional analysis was performed with a Horiba EMAX–5770 energy dispersive X–ray spectroscopy (EDX) system. The DTA curve was obtained by increasing the temperature from a room temperature to 1000°C at a constant heating rate of 10°C/min. Resistivity was measured by a standard four–prove method.

Results and discussion

The effects of composition of the calcined powder on the phase conversion of the 2212 whiskers have been investigated using seven kinds of the calcined powder (nos. 1–7) with different composition. The temperature region where the whiskers can be recovered from the calcined powder is shown in fig. 4–10. For the no. 1 powder, the whiskers can be recovered up to 875°C, whereas they are not found in the powder anymore after the CAP treatment at temperatures higher than 878°C. While the color of the whiskers CAP–treated at 840–855°C is black, it turns gold in the whiskers annealed at 865–875°C. Figure 4–11 shows the change of composition of the CAP–treated whiskers using the no. 1 calcined powder. The atomic ratio is normalized to 1 for the five metallic cations. The atomic ratio of Ca steeply increases between 855 and 865°C accompanying the decrease of Sr, Bi, and Pb ratio. Especially, the content of Bi and Pb decreases less than 1 at.%. This drastic alteration corresponds to the change of the color in the CAP–treated whiskers. Form the X–ray diffraction pattern, Ca_2CuO_3, $(Sr,Ca)_3Cu_5O_8$, and CuO are detected for the whiskers annealed at 865°C, indicating that the superconducting phase decomposes to these phases. The decomposition is found to be promoted in the no. 1

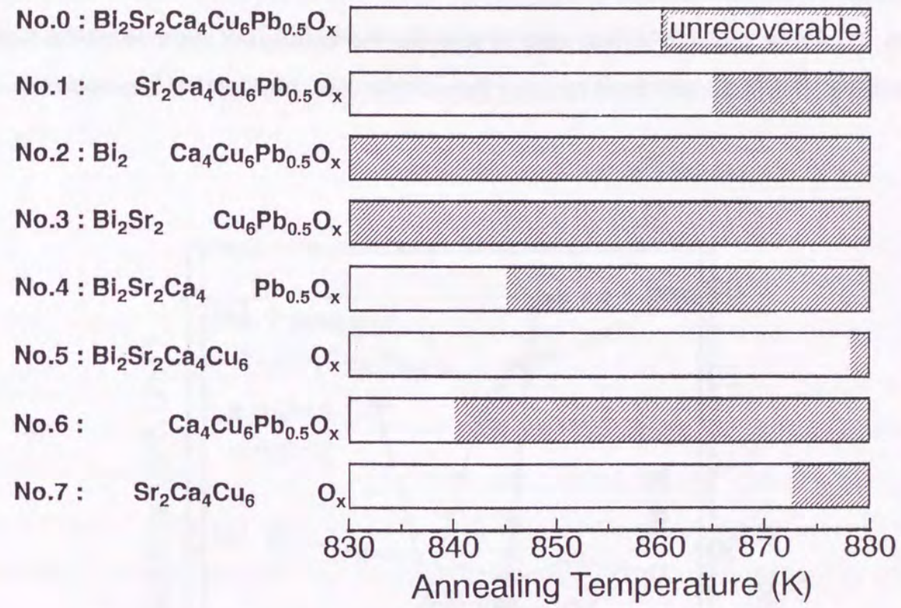

FIG. 4–10. The annealing temperature region where the whiskers can be recovered from the calcined powders in the CAP method.

calcined powder with the deficiency of Bi. The Bi ions are thought to diffuse out from the whiskers to the calcined powder due to the large deference of the Bi concentration between the whiskers and the no. 1 powder. It should be noted that the content of Pb increases with increasing annealing temperature up to 12 at.% at 855°C. X-ray diffraction pattern of the whiskers annealed at 848°C shows the peaks assigned to the 2212 phase, so that the 2212 whiskers with a high Pb/Bi ratio are obtained. It has been reported that the Pb substituted 2212 compound has a potential of no modulation structure [39, 40]. Therefore, it would be interested in studying the modulation structure of the CAP-treated 2212 whiskers obtained by using the no. 1 powder, although it is not discussed.

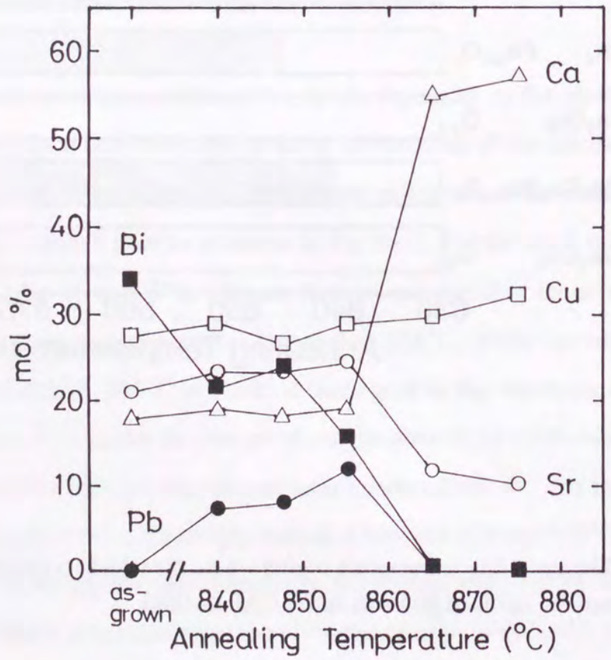

FIG. 4-11. Change of relative atomic ratio for the CAP-treated whiskers at various temperatures using the $Sr_2Ca_4Cu_6Pb_{0.5}O_x$ (no. 1) calcined powder.

The temperature dependence of susceptibility of the CAP-treated whiskers at 855°C is shown in fig. 4-12 and compared with that for the original 2212 whiskers. The volume fraction of the 2223 phase is calculated to be 20%, assuming that the whiskers are consist of the 2212 and the 2223 phases. The volume fraction is estimated as follows. A simulated susceptibility curve is made from the data of the original 2212 whiskers and the pure 2223 whiskers obtained by the CAP treatment using the no. 0 powder, which are normalized at 5 K. The simulated curve with a volume fraction of the 2223 phase (C) is a linear combination of the 2212 and the 2223 data with multiplication factors of $1-C$ and C, respectively. The fractional conversion C is determined by fitting the simulated curve

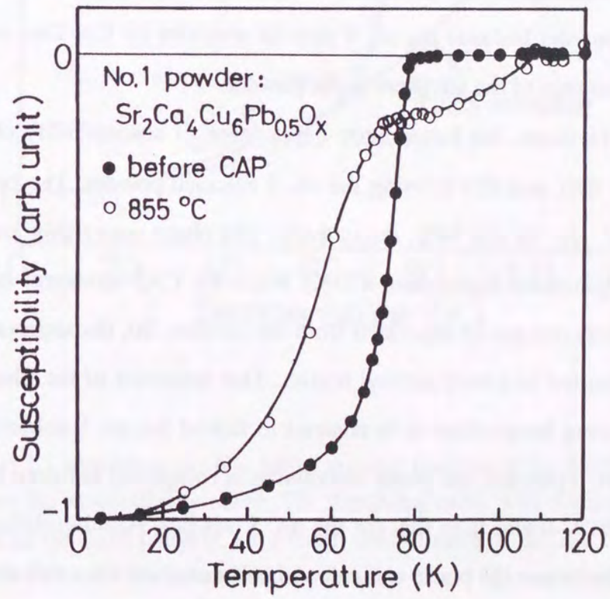

FIG. 4-12. Temperature dependence of susceptibility of the whiskers CAP-treated at 855°C using the no. 1 calcined powder comparing with the original 2212 whiskers.

to the observed data (fig. 4–13). The CAP–treated whiskers at 865 and 875°C show no Meissner signal in the susceptibility curves. The whiskers annealed at 840 and 848°C show no signal of the 2223 phase. The maximum conversion ratio from the 2212 to the 2223 phase is about 20% in the case of the no. 1 calcined powder.

The whiskers are not recovered from the calcined powder of the no. 2 and no. 3 which have the composition without Sr and Ca, respectively. Even at annealing temperatures lower than 830°C, both of the calcined powders are stiffly sintered, and the whiskers are not able to be recovered from the powder. In the case of the no. 4 calcined powder, the whiskers CAP–treated at 840°C are recovered. However, the 2223 phase is not detected in the whiskers by the susceptibility measurement. When the annealing temperature increases higher than 845°C, the whiskers are absent in the powder although it is not stiffly sintered remaining the powder state. In this case, copper in the whiskers is found to diffuse into the powder because the no. 4 powder contains no Cu. This reaction would cause the disappearance of the whiskers in the powder.

Figure 4–14 shows the temperature dependence of susceptibility of the whiskers CAP–treated at 870, and 875°C using the no. 5 calcined powder. The conversion ratio of these whiskers are 18 and 98%, respectively. The phase conversion steeply proceeds at annealing temperatures higher than 870°C. When the CAP treatment is carried out at 878°C, the whiskers can not be recovered from the powder. So, the appropriate annealing temperature is limited to a very narrow region. This behavior of the phase conversion against the annealing temperature is in contrast to that of the no. 0 calcined powder. In the case of the no. 0 powder, the phase conversion is completed between 853 and 858°C which is about 20°C lower than that for the no. 5 powder. Another different point is a temperature region where the phase conversion is observed even a small conversion ratio. The CAP–treated whiskers in the no. 0 powder at 840°C, about 15°C lower than the appropriate annealing temperature, have a conversion ratio of 30% (fig. 4–5). In contrast, the whiskers of 865°C, 10°C lower than the appropriate annealing temperature, show no phase conversion for the no. 5 powder. These differences are attributed to the differnce in

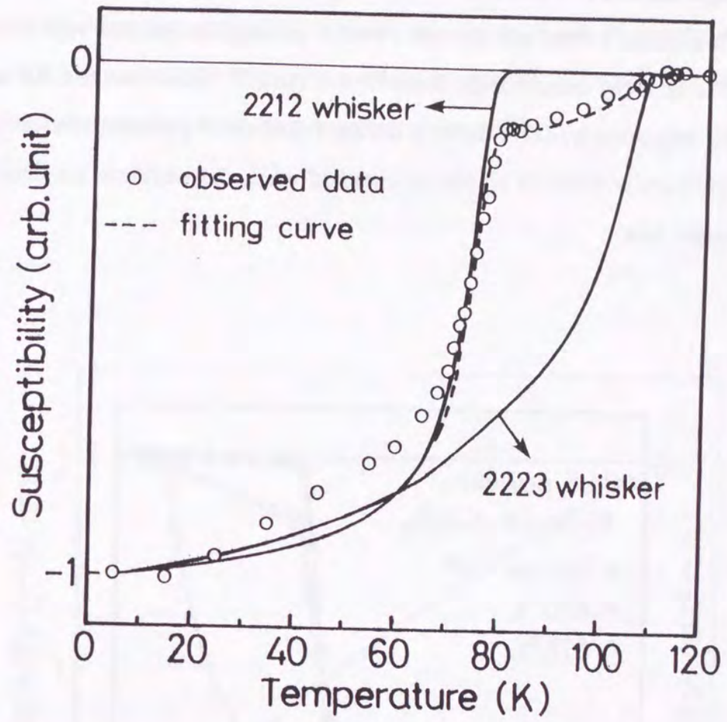

FIG. 4–13. Calculation method of the volume fraction of the 2223 phase (C) from the susceptibility curve. The simulated curve with a volume fraction of the 2223 phase (C) is a linear combination of the 2212 and the 2223 data with multiplication factors of $1–C$ and C, respectively. The fractional conversion C is determined by fitting the simulated curve to the observed data.

the composition of the calcined powder, namely the effects of Pb. In preparing the 2223 compound by the conventional solid state reaction method, it has been reported that the addition of Pb enhances the formation of the 2223 phase by lowering and spreading its formation temperature [41–44]. The similar tendency is observed in the CAP method. Because the Pb addition lowers and spreads a partial melting temperature region, a liquid phase is found to be a key factor for the formation of the 2223 phase in the CAP method. This is strongly supported by DTA data for the no. 0 and no. 5 powders. The fully converted 2223 whiskers without Pb would be obtained when the whiskers are annealed at 875°C for a longer time.

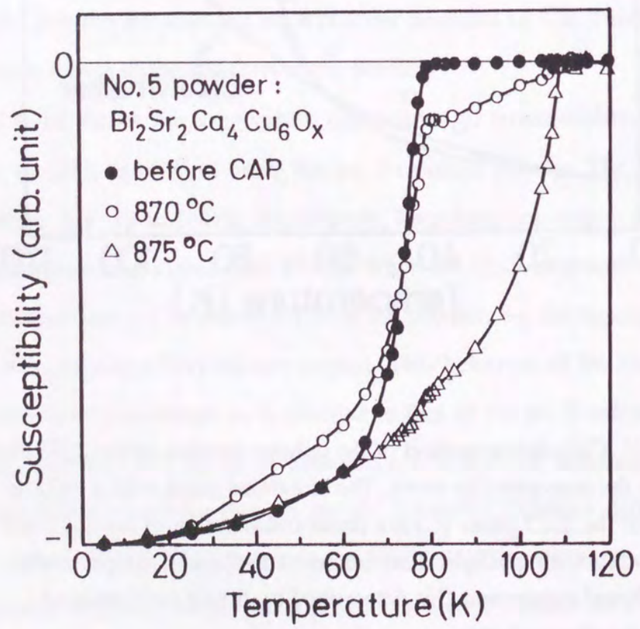

FIG. 4–14. Temperature dependence of susceptibility of the CAP–treated whiskers using the no. 5 calcined powder comparing with the original 2212 whiskers.

Although the whiskers CAP–treated at 875°C contain a small amount of the 2212 phase, a zero resistance state is achieved at temperature higher than 100 K. Figure 4–15 shows the temperature dependence of resistivity for the CAP–treated whisker at 875°C for 120 h using the no. 5 calcined powder. The zero resistance temperature is 101.3 K, which is lower than that of the 2223 whisker with Pb by 5.7 K (fig. 4–4). A small tailing observed in the resistance drop of the whisker without Pb lowers the zero resistance temperature, may be due to an inhomogenity of the whisker.

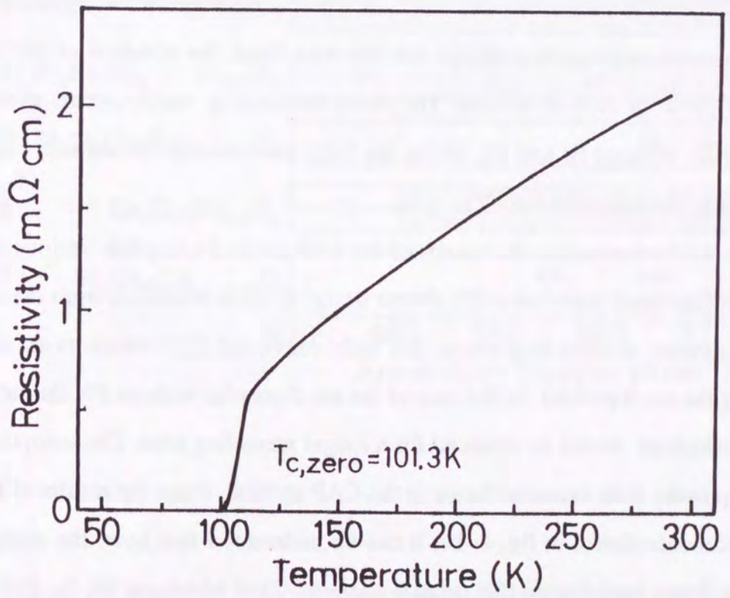

FIG. 4–15. Temperature dependence of resistivity for the whisker CAP–treated at 875°C for 120 h using the no. 5 calcined powder.

In the case of the no. 6 calcined powder, the whiskers CAP–treated at 830°C are recovered. However, the 2223 phase is not detected in the whiskers by the susceptibility measurement. When the annealing temperature increases higher than 840°C, the calcined powder is stiffly sintered and the whiskers are not able to be found in the powder. The no. 7 calcined powder shows a similar behavior to that of the no. 1 powder. Both the powders are different from each other in whether they contain Pb or not. The whiskers can be recovered up to 875°C, whereas they are not found in the powder after the CAP treatment at 878°C anymore. The color of the whiskers CAP–treated at 840–865°C is black, on the other hand, it turns to gold for the whiskers at 875°C. The content of Ca steeply increases between 865 and 875°C accompanying with the decrease in Sr and Bi content. This alteration corresponds to the change of color of the CAP–treated whiskers. From the susceptibility measurements, no 2223 phase is detected in the whiskers CAP–treated at temperatures lower than 855°C. On the other hand, the whiskers of 865°C contain the 2223 phase of 28% in volume. The phase conversion surely occurs even in the calcined powder without Bi and Pb, while the fully converted 2223 whiskers have not been obtained in the case of the no. 7 powder.

Figure 4–16 summarizes the results of the CAP method using the various calcined powders. The fractional conversion (C) shown in fig. 4–16 is evaluated from the susceptibility measurement as described above. The fully converted 2223 whiskers are obtained only by using the no. 0 powder. In the case of the no. 5 powder without Pb, the fully converted 2223 whiskers would be obtained for a longer annealing time. The composition of the calcined powder is an essential factor in the CAP method. From the results of the systematic experiments shown in fig. 4–16, it can be understood that how the composition affects on the phase conversion. To prepare the pure 2223 whiskers, Bi, Sr, Ca, and Cu are the essential elements in the calcined powder. The addition of Pb works to lower and spread the temperature region where the phase conversion occurs, which is the same situation as reported in the solid state reaction method. However, a characteristic point in the CAP method is whether the whiskers can be recovered from the calcined powder or

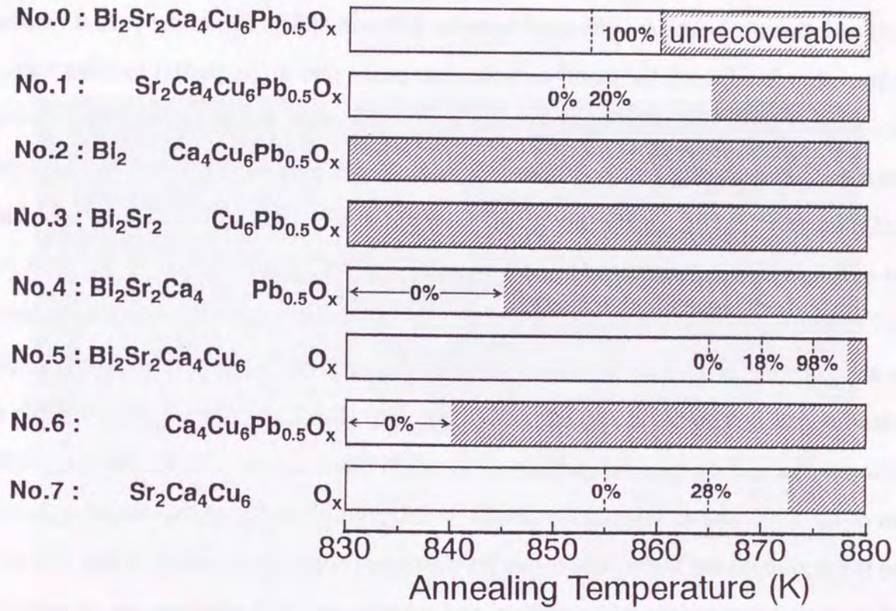

FIG. 4–16. Results of the CAP method using various calcined powder. The annealing time is 150 h.

not. This temperature region for the recovery strongly depends on the composition of the calcined powder.

A liquid phase is necessary for the phase conversion from the 2212 to the 2223 phase as described above, and the melting temperature (T_m) of the calcined powder is an another important parameter. The T_m values of the nos. 0–7 calcined powder determined from the DTA curve are 865 (no. 0), 895 (no. 1), 818 (no. 2), 861 (no. 3), 860 (no. 4), 870 (no. 5), 905 (no. 6), and 965°C (no. 7), respectively. In the case of the no. 0 powder, small endothermic peaks are observed between 820 and 850°C due to the partial melting. On the other hand, such the small endothermic peaks due to the partial melting state is not observed in the other calcined powder. So, a liquid phase due to the partial melting generates just below T_m for the nos. 1–7 powders. It has been reported that the Pb–doped 2223 phase starts to generate at higher than 830°C, and it decomposes to the 2212 phase and a melt at higher than 870°C [5, 30]. Therefore, the T_m values of the no. 1. no. 6, and no. 7 calcined powder are too high to prepare the 2223 phase. In contrast, the T_m value of the no. 2 powder is too low to prepare the 2223 phase. The 2223 phase without Pb starts to decompose at temperature higher than 880°C [45]. The temperature region suitable for the formation and the thermal stability of the 2223 phase is 830–880°C. For the formation of the 2223 phase, this region should overlap with the T_m of the calcined powder and the region where the whiskers can be recovered from the powder. Only the no. 0 and no. 5 powders satisfy this condition, and actually the 2223 whiskers are obtained by the CAP method.

The surface appearances of the starting 2212 whisker and the 2223 whisker obtained using the no. 0 calcined powder are shown in fig. 4–17. The surface of the original 2212 whisker is flat and smooth (fig. 4–17 (a)), while the surface is rough with many steps after the CAP treatment (fig. 4–17 (b)). The edge becomes round, suggesting the existence of a liquid phase around the whiskers during the CAP treatment. Because the annealing temperature is in a partial melting region of the calcined powder as described above, the liquid phase is due to this. The steps and round edges on the CAP–treated

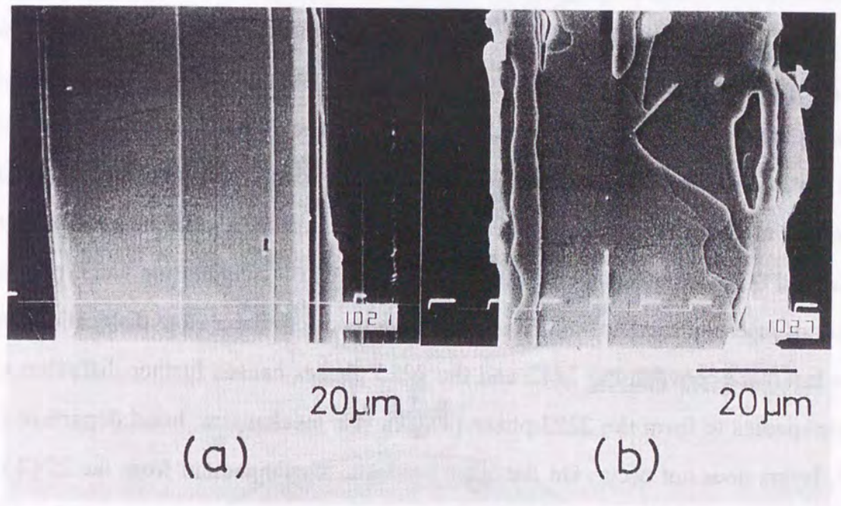

FIG. 4–17. Surface appearances of the (a) original 2212 whisker and (b) CAP–treated 2223 whisker prepared by using the no. 0 calcined powder.

whisker are the evidence for the dissolution of the whisker in the liquid phase. Therefore, the phase conversion is thought to proceed as follows (fig. 4–18). A liquid phase is generated in the powder around the 2212 whisker, which is indicated by black circles. It reacts with the 2212 whisker and nucleation of the 2223 phase occurs at the interface between the liquid phase and the whiskers. By supplying Ca, Cu, and Pb ions into the whisker through the liquid phase, the 2223 phase indicated by hatched lines spreads over the whisker. At the same time, the dissolution of the whisker in the liquid phase occurs during the phase conversion, which causes the irregularities and the round edges on the surface of the 2223 whisker as shown in the surface appearances (fig. 4–17 (b)).

The disproportionation mechanism [27, 28] is unlikely in the CAP method because the 2201 phase is not detected in the CAP–treated whiskers. In addition, when the 2212 whiskers are annealed without the calcined powder, the phase conversion do not taken place. In microscopically, two possible mechanisms can be considered for the phase conversion mechanism, intercalation and rearrangement ones. Atomic species such as Ca, Sr, Cu, and O are inserted into the 2212 phase between the neighboring CuO_2 planes in a manner of insertion mechanism. Feng *et al.* have reported that a edge dislocation formed at the interface between the 2212 and the 2223 phases causes further diffusion of the atomic species to form the 2223 phase [33]. In this mechanism, bond departure in the Bi_2O_2 layers does not occur. On the other hand, the rearrangement from the 2212 to the 2223 phase occurs at the interface, so that the bond departure process is contained in the rearrangement mechanism. In result, some Bi_2O_2 layers are continuous and some layers are discontinuous at the interface. Of these two mechanisms, the rearrangement one is thought to be more probable. If the extra CuO_2 plane intercalates into all the 2212 layers, the strain at the interface would become rather large. To avoid this strain some of the 2212 layers should be remained without receiving the insertion of CuO_2 plane. Such the strain does not exist in the rearrangement mechanism. Considering the *c*–axis lattice parameter, the thickness of 5 layers of the 2223 phase corresponds to that of the 6 layers of the 2212 phase. Actually, such the interface due to the mismatch has been observed in

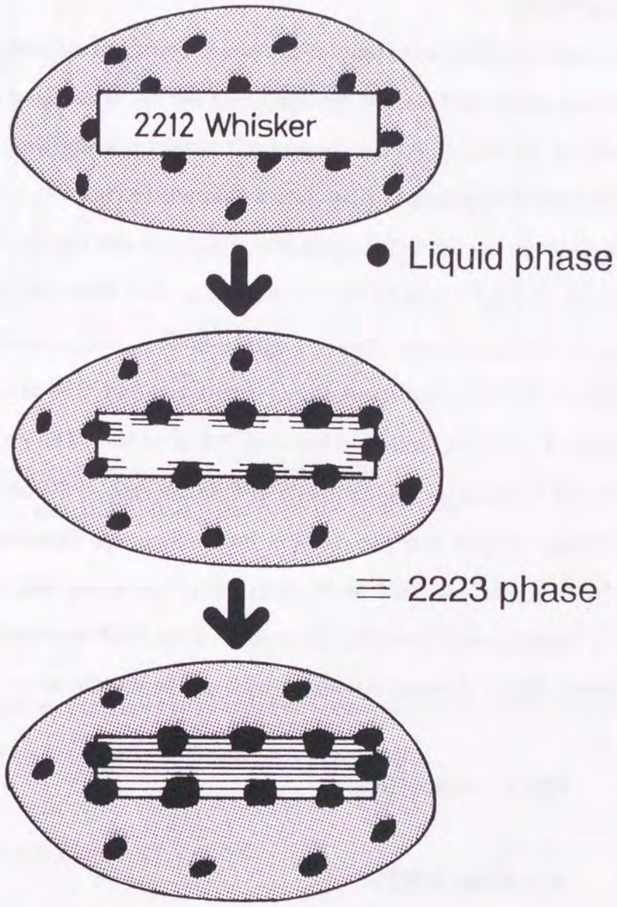

FIG. 4–18. A model for the phase conversion in the CAP method.

a high resolution TEM image for the powder sample [5, 46, 47]. Ca, Sr, Cu, and Pb ions are supplied into the whiskers through a liquid phase and diffused to the interface. They are incorporated in the rearrangement process to make the 2223 phase, and the interface moves to the inner portion of the whisker to increase the 2223 phase during the phase conversion process.

An isothermal kinetics study of the phase conversion from the 2212 to the 2223 phase has been made on the CAP method using the no. 0 calcined powder. Figure 4–19 shows a plot of the fractional conversion (C) versus heating time, t. The C values are determined from the susceptibility data as shown in fig. 4–13. The conversion rate strongly depends on the heating temperature. The fractional conversion in the CAP–treated whiskers at 851, 854, and 857°C reaches up to over 90% for the annealing time of 30, 50, and 90 h, respectively. The C–t curves of these temperatures follow a sigmoid–shaped profile. On the other hand, the C–t curve at 848°C is almost linear with slight upturn, and the C value is limited to less than 0.4 in <150 h. The phase conversion rapidly proceeds at a temperature higher than 850°C in the case of the no. 0 calcined powder.

To obtain insights into the reaction mechanism, the experimental data have been analyzed by a model reported by Hulbert [48]. Assuming that the phase conversion proceeds by nuclei growth models, the results of the CAP treatment have been analyzed by the Johnson–Mehl–Avrami relation, which can be written as

$$C(t) = 1 - \exp[-(Kt)^m] \qquad (4\text{–}1),$$

$$K = A\exp(-E/RT) \qquad (4\text{–}2),$$

where C is the fractional conversion, K is the rate constant, m is the reaction order, A is the preexponential constant, E is the activation energy, R is the gas constant, T is the annealing temperature in Kelvin, and t is the annealing time. This approach considers the nucleation of products at active sites and the rate at which the nucleated particles grow,

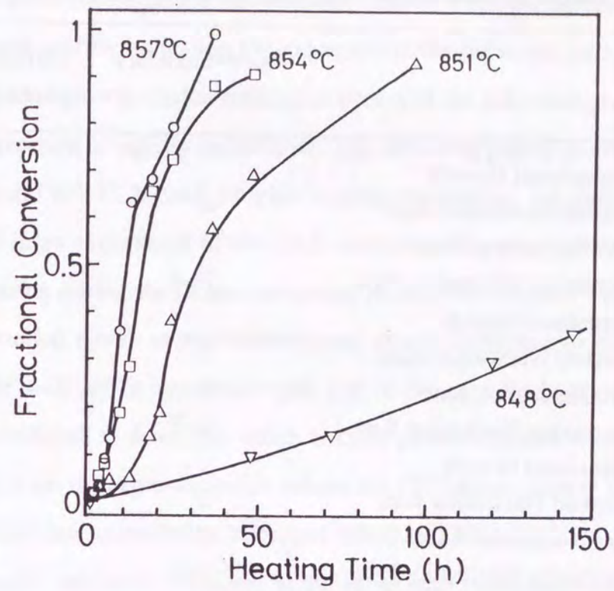

FIG. 4–19. Fractional conversion C–t plots for the whiskers CAP–treated at 857, 854, 851, and 848°C using the no.0 calcined powder.

and has been succeeded to describe the kinetics of phase transformation of various compounds [36, 49, 50]. The equations (4–1) and (4–2) are written as

$$\ln[-\ln(1-C(t))] = m\ln t + m\ln K \qquad (4\text{–}3),$$

$$\ln K = -E/RT + \ln A \qquad (4\text{–}4).$$

The m value is a parameter related to i) reaction mechanism, ii) nucleation rate, iii) geometry of the nuclei (table 4–2 [48]), so that the m value gives us the information on the phase conversion mechanism from the 2212 to the 2223 phase.

Table 4–2. List of m value for the various conditions [48].

	Phase–boundary controlled	Diffusion controlled
Three–Dimensional Growth		
Constant Nucleation Rate	4	2.5
Zero Nucleation Rate	3	1.5
Decreasing Nucleation Rate	3–4	1.5–2.5
Two–Dimensional Growth		
Constant Nucleation Rate	3	2
Zero Nucleation Rate	2	1
Decreasing Nucleation Rate	2–3	1–2
One–Dimensional Growth		
Constant Nucleation Rate	2	1.5
Zero Nucleation Rate	1	0.5
Decreasing Nucleation Rate	1–2	0.5–1.5

In fig. 4–20, ln[–ln(1–C)] is plotted against lnt. The m values determined from the data ln[–ln(1–C)]>–3 in fig. 4–20 are 1.78, 1.50, 1.74, and 1.33 for 857, 854, 851, and 848°C, respectively. In the case of 848°C, the fractional conversion is limited to be less than 0.4. So, further discussion on the conversion mechanism is done for the results of 857, 854, and 851°C. The obtained m values (1.50–1.78) correspond to diffusion controlled three– or two–dimensional growth in table 4–2. As for the nucleation rate, it is unlikely that the nucleation rate is constant. In the CAP method, the nucleation of the 2223 phase is thought to occur at the interface between the whiskers and the liquid phase as shown in fig. 4–18. No nucleation spontaneously occurs inside the whiskers. This is supported by the fact that the apparent fractional conversion determined from the susceptibility measurement for the as–recovered CAP–treated whiskers is larger than that for the sample crushed into powder. This fact indicates that the nucleation and growth of the

2223 phase starts at the surface of the whiskers. The C–t curves, especially at 851°C, are sigmoid–shaped profile, indicating the existence of the induction period. In the frame–work of the nuclei growth model, nucleation occurs in the induction period and after that the phase conversion is rapidly accelerated. The induction period is not clear in the C–t curves at 854 and 857°C. In such a higher heating temperature, the nucleation is found to be completed in an early stage of the CAP treatment. Therefore, the nucleation rate is zero or decreasing during the phase conversion in the CAP method. The m values of the diffusion controlled three– or two–dimensional growth with zero or decreasing nucleation rate (table 4–2) are in agreement with that of the experimental values (1.50–1.78). Although it is difficult to determine which is more probable model, tree– or two–dimensional growth, from the experimental m values, the 2223 phase is more likely to fit to the two–dimensional one considering its crystal structure. Thick single crystals in the direction of the c–axis are hardly obtained in the Bi–system superconductors. Therefore, the diffusion controlled two–dimensional growth with decreasing nucleation rate is found to be most provable model for the phase conversion in the CAP method.

Figure 4–21 shows the lnK vs. 1/T plot. The apparent activation energy, E, calculated from the slop has a value of 1900 kJ/mol. Three experimental data of 857, 854, and 851°C are used to calculate the activation energy. The activation energy obtained here is comparable to that reported by Zhu and Nicholson [36] for bulk sample heated in air (E=1513 kJ/mol), while larger than that for bulk sample heated in 7.5% O_2 [38] (E=460 kJ/mol). As the CAP treatment has been done in air, this result indicates that the formation of the 2223 phase is easier in a lower oxygen partial pressure. Endo *et al.* have reported that the formation of the 2223 phase is much enhanced in a lower oxygen partial pressure due to the expansion of a temperature region of partial melting [7]. Therefore, the obtained apparent activation energy in the present experiment includes the effect of the partial melting of the calcined powder surrounding the whiskers. Such a high activation energy is unexpected from a simple diffusion processe. It seems more likely that the apparent activation energy for the phase conversion in the CAP method reflects not only

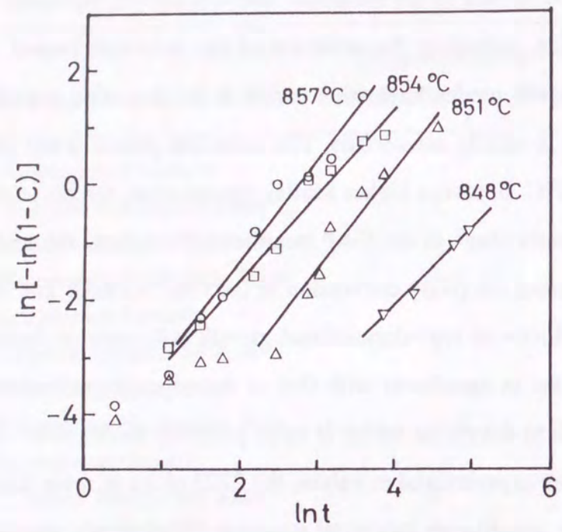

FIG. 4–20. Plot of ln[−ln(1−*C*)] vs lnt of the whiskers CAP–treated at 857, 854, 851, and 848°C using the no. 0 calcined powder.

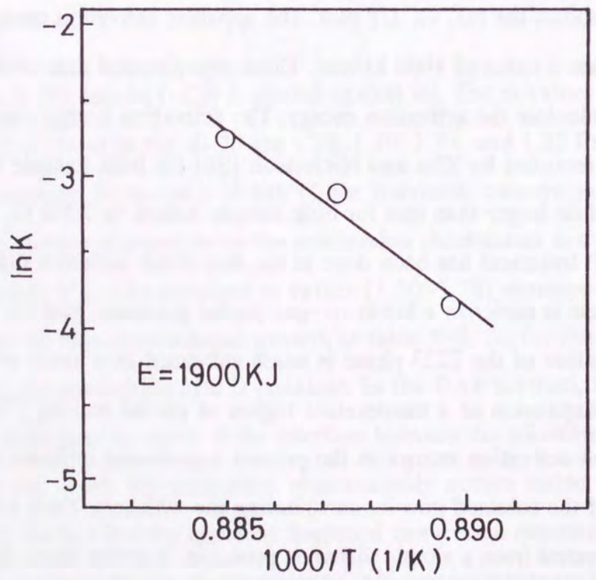

FIG. 4–21. Relation between lnK and 1/T.

the diffusion step but also the generation of the liquid phase needed for the initiation of the phase conversion (fig. 4–18) and the rearrangement at the interface between the 2212 and the 2223 phase including a bond departure process.

In summary, the CAP treatment has been applied to the 2212 whiskers using the calcined powder with various compositions. To obtain the pure 2223 whiskers, the composition of the calcined powder is important. The melting temperature of the calcined powder should be overlapped with the temperature region at which the whiskers can be recovered from the powder and the region of the 2223 phase formation. Only the $Bi_2Sr_2Ca_4Cu_6Pb_{0.5}O_x$ (no. 0) and $Bi_2Sr_2Ca_4Cu_6O_x$ (no. 5) powders satisfy these conditions, and actually the 2223 whiskers are obtained by the CAP method. The phase conversion is thought to proceed as follows. A liquid phase is generated in the powder around the 2212 whiskers. It reacts with the 2212 whiskers, resulting in the nucleation of the 2223 phase at the interface between the liquid phase and the whiskers. By supplying Ca, Cu, and Pb ions into the whiskers through the liquid phase, the 2223 phase spreads into the whiskers remaining the outline of the original crystal shape. From the kinetic study on the CAP method, the diffusion controlled two–dimensional growth with decreasing nucleation rate is most provable model for the phase conversion from the 2212 to the 2223 phase.

4–4. Critical Current Density

Copper based oxide superconductors, type II superconductors, have an upper critical field (H_{c2}) large enough to be used in practical uses, and have critical temperature (T_c) exceeding the liquid nitrogen temperature in the Y, Bi and Tl systems. However, critical current density (J_c) for the bulk materials is still rather low especially in magnetic fields. Accordingly, attention has been focused on the transport properties as a function of temperature, external magnetic field, and/or orientation of crystal relative to the external field. In the Bi system, the transport characteristics of the $Bi_2Sr_2CaCu_2O_x$ (2212) phase have been well investigated not only on polycrystalline bulk materials [51] but also on single crystals [52–54]. On the other hand, the J_c data of the $Bi_2Sr_2Ca_2Cu_3O_{10}$ (2223) compound have been limited only to polycrystalline Ag–sheathed wires [55–60], tapes [61, 62] and sintered pellets [63, 64], because single crystals of the 2223 phase with a size large enough to measure the transport J_c have not been obtained. This section describes the temperature and magnetic field dependence of J_c for the 2223 whiskers prepared by the CAP method.

Experimental

The 2223 whiskers were prepared by the CAP method as described in detail in section 4–2. The starting 2212 whiskers were prepared by heating a melt–quenched glass plate in a stream of O_2 gas at 865°C for 120 h (Chapter 2). The 2212 whiskers thus obtained were then embedded into a powder with the composition of $Bi_2Sr_2Ca_4Cu_6Pb_{0.5}O_x$ which had been calcined at 820°C for 20 h. The powder containing the whiskers was heated at 853°C for 180 h in air. After the heating, the whiskers were mechanically separated from the powder. The 2223 whiskers have the dimensions of 1–5 μm thick, 10–100 μm wide and 1–4 mm long. The 2223 whiskers maintain their original shape and

have the layered structure, while the smoothness of the surface is rather deprived due to the contact with the powder during the heating. J_c was measured by a standard four–probe method with a voltage criterion of 1 μV/cm. Fine (25 μm diameter) gold wires were attached to the sample using a silver epoxy which was fired at 350°C for 1 h in air. The J_c was measured in various constant magnetic fields. The magnetic field was applied parallel or perpendicular to the *ab* plane but always perpendicular to the current direction.

Results and discussion

The temperature dependence of the J_c in an ambient field for the 2223 whisker is shown in fig. 4–22 compared with the as–grown 2212 whisker. The zero–resistance temperature of the 2223 whisker used for the J_c measurement is 105.5 K. Both the 2212 and the 2223 whiskers show a similar behavior each other in the J_c–T curve, while the increase of J_c against temperature for the 2223 whisker is rather small. The 2223 whisker shows a J_c value of 1.0×10^5 A/cm^2 at 70 K and 6.1×10^4 A/cm^2 at 77 K. The highest J_c value in the 2223 samples is 7.3×10^4 A/cm^2 at 77 K. This value is comparable to the high quality 2212 single crystal grown from alkali chloride flux (5×10^4A/cm^2) [52], and higher than the polycrystalline samples [55–64]. Although the J_c decreases with the increase of temperature, it is still above 1×10^4 A/cm^2 at 96 K.

It is important to understand the mechanism which limits the J_c in the 2223 sample. There are three limiting factors being considered as follows: (1) depairing of the supercurrent, (2) weak links due to a poor superconducting coupling, (3) magnetic flux creep. The depairing current ($J_d(T)$) expected for this material is

$$J_d(T) = J_d(0)(1-t^2)(1-t^4)^{-1/2},$$

where $t=T/T_c$ and $J_d(0)=H_c(0)/3\sqrt{6}\pi\mu_0\lambda(0)=1.9\times10^7$ A/cm^2 [52]. Here $H_c(0)=1.06$ T and

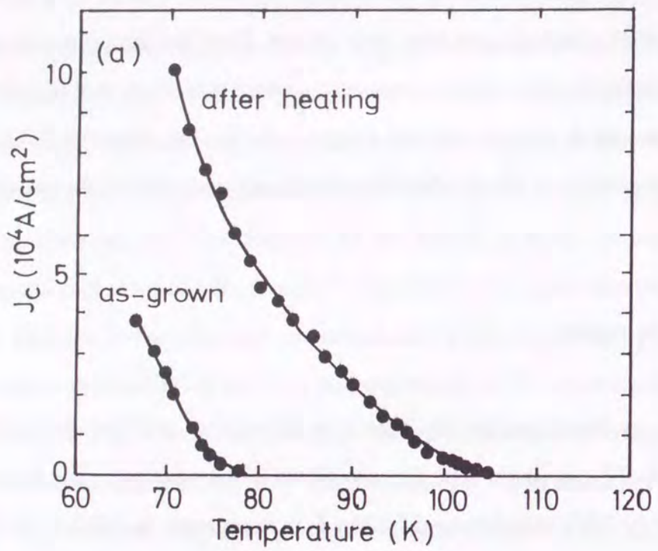

FIG. 4–22. Temperature dependence of J_c in an ambient field for the 2212 and the 2223 whiskers.

$\lambda(0)$=190 nm are used [65]. The J_d value is calculated to be 1.05×10^7 A/cm^2 at 77 K. For the zero applied field, the observed J_c (77 K) is smaller than the J_d (77 K) by a factor of 150. It has been reported that the observed J_c (77 K) is roughly a factor of 15 less than J_d (77 K) for the high quality $YBa_2Cu_3O_x$ and Bi–2212 single crystals [52]. In order to examine the possibility of the weak links in the 2223 whisker, we have analyzed the temperature dependence of J_c. The value of n in the relation of $J_c \propto (1-t)^n$, t being the reduced temperature T/T_c, gives the information on the weak links. In the polycrystalline superconductor with superconductor – normal metal – superconductor (SNS) junctions, a power law dependence with n=2 for T close to T_c has been predicted by de Gennes [66]. When superconducting grains are separated by an insulator (SIS junctions), the

model of $J_c \propto (1-t)$ has been proposed [67]. In the case of SINS junction, a 3/2 power dependence of J_c has been proposed on the basis of a proximity junction tunneling model [68, 69]. These relations are based on a condition that the coherence length is much lager than the lattice parameter. Recently, Deutscher have predicted the n=2 for the high–T_c oxide superconductor such as the Y–Ba–Cu–O compound in which SNS junctions are formed at twin boundaries inside the grains [70]. For the superconductor with a short coherence length of several tens of angstroms, the twin boundaries are considered to act as the normal metallic grain boundaries for the polycrystalline superconductor with a large coherence length.

Figure 4–23 shows the logarithmic plot of J_c versus (1–t) near T_c for the 2223 whisker. For temperatures with $1-t<0.03$ the straight line has a slope of n=2.0. The present result of n=2 for the 2223 whisker well agrees with the proposal of Deutscher, suggesting the existence of the similar varier as the twin boundary observed in the $YBa_2Cu_3O_x$ compound. The 2223 whiskers are grown by the diffusion of Ca, Cu, and Pb ions into the 2212 whiskers through a liquid phase (section 4–3). The phase conversion is initiated at many points on the surface of the 2212 whisker. Therefore, the orientation of the *a*– and *b*–axis can not be arranged in one direction in the CAP–treated 2223 whiskers, in contrast to the 2212 whiskers. The 2223 whiskers are thought to have twin boundaries where the *a*– and *b*–axis is discrete. This would be the reason that the 2223 whisker shows n=2 dependence in the relation of $J_c \propto (1-t)^n$ as in the case of the Y–Ba–Ca–O compound.

The magnetic field dependence of the J_c for the 2223 whisker and the 2212 whisker at 77 K is shown in fig. 4–24. The 2212 whisker contains Li as a dopant which is effective for increasing T_c (chapter 5), and has a zero resistance temperature of 81 K, higher than the liquid nitrogen temperature. A maximum of the J_c value is usually obtained when the magnetic field is aligned along the *ab* plane ($H \perp c$), and gradually decreases with the increase of magnetic field both for the 2212 and 2223 whiskers. The J_c is as high as 1×10^4 A/cm^2 for the 2223 whisker at H=1 T in the case of $H \perp c$. It is a

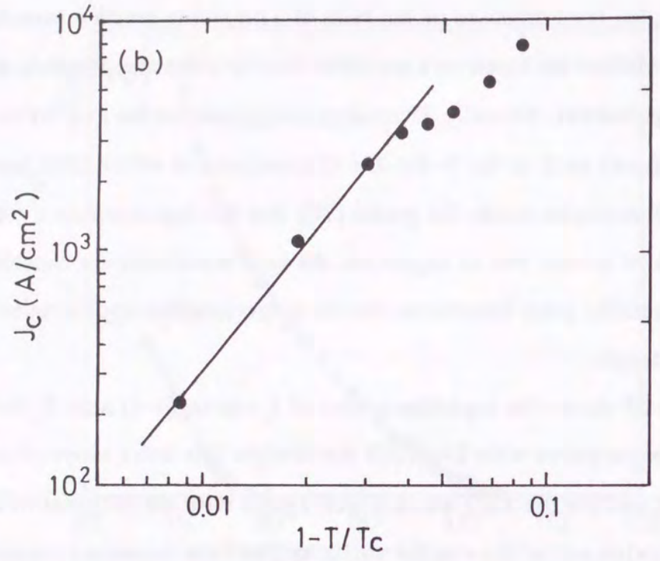

FIG. 4–23. Logarithmic plot of J_c vs. $(1-T/T_c)$ for the 2223 whisker.

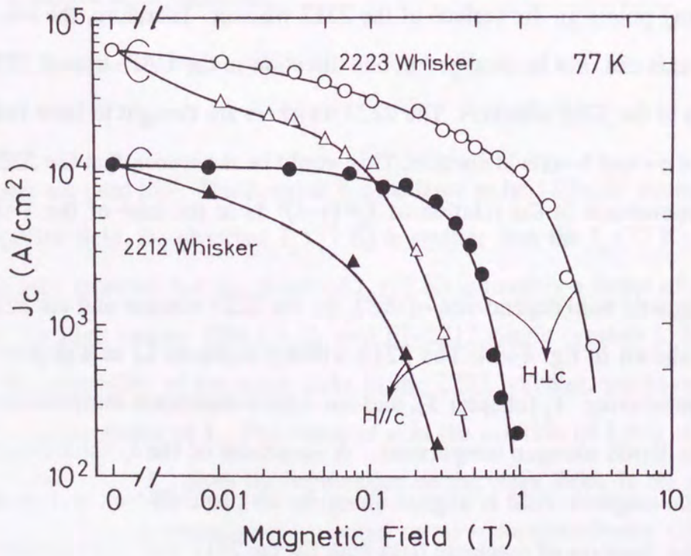

FIG. 4–24. Magnetic field dependence of the critical current density for the 2212 and the 2223 whiskers at 77 K.

hundred times larger than that of the 2212 whisker ($1x10^2$ A/cm^2) at 1 T. This would be attributed to the difference in the temperature margin between the zero resistance temperature and 77 K. For practical applications at the liquid nitrogen temperature, it is necessary to produce wires or tapes consisting of the 2223 phase. It is considered that the 2212 phase is suitable for practical uses at the liquid helium temperature.

The anisotropy in J_c of the 2223 whisker between H⊥*c* and H ∥ *c* is larger than that of the Ag sheathed polycrystalline tapes [56], especially in a higher magnetic field. This is interpreted by the difference in the degree of orientation. The polycrystalline sample often shows two steps of J_c drop in the J_c–H curve. The first step is due to a week coupling limitation on J_c, and the second one is attributed to the flux flow [71]. On the other hand, the first J_c drop is not observed for the whiskers in H⊥*c*, suggesting there is no week coupling such as grain boundaries along the whisker axis.

In summary, temperature and magnetic field dependence of J_c have been measured on the CAP–treated 2223 whiskers. The whisker yields a maximum J_c of $7.3x10^4$ A/cm^2 at 77 K, and J_c is higher than $1x10^4$ A/cm^2 even at 96 K in zero applied field. The 2223 whisker shows n=2 dependence in $J_c \propto (1-t)^n$ for T close to T_c. At 77 K the 2223 whisker shows the J_c values above $1x10^4$ A/cm^2 up to 1T, in contrast to the 2212 whisker ($1x10^2$ A/cm^2, H=1 T) which shows a steep decrease in J_c in magnetic field above 0.2 T.

4–5. Upper Critical Field and Anisotropy of $Bi_2Sr_2Ca_2Cu_3O_x$ Whiskers

One important feature of the high–T_c oxide superconductors is the degree of anisotropy of their superconducting properties derived from their layered crystal structure. It is essential for the understanding of the physical properties of these compounds to reveal what the significant factor for determining the anisotropy are. In the Tl and Bi systems, isostructural compounds with different number of CuO_2 planes are well known. These are considered to be a good model to examine the correlation between the degree of anisotropy and the number of CuO_2 planes. The evaluation of anisotropy for the cuprate superconductors has been made by upper critical field (H_{c2}), critical current density, resistivity, thermopower, fluctuation effects in conductivity, specific heat, and electronic structure, and others. Among these, the upper critical field is intrinsic to the superconductor because the H_{c2} is associated with microscopic currents on a length scale given by the vortex size [72]. For the $Tl_2Ba_2Ca_{n-1}Cu_nO_y$ (n=1, 2, 4) compounds, strong correlation between the upper critical field and the number of CuO_2 layers has been reported [73]. On the other hand, in the $Bi_2Sr_2Ca_{n-1}Cu_nO_x$ (n=1, 2, 3) compounds, although they are the more widely studied system, only for the $Bi_2Sr_2CaCu_2O_x$ (2212) has the anisotropy of H_{c2} been sufficiently studied [72]. The anisotropy study has been limited to only the polycrystalline samples for the 110 K $Bi_2Sr_2Ca_2Cu_3O_x$ (2223) compound [74–76] because large crystals of high quality have not previously been obtained.

This section describes the anisotropy of H_{c2} determined by the measurement of resistive transition curves in magnetic fields for the 2223 compound with T_c over 100 K. The 2223 whiskers are used for the measurement. The magnetic fields up to 7.5 T are applied parallel and perpendicular to the CuO_2 plane. An anisotropy factor of 31 has been obtained for H_{c2} defined at the conventional 50% value of the extrapolated normal–state resistivity in the magnetoresistance curves. The degree of anisotropy is discussed compared with the 2212 compound.

Experimental

The 2212 whiskers were prepared by heating glassy plates in a stream of O_2 gas, as previously described (chapter 2). The 2223 whiskers were prepared by the CAP method (section 4–2). The resistivity of the 2223 whisker used in this experiment decreases sharply at 110 K, and the zero–resistance state is achieved at 106.5 K. The Meissner curve shows a sharp decrease at around 110 K without any signal around 80 K due to the 2212 phase. The resistivity of the 2223 whisker is 380 μΩcm at room temperature and decreases linearly against temperature down to 130 K.

The magnetoresistance was measured by a standard four–probe method using a dc current of 0.05–0.5 mA along the *ab* plane. The electrical contact was made by using gold wires of 25 μm in diameter with silver epoxy. A magnetic field up to 7.5 T was applied parallel and perpendicular to the *c*–axis with a superconducting solenoid. The current was always perpendicular to the magnetic field. The accuracy of the alignment of magnetic field and sample orientation is approximately one degree. The 2223 whisker has some steps on the surface because of erosion during the annealing in the calcined powder. The result of scanning tunnel microscope (STM) observation indicates that the plateaus at the both sides of the step are flat and smooth, and they are mutually parallel. Therefore, magnetic field was actually aligned parallel and perpendicular to the *c*–axis within the experimental error of one degree.

Results and discussion

Figure 4–25 shows the resistive superconducting transition under the magnetic fields (H) up to 7.5 T perpendicular and parallel to the *c*–axis. As observed in other superconducting cuprates, the onset of superconductivity is far less sensitive to the field than the foot of the transition. A remarkable field–broadened transition is observed when

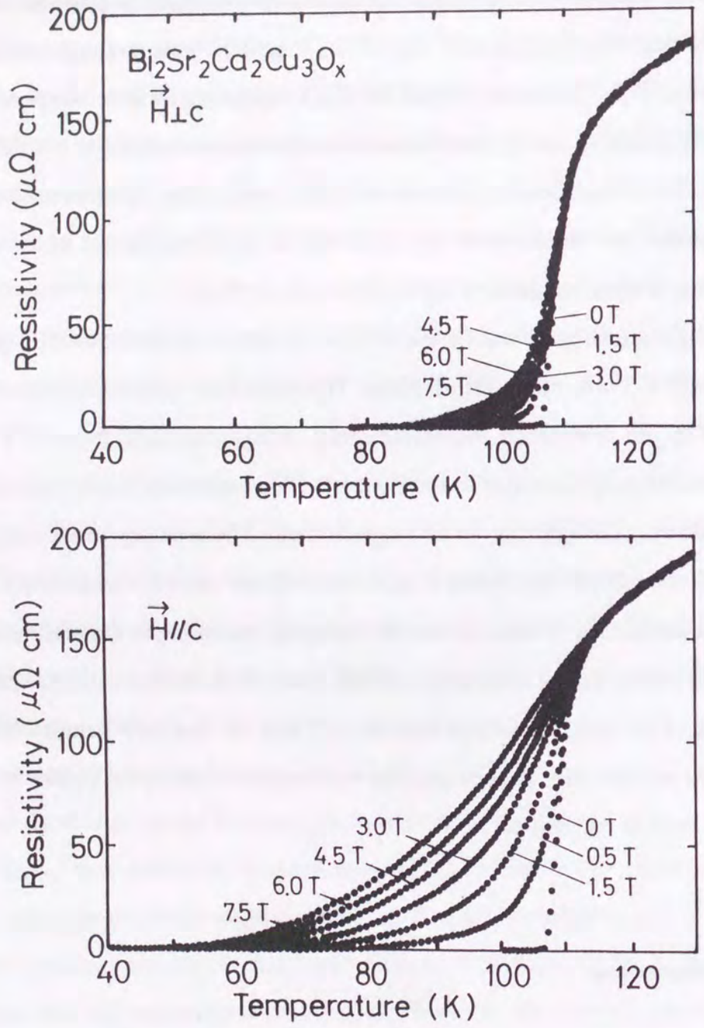

FIG. 4–25. Resistive transitions of the 2223 whisker in various magnetic fields perpendicular and parallel to the c–axis.

the field is parallel to the c–axis (H ∥ c). On the other hand, transition curves are less sensitive in perpendicular fields (H⊥c).

These data for H ∥ c–axis and H⊥c–axis in the low resistivity region replotted as logρ vs T^{-1} are shown in figs. 4–26 and 4–27. Palstra *et al.* have reported that the resistivity (under 1% of the normal–state resistivity) is thermally activated and described by an Arrhenius law, $\rho=\rho_0\exp(-U_0/T)$, for the 2212 single crystal [77]. As shown in fig. 4–26, the resistivity depends exponentially on T^{-1} over the wide resistivity range for the 2223 whisker, resulting a thermally activated behavior. The same behavior is obtained for the H⊥c–axis plotting (fig. 4–27). The activation energy U_0 has been calculated by fitting the Arrhenius law. The U_0 values are 1500, 940, 750, 700, 620, and 580 K for the H ∥ c–axis field of 0.5, 1.5, 3, 4.5, 6, and 7.5 T, and 2000, 1600, 1450, 1350, and 1280 K for the H⊥c–axis field of 1.5, 3, 4.5, 6, and 7.5 T, respectively. Figure 4–28 shows the activation energy U_0 as a function of magnetic field. The U_0 values are expressed by a power law: $U_0=1100H^{-0.30}$ K for 1.5 T<H(∥ c–axis)<7.5 T, and $U_0=2200H^{-0.27}$ K for 1.5 T<H(⊥c–axis)<7.5 T. The anisotropy in U_0 (factor of 2) is comparable to the 2212 single crystal [77]. However, the U_0 values are two or three times larger than that for the 2212 phase [77–79] and smaller than that of $YBa_2Cu_3O_x$ [79]. Because the activation energy U_0 has been thought to be related to the potential energy of flux pinning, it strongly depends on microstructual defects and can be enhanced by the introduction of effective pinning centers. If the single crystals are perfect, they would contain no pinning centers, unless they have intrinsic pinning centers [80]. In order to reveal the origin of the difference of U_0, microstructual effects or intrinsic pinning, between the 2223 and 2212 phases, microstructual studies are necessary.

The strong broadening of the transition curve in a magnetic field leads to quite different temperature dependence of H_{c2}, so the slopes of H_{c2}–T curve at T_c will depend strongly on the method of evaluation. Some definitions for H_{c2} from the magnetoresistance curve have been reported: $\rho(T)/\rho_N(T)=0.15$, 0.3, 0.5, 0.6, and 0.9, and $\rho=0$, which was obtained by extrapolation of the linear part of transition curve, where $\rho_N(T)$ is the

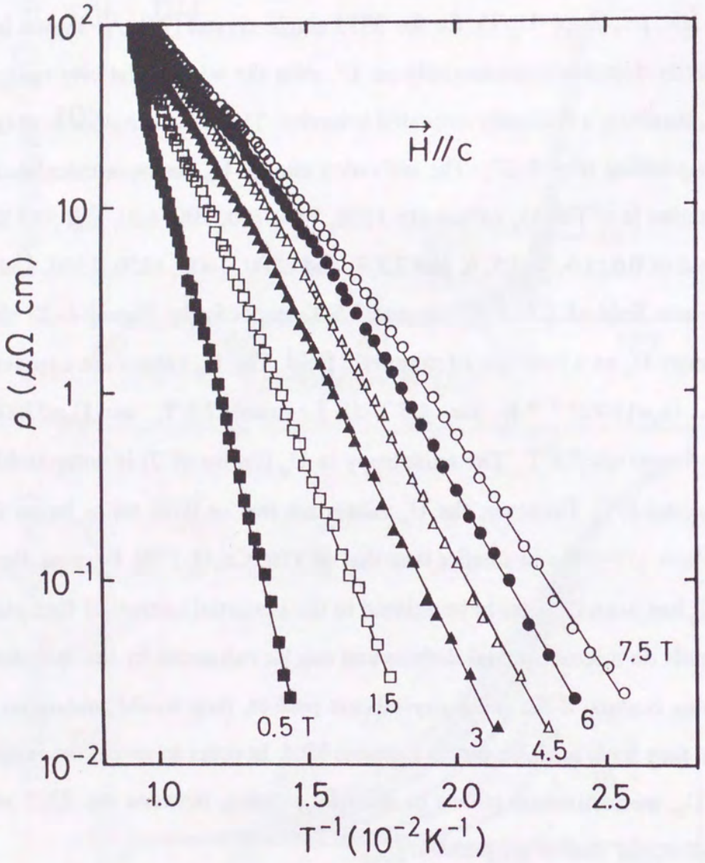

Fig. 4–26. Arrhenius plot of the resistivity of the 2223 whisker in magnetic fields parallel to the *c*–axis.

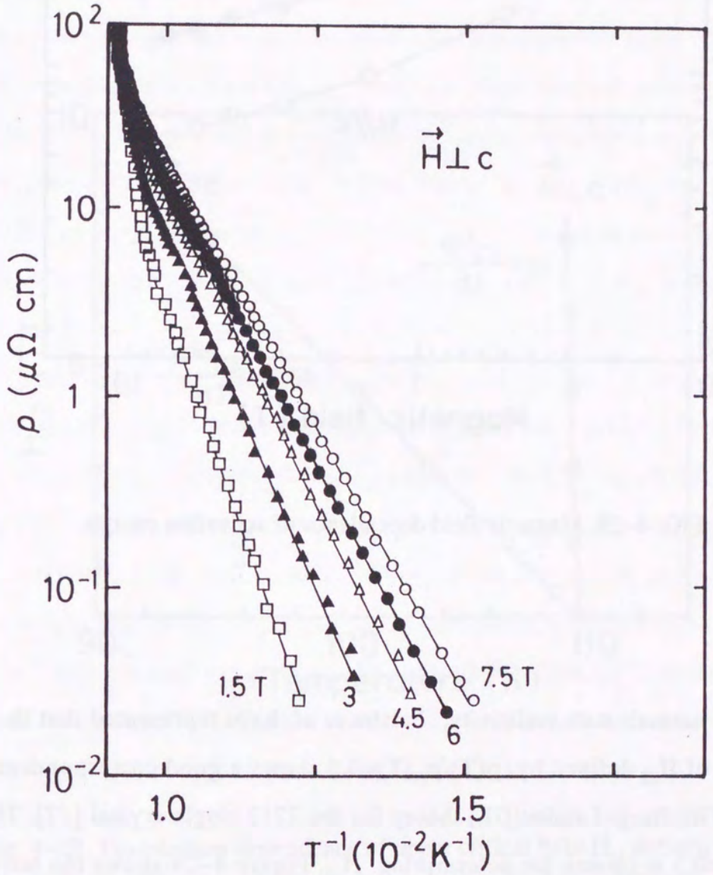

Fig. 4–27. Arrhenius plot of the resistivity of the 2223 whisker in magnetic fields perpendicular to the *c*–axis.

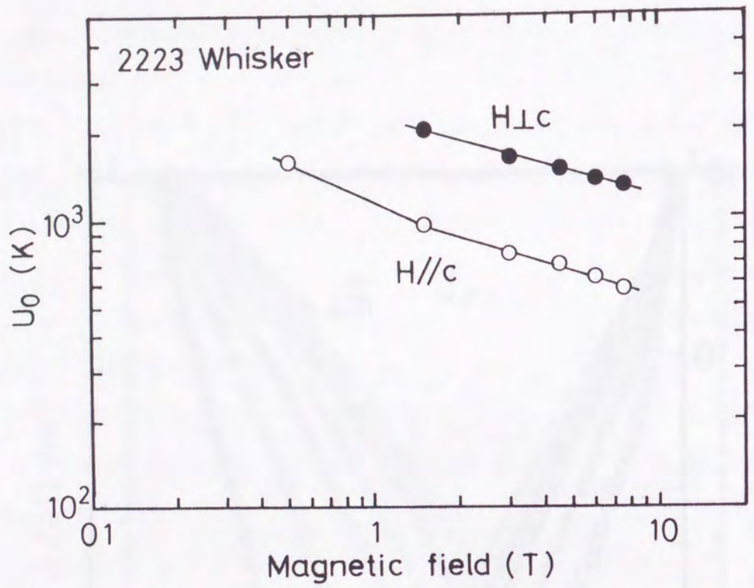

FIG. 4–28. Magnetic field dependence of activation energy.

extrapolated normal–state resistivity. Palstra *et al.* have represented that the angular dependence of H_{c2} defined by $\rho(T)/\rho_N(T)=0.5$ shows a good correspondence to the anisotropic Ginzburg–Landau(GL) theory for the 2212 single crystal [77]. Therefore, $\rho(T)/\rho_N(T)=0.5$ is chosen for determining H_{c2}. Figure 4–29 shows the temperature dependence of upper critical field. The 2223 whisker shows a linear relation for the H_{c2}–T curve for the alignments of H ∥ *c* and H⊥*c*. The H_{c2}–T curves with a slightly upward curvature near T_c have been observed for $YBa_2Cu_3O_x$ [81, 82], $Bi_2Sr_2CaCu_2O_x$ [83], $Tl_2Ba_2Ca_{n-1}Cu_nO_x$ (n=1, 2, 4) [73, 84], and $Nd_{1.85}Ce_{0.15}CuO_x$ [85] single crystals or thin films. However, a linear relation is also observed for 2212 thin films [86]. Suzuki and

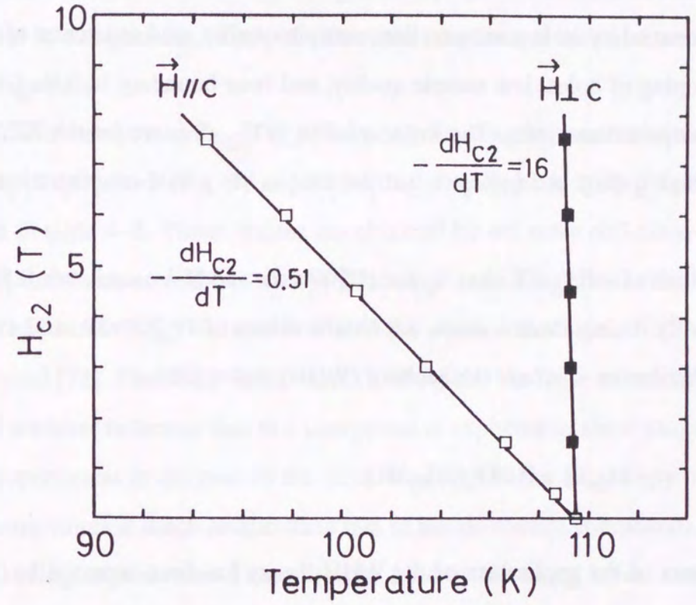

Fig. 4–29. Temperature dependence of upper critical field H_{c2} defined at the conventional 50% value of the extrapolated normal–state resistivity in the magnetoresistance curves.

Hikita have reported H_{c2}–T behavior for $La_{2-x}Sr_xCuO_4$ (x=0.1, 0.15, 0.3) thin films, which show slightly downward curvature, near linear relation, and upward curvature, respectively [87]. In these samples, $La_{1.85}Sr_{0.15}CuO_4$ compound shows the highest T_c value, i.e., has most optimum hole concentration. Han *et al.* have examined the H_{c2}–T behavior for various doped 2223 polycrystalline samples and suggested that increased sample quality leads to a more linear H_{c2} relation and second phase contributions may play a crucial role in the curvature [76]. The H_{c2}–T behavior defined by $\rho(T)/\rho_N(T)=0.5$ would be influenced by hole concentration, sample quality, and existence of impurity phase. Over doping of holes, low sample quality, and twin boundary in $YBa_2Cu_3O_x$ [88] tend to give an upward curvature. The linear relation in H_{c2}–T curve for the 2223 whisker assures of its high quality and indicates that the sample has a hole concentration near the optimum one.

The values of $-dH_{c2}/dT$ near T_c for H ∥ *c*–axis and H⊥*c*–axis are 0.51 and 16 T/K, respectively. Using these values, we obtain values of $H_{c2}(0)$=39 and 1210 T by applying the Werthamer–Helfand–Hohenberg (WHH) theory [89],

$$H_{c2}(0) = 0.69T_c(dH_{c2}/dT).$$

The effectiveness of the application of the WHH theory has been reported by Tajima *et al.* [82]. They have directly measured H_{c2} for the $YBa_2Cu_3O_x$ single crystal at 4.2 K by applying a pulsed magnetic field up to 50 T, and observed a good agreement with a prediction of WHH theory. The $H_{c2}(0)$ values are used to calculate the coherence length (ξ) from the Ginzburg–Landau relation:

$$\xi^2_{ab}(0) = \Phi_0/2\pi H_{c2}^{\parallel c}(0)$$

and

$$\xi_c(0) = \Phi_0/2\pi H_{c2}^{\perp c}(0)\xi_{ab}(0),$$

where Φ_0 is the flux quantum. We then obtain $\xi_{ab}(0)$=29 Å and $\xi_c(0)$=0.93 Å , and an anisotropy ratio of 31. It should be noted that the coherence lengths would be overestimated because the H_{c2} values are estimated from the field–broadened transition curves, which involve thermally activated resistivity as shown in figs. 4–26 and 4–27. The intrinsic coherence lengths would be shorter than the values obtained here. However, it is significant to compare the values of coherence lengths and the anisotropy with that for other compounds.

Critical temperatures, $-dH_{c2}/dT$, coherence lengths, and anisotropy ratios for $Bi_2Sr_2Ca_{n-1}Cu_nO_x$ (n=2 [72], 3) and $Tl_2Ba_2Ca_{n-1}Cu_nO_x$ (n=1, 2, 4) [73, 80] compounds are listed in table 4–3. These values are obtained by the same definition of H_{c2} [$\rho(T)/\rho_N(T)=0.5$] and the same analysis with WHH theory and GL relations. The $\xi_{ab}(0)$ value of 29 Å in the present 2223 whisker is almost the same as the value of 27 Å for the 2212 single crystal [72]. The small $\xi_c(0)$ value (0.93 Å) and the large anisotropy ratio (31) for the 2223 whisker indicates that this compound is expected to show strong two dimensional properties as in the case of the 2212 compound. The anisotropy ratio of the Tl–system compounds is much smaller than that of the Bi–system compounds, although they have an analogous structure. Therefore, the kind of "blocking layer" that separates the CuO_2 layers is one of the intrinsic factors for determining the degree of anisotropy. For the $Tl_2Ba_2Ca_{n-1}Cu_nO_x$ (n=1, 2, 4) compounds, Mukaida *et al.* have reported that the $\xi_c(0)$ decreases as the number of CuO_2 layers decreased, while the $\xi_{ab}(0)$ is almost independent of n [73]. Although the coherence lengths, especially $\xi_c(0)$, would be overestimated due to misalignment, the same tendency is observed for the $Bi_2Sr_2Ca_{n-1}Cu_nO_x$ (n=2, 3). These results suggests that the ratio of thickness between "blocking layer (Bi_2O_2)" and "mediating layer" [90] which contains CuO_2 layers inside the blocking layer would be another important factor for determining the degree of anisotropy.

In conclusion, the magnetoresistance for the 2223 whisker has been measured.

Table 4–3. Critical temperature, $-dH_{c2}/dT$, coherence lengths, and anisotropy ratio for $Bi_2Sr_2Ca_{n-1}Cu_nO_x$ (n=2, 3) and $Tl_2Ba_2Ca_{n-1}Cu_nO_x$ (n=1, 2, 4) compounds.

compounds	$T_{c,zero}$ (K)	$-dH_{c2}^{\parallel c}/dT$ (T/K)	$-dH_{c2}^{\perp c}/dT$ (T/K)	$\xi_{ab}(0)$ (Å)	$\xi_c(0)$ (Å)	Anisotropy ratio	Ref.
$Bi_2Sr_2Ca_2Cu_3O_x$	106.5	0.51	16	29	0.93	31	present
$Bi_2Sr_2CaCu_2O_x$	81	0.75	45	27	0.45	60	[72]
$Tl_2Ba_2CuO_x$	86	0.36	5	52	3	14	[73]
$Tl_2Ba_2CaCu_2O_x$	97	0.4	1.8	31	6.8	4.5	[73]
$Tl_2Sr_2Ca_3Cu_4O_x$	93	0.25	1.1	45	10	4.4	[73, 82]

Linear relation is obtained in H_{c2}–T curve defined at $\rho(T)/\rho_N(T)=0.5$, and according to the WHH theory and the GL relations, the coherence lengths of $\xi_{ab}(0)=29$ Å and $\xi_c(0)=0.93$ Å are obtained for the 2223 phase. The large anisotropic factor of coherence length (31) and the small $\xi_c(0)$ value indicate that the 2223 compound is expected to show strong two dimensional properties.

References

[1] C.Michel, H.Hervieu, M.M.Bolel, A.Grandia, F.Deslandes, J.Provost and B.Raveau, Z.Phys., **B68**, 421(1987).

[2] J.Akimitsu A.Yamazaki, H.Sawa, and H.Fujiki, Jpn.J.Appl.Phys., **26**, L2080(1987).

[3] H.Maeda, Y.Tanaka, M.Fukutomi, and T.Asano, Jpn.J.Appl.Phys., **27**, L209(1988).

[4] J.L.Tallon, R.G.Buckley, P.W.Gilberd, M.R.Preland,I.W.M.Brown, M.E.Bowden, L.A.Christian, and R.Goguel, Nature, **333**, 153(1988).

[5] T.Hatano, K.Aota, S.Ikeda, K.Nakamura and K.Ogawa, Jpn.J.Appl.Phys., **27**, L2055(1988).

[6] D.Shi, M.Tang, K.Vandervoort, and H.Claus, Phys.Rev. B, 39, 9091 (1989).

[7] U.Endo, S.Koyama, and T.Kawai, Jpn.J.Appl.Phys., **27**, L1476 (1988).

[8] A.Sumiyama, T.Yoshitomi, H.Endo, J.Tsuchiya, N.Kijima, M.Mizuno, and Y.Oguri, Jpn.J.Appl.Phys., **27**, L542(1988).

[9] S.A.Sunshine, T.Siegrist, L.F.Schneemeyer, D.W.Murphy, R.J.Cava, B.Batlogg, R.B.VanDover, R.M.Fleming, S.H.Glarum, S.Nakahara, R.Farrow, J.J.Krajewski, S.M.Zahurak, J.V.Waszczak, J.H.Marshall, P.Marsh, L.W.Rupp,Jr., and W.F.Peck, Phys.Rev. B, **38**, 893 (1988).

[10] M.Takano, J.Takada, K.Oda, H.Kitaguchi, Y.Miura, Y.Ikeda, Y.Tomii, and H.Mazaki, Jpn.J.Appl.Phys., **27**, L1041(1988).

[11] Y.Hidaka, Y.Tanaka, M.Fukutomi, and T.Asano, Jpn.J.Appl.Phys., **27**, L209(1988).

[12] J.J.Lin, E.L.Benitez, S.J.Poon, M.A.Subramanian, J.Gopalakrishnan, and A.W.Sleight, Phys.Rev.B **38**, 5095(1988).

[13] T.F.Ciszek, J.P.Goral, C.D.Evans and H.Katayama-Yoshida, J.Cryst.Growth, **91**, 312(1988).

[14] S.Kishida, H.Tokutake, S.Nakanishi, H.Fujimoto, K.Nishimori, N.Ishihara, Y.Watanabe, and W.Futo, J.Cryst.Growth, **99**, 937(1990).

[15] L.F.Schneemeyer, R.V.van Dover, S.H.Clarum, S.A.Sunshine, R.M.Fleming, B.Batlogg, T.Siegrist, J.H.Marshall, J.V.Waszczak, and L.W.Rupp, Nature, **332**, 423(1988).

[16] T.Shishido, D.Shindo, K.Ukei, T.Sasaki, N.Toyota, and T.Fukuda, Jpn.J.Appl.Phys., **28**, L791(1989).

[17] Y.Kubo, K.Michisita, Y.Higashida, M.Mizuno, H.Yokoyama, N.Shimizu, E.Inukai, N.Kuroda, and H.Yoshida, Jpn.J.Appl.Phys., **28**, L606(1989).

[18] R.S.Feigelson, D.Gazit, D.K.Fork, and T.H.Geball, Science, **240**, 1642 (1988).

[19] D.Gazit and R.S.Feigelson, J.Cryst.Growth, **91**, 318(1988).

[20] S.Takekawa, H.Nozaki, A.Umezono, K.Ksuda, and H.Kobayashi, J.Cryst.Growth, **92**, 687(1988).

[21] K.Shigematsu, H.Takei, I.Higashi, K.Hoshino, H.Yakahara, and M.Aono, J.Cryst.Growth, **100**, 661(1990).

[22] H.Komatsu, Y.Kato, S.Miyashita, T.Inoue, and S.Hayashi, Physica C, **190**, 14(1991).

[23] I.Matsubara, H.Tanigawa, T.Ogura, H.Yamashita, M.Kinoshita, and T.Kawai, Appl.Phys.Lett., **58**, 409 (1991).

[24] I.Matsubara, H.Tanigawa, T.Ogura, H.Yamashita, M.Kinoshita, and T.Kawai, Proc. of the 3rd International Symposium on Superconductivity, 786 (1991).

[25] D.Shi, M.S.Moley, J.G.Chen, M.Xu, K.Vandervoort, Y.X.Liao, A.Zangvil, J.Akujieze, and S.Segre, Appl.Phys.Lett., **55**, 699 (1989).

[26] A.Kapitulnik, M.R.Beasley, C.Castellani, and C.DiCastro, Phys.Rev. B, **37**, 537 (1988).

[27] H.Nobumasa, K.Shimizu, Y.Kitano, and T.Kawai, Jpn.J.Appl.Phys., **27**, L846 (1988).

[28] N.Kijima, H.Endo, J.Tsuchiya, A.Sumiyama, M.Mizuno, and Y.Oguri, Jpn.J.Appl.Phys., **27**, L1852 (1988).

[29] T.Uzumaki, K.Yamanaka, N.Kamehara, and K.Niwa, Jpn.J.Appl.Phys., **28**, L75 (1989).

[30] Y.Chen and R.Stevens, J.Am.Ceram.Soc., **75**, 1150 (1992).

[31] P.E.Morgan, R.M.Housley, J.R.Porter, and J.J.Ratto, Physica C, **176**, 279 (1991).

[32] D.Shi, M.Tang, M.S.Boley, M.Hash, K.Vandervoort, H.Claus, and Y.L.Lwin, Phys.Rev.B, **40**, 2247 (1989).

[33] Q.Feng, H.Zhang, S.Feng, X.Zhu, K.Wu, Z.Liu, and L.Xue, Solid State Commun., **78**, 609 (1991).

[34] G.K.Pakam, R.B.Tripathi, M.Sharma, D.K.Suri, S.U.M.Rao, K.C.Nagpal, and B.K.Das, Solid State Commun., **80**, 271 (1991).

[35] J.Thuchiya, E.Hozumi, N.Kijima, A.Sumiyama, M.Mizuno, and Y.Oguri, Jpn.J.Appl.Phys., **28**, L1918 (1989).

[36] W.Zhu and P.S.Nicholson, J.Mater.Res., **7**, 38 (1992).

[37] S.Chaudhry, N.Khare, and A.K.Gupta, J.Mater.Res., **7**, 2027 (1992).

[38] J.S.Luo, N.Merchant, V.A.Maroni, D.M.Gruen, B.S.Tani,W.L.Carter, and G.N.Riley Jr., Appl.Supercon., **1**, 101 (1993).

[39] V.Manivannan, J.Gopalakrishman, and C.N.R.Rao, Phys.Rev.B, **43**, 8686 (1991).

[40] Y.Iwai, N.Sato, T.Sasagawa, H.Saito, and M.Takata, Physica C, **186–189**, 641 (1991).

[41] R.Ramesh, G.Thomas, S.Green, C.Jiang, Y.Mei, M.L.Rudee, and H.L.Luo, Phys.Rev.B, **38**, 7070 (1988).

[42] E.Chavira, R.Escudero, D.Rios–Jara, and L.M.Leon, Phys.Rev.B, **38**, 9272(1988).

[43] B.L.Ramakrishna, J.C.Barry, Z.Iqbal, E.W.Ong, A.Bose, and H.Eckharadt, Physica C, **158**, 203 (1989).

[44] S.Narumi, H.Ohfsu, I.Iguchi, and R.Yoshizaki, Jpn.J.Appl.Phys., **28**, L27 (1989).

[45] H.Endo, J.Thuchiya, N.Kijima, A.Sumiyama, M.Misuno, and Y.Ogiri, Jpn.J.Appl.Phys., **27**, L1906 (1988).

[46] S.Horiuchi, K.Shoda, H.Nozaki, Y.Onoda, and Y.Matsui, Jpn.J.Appl.Phys, **28**, L621 (1989).

[47] *High Temperature Superconductors*, ed. P.Vincenzini (Elsevier Science Publishers, 1991) p. 293.

[48] S.F.Hulbert, J.Br.Ceram.Soc., **6**, 11 (1969).

[49] D.Ternbull, *Solid State Physics*, Vol.3 (Academic Press, New York, 1956) p. 252.

[50] R.Chiba and N.Funakoshi, J.Non–Cryst.Solids, **38–39**, 741 (1980).

[51] K.Heine, J.Tenbrink, and M. Thoner, Appl.Phys.Lett., **55**, 2441 (1989).

[52] R.B.van Dover, L.F.Schneemeyer, E.M.Gyorgy, and J.V.Waszczak, Appl.Phys.Lett., **52**, 1910 (1988).

[53] Donglu Shi, Ming Tang, Y.C. Chang, P.Z.Jiang, K.Vandervoort, B.Malecki, and D.J.Lam, Appl.Phys.Lett., **54**, 2358 (1989).

[54] S.Nomura, Y.Yamada, T.Yamashita, and H.Yoshino, J.Appl.Phys., **67**, 547 (1990).

[55] T.Hikata, K. Sato, and H.Hitotsuyanagi, Jpn.J.Appl.Phys., **28**, L82 (1989).

[56] Y.Yamada, K.Jikihara, T.Hasebe, T.Yanagiya, S.Yasuhara, M.Ishihara, T.Asano, and Y.Tanaka, Jpn.J.Appl.Phys., **29**, L456 (1990).

[57] K.Sato, T.Mikata, M.Ueyama, T.Kato, T.Masuda, N.Nagata, K.Iwata, and T.Misui, IEEE Trans. Magn., **27**, 1231 (1991).

[58] Y.Yamada, B.Obst, and R.Flukiger, Supercond. Sci. Technol., **4**, 165 (1991).

[59] L.R.Motowidlo, E.Gregory, P.Haldar, J.A.Rice, and R.D.Blaugher, Appl.Phys.Lett., **59**, 736 (1991).

[60] K.Chen, L.Homg, H.S.Koo, C.Y.Shei, L.P.Wang, C.Chiang, T.J.Yang, W.H.Lee, and P.T.Wu, Appl.Phys.Lett., **59**, 1635 (1991).

[61] M.Mimura, H.Kumakura, K.Togano, and H.Maeda, Appl.Phys.Lett., **54**, 1582 (1989).

[62] H.Kumakura, K.Togano, H.Maeda, E.Yanagisawa, and T.Morimoto, Jpn.J.Appl.Phys., **28**, L176 (1989).

[63] Y.Tanaka, T.Asano, K.Jikihara, M.Fukutomi, J.Machida, and H.Maeda, Jpn.J.Appl.Phys., **27**, L1655 (1988).

[64] M.Matsuda, Y.Iwai, M.Takata, M.Ishii, T.Yamashita, and H.Koinuma, Jpn.J.Appl.Phys., **27**, L1650 (1988).

[65] Q.Li, M.Suenaga, J.Gohng, D.K.Finnemore, T.Hikata, and K.Sato, Phys.Rev. B, **46**, 3195(1992).

[66] P.G.de Gennes, Rev.Mod.Phys., **36**, 225 (1964).

[67] V.Ambegaokar, and A. Baratoff, Phys.Rev.Lett., **10**, 486 (1963).

[68] S.Greenspoon and H.J.T.Smith, Canad.J.Phys, **49**, 1350 (1971).

[69] S.Nagata and H.C.Yang, Physica B, 108, 997 (1981).

[70] Deutscher and K.A.Muller, Phys.Rev.Lett., **59**, 1745 (1987).

[71] J.W.Ekin, T.Larson, A.M.Herman, Z.Z.Sheng, K.Togano, and H.Kumakura, Physica **C162–164**, 671 (1989).

[72] T.T.M.Palstra, B.Batlogg, L.F.Schneemeyer, and R.J.Cava, Phys.Rev. B **38**, 5102 (1988).

[73] H.Mukaida, K.Kawaguchi, M.Nadao, H.Kumakura, D.R.Dietderich, and K.Togano, Phys.Rev. B **42**, 2659 (1990).

[74] N.Kobayashi, H.Kawabe, K.Kusaba, M.Kikuchi, Y.Shono and Y.Muto, Physica C **162–164**, 27 (1989).

[75] C.G.Cui, J.L.Zhang, S.L.Li, J.Li, F.Shi, S.Z.Zhou, Z.H.Shi, and J.Dou, Solid State Commun., **70**, 287 (1989).

[76] S.H.Han, Z.Hegedus, M.Andersson, M.Nygren, O.Rapp, Y.F.Yan, Q.Chen, Y.N.Wei, and Y.S.He, Physica C **169**, 250 (1990).

[77] T.T.M.Palstra, B.Batlogg, L.F.Schneemeyer, and J.V.Waszczak, Phys.Rev.Lett., **61**, 1662 (1988).

[78] Y.Jia and J.A.Wilson, Solid State Commun., **71**, 191 (1989).

[79] N.Kobayashi, H.Iwasaki, H.Kawabe, K.Watanabe, H.Yamane, H.Kurosawa, H.Hasumoto, T.Hirai, and Y.Muto, Physica C, **159**, 295 (1989).

[80] M.Murakami, M.Morita, and N.Koyama, Jpn.J.Appl.Phys., **28**, L1754 (1989).

[81] B.J.Dalymple and D.E.Prober, J.Low Temp.Phys., **56**, 545 (1987).

[82] Y.Tajima, M.Hikita, T.Ishii, H.Fute, K.Sugiyama, M.Date, A.Yamagishi, A.Katsui, Y.Hidaka, T.Iwata, and S.Tsurumi, Phys.Rev.B, **37**, 7956 (1988).

[83] Y.Koike, T.Nakanomyo, and T.Fukase, Jpn.J.Appl.Phys., **27**, L1057 (1988).

[84] K.Togano, H.Kumakura, H.Mukaida, K.Kawaguchi, and M.Nakao, Jpn.J.Appl.Phys., **28**, L907 (1989).

[85] M.Suzuki and M.Hikita, Phys.Rev.B, **41**, 9566 (1990).

[86] J.H.Kang, R.T.Kampwirth, and K.E.Gray, Appl.Phys.Lett., **52**, 2080 (1988).

[87] M.Suzuki and M.Hikita, Jpn.J.Appl.Phys., **28**, L1368 (1989).

[88] J.S.Moodera, R.Meservey, J.E.Tkaczyk, C.K.Hao, G.A.Gibson, and P.M.Tedrow, Phys.Rev.B, **37**, 619 (1988).

[89] N.R.Werthamer, E.Helfand, and P.C.Hohemberg, Phys.Rev. **147**, 295 (1966).

[90] N.Nobumasa, K.Simizu, and T.Kawai, Physica C **167**, 515 (1990).

Chapter 5

Effects of Li–Doping on the Superconducting Properties of Bi–based Superconducting Whiskers

5–1. Introduction

The critical temperature (T_c) of p–type cuprate superconductors depends on several parameters. Hole concentration is one of the most important factors for determining T_c. For the Y and the La–systems, the change of the oxygen content and the substitution of alkaline earth metal (Ca, Sr, Ba) for the La site are the main ways for alternating the hole concentration, respectively. On the other hand, lots of factors have been reported to change T_c in the Bi–system. Content of oxygen [1–4], defects in alkaline earth metal sites [5], and substitution of Bi for alkaline earth metal [6] influence on the hole concentration. Substitution of Ba in the Sr site changes the structural parameters such as Cu–O bond length in the CuO_2 plane and the distance between the CuO_2 layers, resulting in the alternation of T_c [7–11]. Because the superconducting phases of the Bi–system allow a wide range of compositional alternation for building themselves, such defects or intrasubstitution as described above are observed. This makes for a complex situation in the Bi–system compared with the La– and the Y–systems. Therefore, a study of effects of substitution on T_c in the Bi–system needs a careful analysis taking into account other possible factors influencing on T_c in a proper way.

In many reports on substitutional experiments in the Bi–system, Li–doping has attracted much attentions because of the effectiveness in increasing T_c for the $Bi_2Sr_2CaCu_2O_x$ (2212) phase. The Li–doping has been achieved by various methods, such as conventional powder reaction method [12–14], electorochemical method [15,16], melt–processing [17,18], laser ablation method [19], floating zone method [20], and chemical reaction method using n–butyl lithium [21,22]. These methods have confirmed

the effectiveness of Li–doping on T_c of the 2212 compound. Although several mechanisms have been proposed for the effectiveness of Li–doping such as optimization of hole concentration [14,15,17,21,22], change of cation ratio [17], and the change of electronic structure [13], the detailed mechanism has not been authenticated yet.

As for the $Bi_2Sr_2Ca_2Cu_3O_x$ (2223) compound, it has attracted much attention in the field of superconductivity research because of its high T_c over 100K. This material, however, is so delicate to synthesize that no one has reported the formation of single crystals of this compound. Even in the substitution experiment for the polycrystalline compound, only Pb doping has been proved to be effective to stabilize the 2223 phase, although no effect has been observed on the T_c value. That is, the improvement of T_c by the doping of other element has been unsuccessful. Because of these difficulty, the fundamental superconducting properties of the 2223 phase have not been sufficiently examined. This undeveloped field is one of the most interesting themes for the understanding of high T_c superconductivity.

In this chapter, the preparation of the Li–doped 2212 whiskers by the glass annealing method and the enhancement of T_c by doping Li in them are described [23,24]. In addition, Li–doped 2223 whiskers have been prepared by the CAP method as described in the previous chapter. Both the phase conversion from the 2212 phase to the 2223 phase and Li–doping have been simultaneously achieved by this method. The Li–doping into the 2223 phase would give us further important insights into the role of Li in the Bi–based superconductors. It has been confirmed that the Li–doping is effective in increasing T_c in the 2223 phase, too [25]. It is important to know the content and site of the doped Li ions in order to understand the reason for the increase of T_c. However, these factors are still unclear because the Li–doped 2212 sample has been limited in powder or polycrystalline bodies. For clarifying the role of Li, high quality samples doped with Li are required. Recently, preparation of the Li–doped 2212 single crystals by a self–flux method has been reported [26]. The Li–doped 2212 and 2223 whiskers are also considered to be useful for clarifying the reason of the enhancement of T_c. The enhancement

mechanism of T_c by Li–doping is discussed from the results of compositional analysis, measurement of the *c*–axis lattice parameter, and the annealing experiment under a reduced pressure to change the oxygen content [27].

5–2. Effects of Li–doping on the Superconducting Properties of $Bi_2Sr_2CaCu_2O_x$ Whiskers

In this section, the superconducting properties of Li–doped $Bi_2Sr_2CaCu_2O_x$ (2212) whiskers grown from the melt–quenched glass plate with various initial compositions are described. To clarify the effect of Li–doping, the influence of other elements, Na, K, Ga, Ge, Sb, Te, and Pb on the growth of whiskers and on the superconducting properties has also been examined. The zero resistance temperature ($T_{c,zero}$) of the Li–doped whiskers increases with increasing the Li content up to 82 K for the 2212 phase. The 2212 whiskers contain the $Bi_2Sr_2Ca_2Cu_3O_x$ (2223) phase as a minor phase, and the ability of $T_{c,zero}$=112 K for the 2223 phase has been obtained as determined by extrapolation of the resistance drop. A maximum critical current density (J_c) of $3.4x10^4$ A/cm^2 at 77 K and $3x10^5$ A/cm^2 at 66 K in a zero applied field is obtained for these whiskers. The magnetic field dependence of J_c with H ∥ *c* and H⊥*c* has also been examined for the Li–doped whisker at 77 K.

Experimental

Powders of Bi_2O_3, $SrCO_3$, $CaCO_3$, CuO and the oxides or carbonates of additional elements were mixed as listed in table 5–1. Powders of Li_2CO_3, Na_2CO_3, K_2CO_3, Ga_2O_3, GeO_2, Sb_2O_5, TeO_2 and PbO were used as source materials for additional elements. The mixed powders were melted in an alumina crucible at 1200°C for 30 min in air. The melts were poured onto a steel plate and were pressed quickly. The thickness of the resulting quenched glass plates was 0.5–1.0 mm. The glass plates were heated on an alumina boat at 840 or 860°C (table 5–1) for 120 h in a stream of O_2 gas (150 ml/min) and were cooled to room temperature in the furnace. Whiskers grew perpendicularly to the surface of the crystallized glass plates for all the samples. The dimensions of the

whiskers were 1–10 μm thick, 10–500 μm wide and 1–10 mm long.

The temperature dependence of the resistance and J_c were measured by the standard four–probe method. Determination of growing phase and the *c*–axis lattice parameter was carried out using a RIGAKU X–ray diffractometer equipped with a Cu–Kα wavelength. The susceptibility was measured with a superconducting quantum interference device (SQUID: Quantum Design $MPMS_2$) magnetometer. The content of Li in the Li–doped 2212 whiskers was determined by atomic absorption analysis. The DTA curve was obtained by increasing the temperature from a room temperature to 1000°C at a constant heating rate of 10°C/min.

Table 5–1. List of sample, initial composition, and heating temperature.

	Composition						
Sample	Bi	Sr	Ca	Cu	Li	Other elements	Heating temp.,°C
undoped	2	1.9	2.2	4	--	--	860
Li(0.25)	2	1.9	2.2	4	0.25	--	840
Li(0.5)	2	1.9	2.2	4	0.5	--	840
Li(0.75)	2	1.9	2.2	4	0.75	--	840
Li(0.7)	2.2	1.8	1.05	1.45	0.7	--	840
Na(0.5)	2	1.9	2.2	4	--	0.5(Na)	840
K(0.5)	2	1.9	2.2	4	--	0.5(K)	840
Ga(0.5)	2	1.9	2.2	4	--	0.5(Ga)	840
Ge(0.5)	2	1.9	2.2	4	--	0.5(Ge)	840
Sb(0.5)	2	1.9	2.2	4	--	0.5(Sb)	840
Te(0.5)	2	1.9	2.2	4	--	0.5(Te)	840
Pb(0.5)	2	1.9	2.2	4	--	0.5(Pb)	840

Results and discussion

Additional elements have been chosen from alkaline metal (Li, Na, K), IIIb group (Ga), IVb group (Ge, Pb), Vb group (Sb) and VIb group (Te). Heating temperature of the glass plates for the whisker growth is listed in table 5–1. The most appropriate growing temperature for the samples is different from each other. In the case of undoped sample, which is regarded as the standard sample without additional elements, the whisker growth is not observed at 840°C. A higher heating temperature (860°C) is necessary to grow the undoped whiskers. A heating temperature of 840°C is suitable for the whisker growth in other samples containing additional element in the glass plate. In the DTA measurements of the glass plates, three endothermic peaks are observed in the range of 800 to 930°C in each sample. It has been reported that the lower two peaks are due to partial melting and the higher one is due to decomposition [28]. These peaks of the undoped sample are sifted toward higher temperatures than those of the other samples. Thus the additional elements listed in table 5–1 are effective to decrease the melting temperature in Bi–Sr–Ca–Cu–O system. The temperature for the whisker growth lies in the range of three endothermic peaks, indicating that the partial melting state is necessary to grow the whiskers.

Figure 5–1 shows the temperature dependence of resistance (R–T) for the 2212 whiskers grown from the glass plate containing the additional elements. Two steps in the resistance curve are observed for all the whiskers , due to the existence of two phases, 2212 phase and 2223 phase, in the whiskers. The $T_{c,zero}$ is in the range of 70–75 K for the Na(0.5), K(0.5), Ga(0.5), Ge(0.5), Sb(0.5), Te(0.5), and Pb(0.5) whiskers, whereas the $T_{c,zero}$ of the Li(0.5) whisker is 82 K higher by several degrees than the other whiskers. The same situation is in the onset temperature ($T_{c,on}$) of the 2223 phase. The $T_{c,on}$ of the Li(0.5) whisker is 110 K which is higher by 5 K than the other whiskers. Therefore, only Li is effective for raising T_c for both the 2212 and the 2223 phases. This is also confirmed by the susceptibility measurement. Figure 5–2 shows the temperature dependence

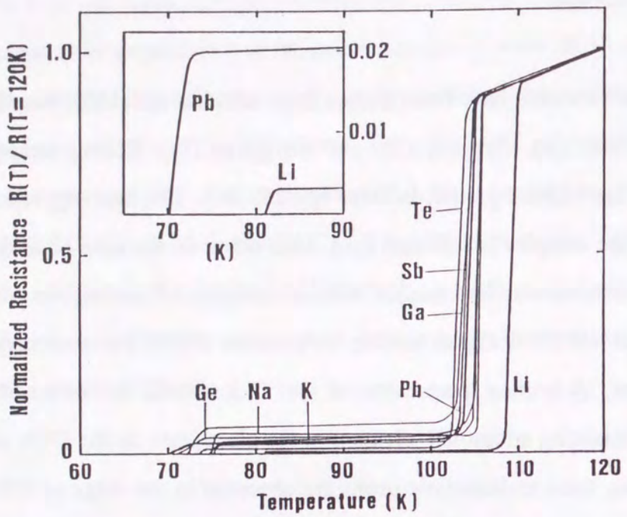

FIG. 5–1. Temperature dependence of the normalized resistance for the Li(0.5), Na(0.5), K(0.5), Ga(0.5), Ge(0.5), Sb(0.5), Te(0.5), and Pb(0.5) whiskers. The inset shows the temperature region 65–90 K.

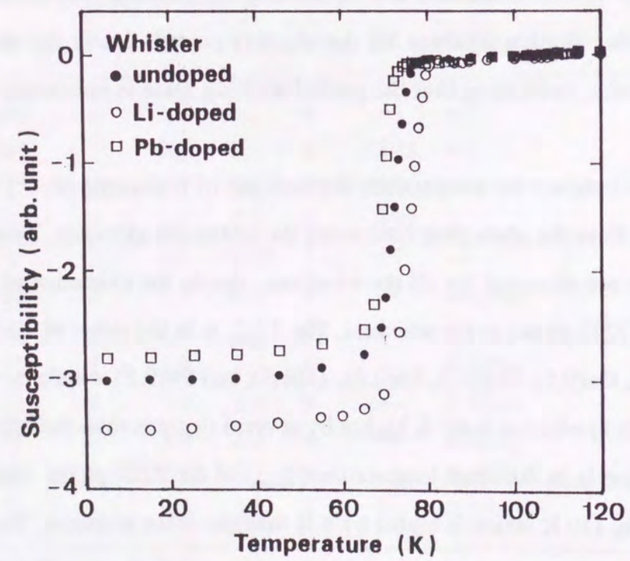

FIG. 5–2. Magnetic susceptibility data of the undoped, Pb(0.5), and Li(0.5) whiskers.

of susceptibility for the undoped, Pb(0.5), and Li(0.5) whiskers. The whiskers are found to contain the 2223 phase about 1% of the volume fraction, which causes the first resistance drop. The diamagnetic signal steeply increases at the onset temperature of the 2212 phase, and it nearly saturates at temperature 10 K below the $T_{c,on}$. The $T_{c,on}$ temperature of the 2212 phase in the Li–doped whiskers is higher than those of the undoped and the Pb(0.5) whiskers by 5 K.

The relationship between the superconductivity and the amount of Li in the 2212 whiskers is interested. Figure 5–3 shows the R–T behavior for the undoped and Li–doped whiskers. Both the first and second $T_{c,on}$ temperatures of the Li–doped whiskers are higher than those of the undoped one. The first $T_{c,on}$ values of the Li–doped samples

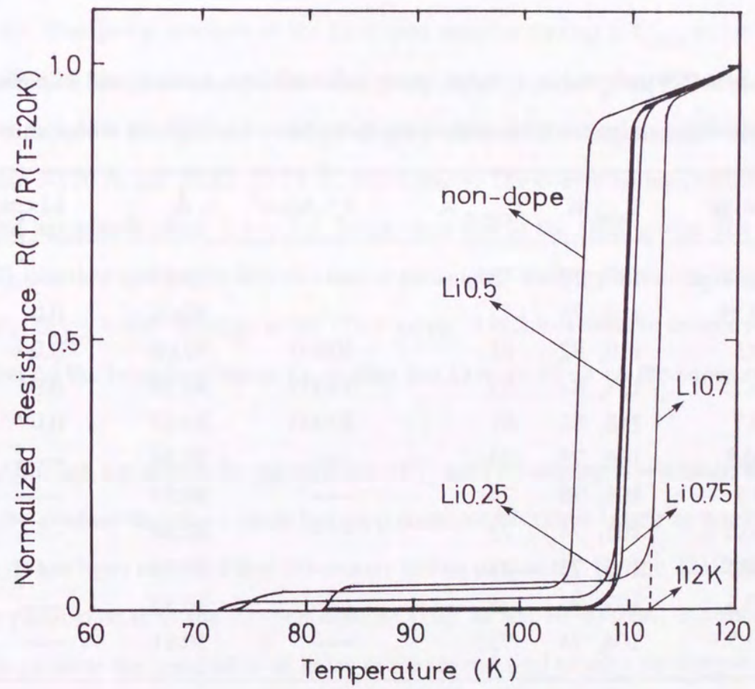

FIG. 5–3. Temperature dependence of the normalized resistance for a series of Li–doped 2212 whiskers.

are above 110 K. Especially for Li(0.7) sample which contains the highest amount of Li in the initial composition, the resistance drop occurs at 113 K, and the zero–resistance state is expected at 112 K by extrapolating the resistance drop, and this value is higher than that has been reported for the 2223 phase [29]. The results of the T_c value, J_c value, the *c*–axis lattice parameter, and Li content in the whiskers are summarized in table 5–2. In a series of the Li–doped samples, the $T_{c,on}$ and $T_{c,zero}$ values are enhanced with increasing Li content in the initial composition. The Li content in the whiskers, with the expression against $Bi_2Sr_2CaCu_2O_8$ formula, increases from 0.02 to 0.07 depending on the initial composition. The first $T_{c,on}$ due to the 2223 phase shows a good correlation with the analyzed Li content in the whisker. The $T_{c,zero}$ value changes critically at the content between Li(0.25) and Li(0.5), and exceeds the liquid nitrogen temperature in Li(0.5),

Table 5–2. The T_c value, J_c value, the *c*–axis lattice parameter, and Li content of the whiskers grown from melt–quenched plate with different composition.

Sample	$T_{c,on}$, K	$T_{c,zero}$, K	J_c[a], A/cm^2	*c*, Å	Li content[b]
non–dope	107, 77	72	---	30.57	---
Li0.25	110, 75	72	---	30.66	0.02
Li0.5	110, 82	81	30000	30.66	0.04
Li0.75	111, 83	82	34000	30.70	0.05
Li0.7	113, 82	81	29000	30.67	0.07
Na0.5	106, 75	74	---	30.59	---
K0.5	106, 75	74	---	30.57	---
Ga0.5	105, 74	73	---	30.56	---
Ge0.5	106, 75	71	---	30.54	---
Sb0.5	105, 76	75	---	30.52	---
Te0.5	104, 74	73	---	30.51	---

[a]At 77 K in a zero magnetic field.
[b]Determined by atomic absorption analysis and calculated against $Bi_2Sr_2CaCu_2O_8$.

Li(0.75), and Li(0.7) whiskers. One of the Li(0.75) whiskers showed a zero–resistance state at 107 K, which is regarded as the case where the voltage terminals were connected with the 2223 crystal. This situation is rarely achieved because the 2223 crystals exist in the midlayer, provably like the intergrowth between the 2212 crystals.

The $T_{c,on}$ and $T_{c,zero}$ values of Na(0.5), K(0.5), Ga(0.5), Ge(0.5), Sb(0.5), Te(0.5), and Pb(0.5) whiskers are comparable to those for the undoped sample. These additional elements are not effective in improving the superconductivity of the whiskers, and only Li is effective for raising T_c of the 2212 and the 2223 phases. Consequently, the resulting whiskers are comparable to the undoped whiskers in superconductivity, and the additional elements work to decrease the whisker growing temperature.

The relationship between the *c*–axis lattice parameter and the $T_{c,zero}$ value is shown in fig. 5–4. The samples can be classified into two groups depending on their lattice parameter. One group consists of the Li–doped samples having a $T_{c,zero}$ value above the liquid nitrogen temperature, and the other group consists of samples without Li having a $T_{c,zero}$ value below 77 K. The *c*–axis lattice parameters of the former and the latter group are 30.66–30.70 Å and 30.51–30.59 Å, respectively. The *c*–axis lattice parameter of the Li–doped samples is about 0.1–0.2 Å longer than that of the other group. The sample of Li(0.25) is rather special, in that the lattice parameter belongs to the Li–doped group, while the $T_{c,zero}$ value belongs to the other group. It is found that the sample of Li(0.25) is located on the boundary where Li–doping can have an effect on the superconductivity or not.

Although the reason for the increase of T_c with Li–doping is not clear, it is experimentally evident that the *c*–axis lattice parameter becomes larger as a result of Li–doping. It has been reported that the *c*–axis lattice parameter for the 2212 phase is inversely proportional to the oxygen content [30]. In the Bi–system, excess oxygen is found to promote the generation of holes in the crystal, and usually the oxygen content is larger than the optimum hole concentration in the 2212 phase. This is the case in the whiskers, because they grow under a stream of O_2 gas. In the Li–doped whiskers, the

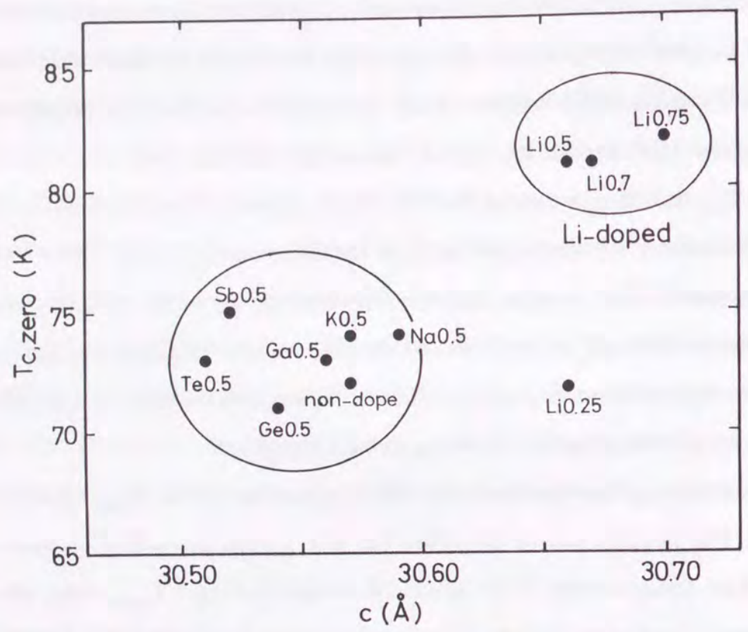

FIG. 5–4. Relationship between the *c*–axis lattice parameter and the $T_{c,zero}$ value of 2212 whiskers grown from a variety of initial compositions.

elongation of the *c*–axis seems to indicate a decrease of the oxygen content, resulting in the optimization of the hole concentration. However, the rise of T_c in both the 2212 and the 2223 phases in this particular whisker cannot be explained only by the reduction of hole concentration, because T_c of the 2223 phase is usually lowered by the reduction of oxygen content [31, 32]. In fact, the $T_{c,zero}$ values over 110 K have been scarcely reported for the 2223 samples. The rise of $T_{c,on}$ for 2223 phase by Li addition and the extrapolated $T_{c,zero}$ value of 112 K observed in the Li(0.7) sample seem to suggest the other mechanism than the optimization of hole concentration. The site of Li in the crystal is not determined in the present experiment. Recently, the possibility of substitution of Cu by Li has been reported in the 2212 bulk material which was synthesized by a solid state

reaction method [12]. This gives us another mechanism that could explain the increase of T_c with Li addition. The electronic structure will be changed by the substitution more directly than through the hole concentration. The mechanism of the enhancement of T_c by Li–doping will be discuss in detail in chapter 5–4.

The maximum J_c values at 77 K in a zero magnetic field for Li–doped whiskers are shown in table 5–2. The J_c values as high as $3x10^4$ A/cm^2 are obtained for the Li–doped whiskers. The narrow transition width as shown in the susceptibility curve (fig. 5–2) can account for the high J_c value even for a small temperature margin between $T_{c,zero}$ and 77 K. The bulk materials obtained by standard solid state reaction have polycrystalline forms and have grain boundaries which decrease the critical current density. Intergrain current and closed intragrain current in sintered Y–Ba–Cu–O samples were measured by using an ac inductive method by Ni *et al.* [33]. The intragrain current density is 10^3 order larger than the intergrain current density, indicating that the grain boundaries are the largest interfering factor against the high J_c value. The ideal situation for high J_c values from a viewpoint of morphology is absence of grain boundaries and the alignment of crystal axes in the sample. The 2212 whiskers nearly satisfy these two conditions, and show a high J_c value.

Figure 5–5 shows the temperature dependence of J_c for the Li–doped (Li(0.5)) whisker compared with those of the undoped and Pb(0.5) whiskers in a zero magnetic field. At 66 K, the J_c of Li(0.5) is as high as $3x10^5$ A/cm^2, and $3x10^4$ A/cm^2 at 77 K. By contrast, the J_c values for the undoped and Pb(0.5) whiskers are $7.3x10^4$ and $4x10^4$ A/cm^2 at 66 K, respectively. The J_c increases continuously with the decrease of temperature in all the samples, while the slope of the increase of J_c is different from each other. Fitting the data near $T_{c,zero}$ shows that J_c follows a power law of $J_c \propto (1-T/T_c)^n$. Deutscher and Müller predicted a n=2 relation for the high T_c oxide superconductors near T_c [34]. The n value has been determined by plotting $\log J_c$ versus $\log(1-T/T_c)$ for Li(0.5) and undoped samples, n=2.2 for Li(0.5) and n=0.9 for the undoped whiskers. When J_c is measured by a transport method, self–field effects cannot be neglected in samples with such a small

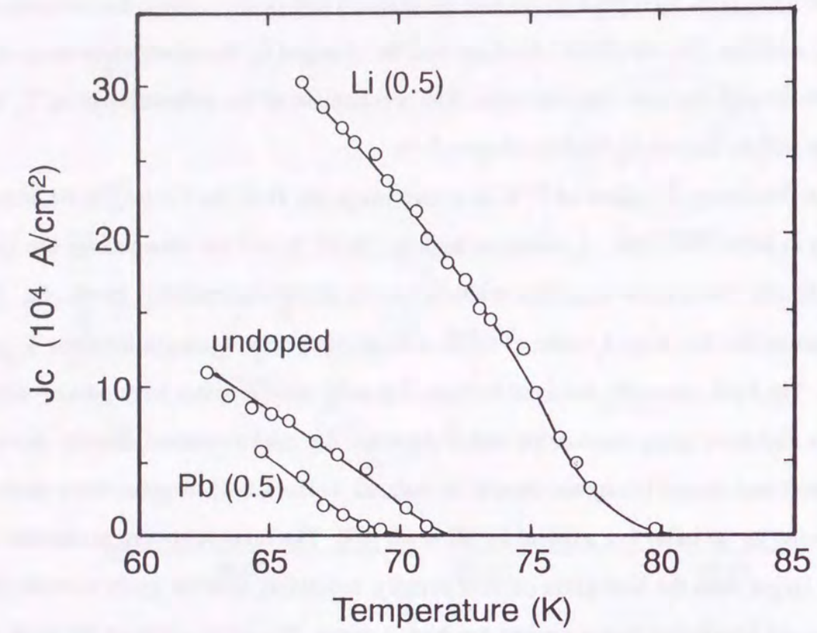

FIG. 5–5. Temperature dependence of J_c for the Li(0.5), Pb(0.5), and undoped whiskers in a zero magnetic field.

cross–section as the whiskers. The difference in the slope of the increase of J_c seems to reflect the difference of pinning force against the self–field flux lines.

Figure 5–6 shows the magnetic field dependence of J_c for H $\parallel$ *c* and H$\perp$*c* at 77 K. The J_c value of the whisker used for this measurement is 1.1×10^4 A/cm^2 in a zero magnetic field. A maximum of the J_c value is usually obtained when the magnetic field is aligned along the *ab* plane. In the case of H$\perp$*c*, the J_c value steeply decreases in the magnetic fields higher than 0.2 T. The steep decrease of J_c in a high magnetic field is attributed to the weakness of pinning force. The whiskers are of a single crystal nature and have no grain boundaries in the direction of growing axis. The similar behavior of J_c has been reported on Ag–sheathed polycrystalline wires [35], indicating that grain boundaries cannot be effective pinning center for flux lines.

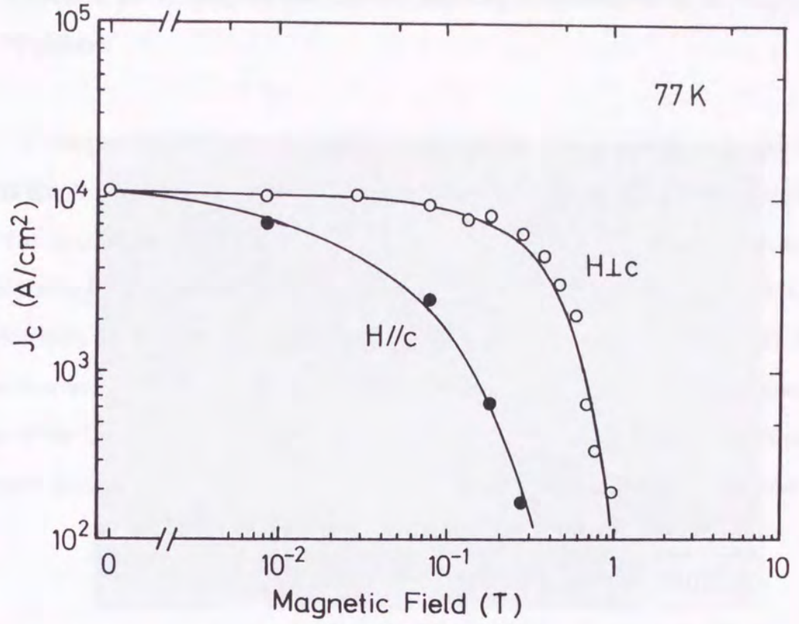

FIG. 5–6. Critical current density as a function of H $\parallel$ *c* and H$\perp$*c* at 77 K in magnetic fields up to 1 T.

Finally, bending property of the Li–doped whiskers is evaluated. The Li(0.5) whiskers are elastically bent up to a radius of curvature of about 0.1 mm (0.5% bending strain calculated for the whisker thickness of 1μm) as shown in fig. 5–7. This bending property is the same level as that of the undoped whiskers, so the flexible 2212 whiskers with $T_{c,zero}$ higher than 77 K can be obtained by Li–doping.

In summary, Li–doping is effective for increasing T_c of the 2212 phase. The T_c value is enhanced with the increase of Li content in the whisker, which can be controlled by changing the initial composition. A maximum J_c value of 3.4×10^4A/cm^2 at 77K and 3×10^5 A/cm^2 at 66 K in a zero magnetic field is obtained for the Li–doped whisker which has a $T_{c,zero}$ value of 82 K. An anisotropy of the J_c with respect to the direction of the

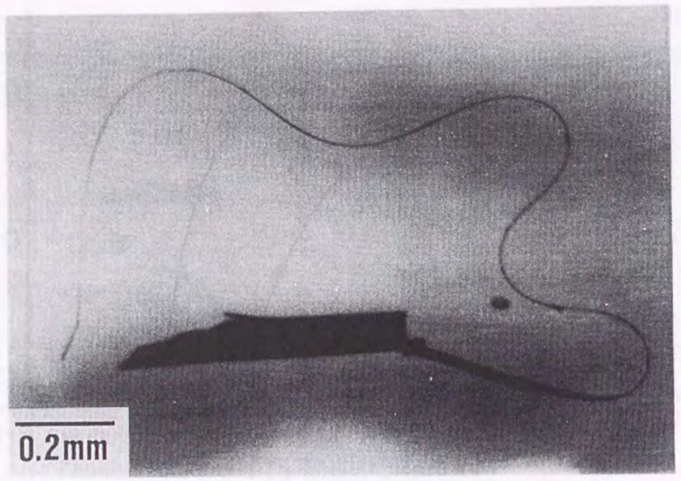

FIG. 5–7. Li–doped 2212 whisker in a bending state.

magnetic field is observed, and J_c decreases steeply in magnetic field higher than 0.2 T for H⊥c. The 2212 whiskers contain a small amount of the 2223 phase. The possibility of a $T_{c,zero}$ higher than 112 K is indicated in the R–T curve. However, the pure Li–doped 2223 whiskers are required to clarify the effect of Li–doping on T_c in the 2223 phase.

5–3. Effects of Li–Doping on the Superconducting Properties of $Bi_2Sr_2Ca_2Cu_3O_x$ Whiskers

Li–doped $Bi_2Sr_2Ca_2Cu_3O_{10}$ (2223) whiskers of single crystals with several millimeters length have been successfully prepared and it is revealed that Li–doping is effective for increasing critical temperature (T_c) of the 2223 phase. By annealing $Bi_2Sr_2CaCu_2O_8$ (2212) whiskers within a very narrow temperature region in a calcined powder with a composition of $Bi_2Sr_2Ca_4Cu_6Pb_{0.5}Li_xO_y$ (x=0.1, 0.2, 0.3 0.4), the 2212 phase is converted to the 2223 phase and Li–doping is achieved at the same time. The T_c value of the Li–doped 2223 whiskers (108.2 K) is reproducibly 1.2 K higher than that of undoped 2223 whiskers prepared by the same method using a calcined powder without Li.

Experimental

The Li–doped and undoped 2223 whiskers were prepared by the CAP method. The 2212 whiskers were placed in a powder with the composition of $Bi_2Sr_2Ca_4Cu_6Pb_{0.5}Li_xO_y$ (x=0.0, 0.1, 0.2, 0.3, 0.4, 0.5) which had previously been calcined at 780°C for 20 h and 820°C for 20 h with an intermediate grinding. It has been reported that the addition of a small amount of lead enhances the growth of the 2223 phase by promoting the nucleation of the 2223 phase and the diffusivity of Ca and Cu [36]. A small amount of lead was added to the calcined powder to take advantage of this property. The powder with whiskers was set between two sintered pellets with the composition of $Bi_2Sr_2Ca_4Cu_6Pb_{0.5}O_x$ to prevent reactions of the calcined powder with an alumina boat (fig. 4–1). After annealing it at a pre–determined temperature (820–860°C) depending on the Li content in the calcined powder for 150 h in air, the whiskers were mechanically removed from the powder. The recovered whiskers have the dimensions of

1–5 μm thick, 10–100 μm wide, and 1–3 mm long.

The magnetic susceptibility was measured using a Quantum Design $MPMS_2$ magnetometer equipped with a superconducting quantum interference device (SQUID) detector in a magnetic field of 3 Oe from 5 to 120 K. The composition was determined with a Horiba EMAX–5770 energy dispersive X–ray spectroscopy (EDX) system. The Li content was determined by atomic absorption analysis. The DTA curve was obtained by increasing the temperature from a room temperature to 1000°C at a constant heating rate of 10°C/min. The temperature dependence of resistance was measured by the standard four–probe method.

Results and discussion

There are two ways for preparing the Li–doped 2223 whiskers, as follows:

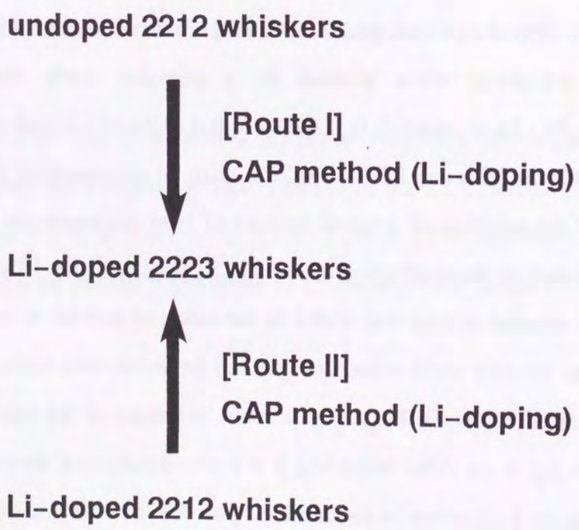

Two kinds of the 2212 whiskers are used as the starting whiskers in the CAP method. One is the undoped 2212 whiskers (route I) and the other is the Li–doped 2212 whiskers (route II). The experimental conditions are summarized in table 5–3. Six kinds of calcined powders of $Bi_2Sr_2Ca_4Cu_6Pb_{0.5}Li_xO_y$ with various Li content, x=0.0, 0.1, 0.2, 0.3, 0.4, and 0.5 were used. The experimental number from 1 to 6 and from 7 to 8 in table 5–3 correspond to the route I and route II, respectively. In the case of the x=0.0 calcined powder, Li does not enter into the whiskers during the CAP treatment. Phase conversion occurs and the undoped 2223 whiskers are obtained (no. 1). The starting 2212 whiskers

Table 5–3. Experimental conditions of CAP method.

No.	2212 Whiskers	Calcined Powder $Bi_2Sr_2Ca_4Cu_6Pb_{0.5}Li_xO_y$	Temperature (°C)	Time (h)
1	undoped	x=0.0	840, 845, 848 850, 853, 855 858, 860	150
2	undoped	x=0.1	840, 845, 848 850, 853	150
3	undoped	x=0.2	835, 838, 840 843, 845	150
4	undoped	x=0.3	835, 838, 840 843	150
5	undoped	x=0.4	833, 835, 838 840	150
6	undoped	x=0.5	830, 833, 835 838	150
7	Li–doped	x=0.0	853	150
8	Li–doped	x=0.2	843	150

used in route II contain Li, which is confirmed by the atomic absorption analysis. The Li content is 0.04 relative to the chemical formula of $Bi_2Sr_2CaCu_2O_8$. In experiment no. 7, Li is not further supplied from the calcined powder to the whiskers. So, in the series of CAP experiments we have prepared four kinds of the 2223 whiskers:

(1) undoped 2223 whiskers (no. 1);

(2) Li–doped 2223 whiskers (Li is supplied to the undoped 2212 whiskers from the calcined powder during the CAP treatment (no. 2 – no. 6));

(3) Li–doped 2223 whiskers (the starting 2212 whiskers contain Li whereas further Li is not supplied from calcined powder during the CAP treatment (no. 7));

(4) Li–doped 2223 whiskers (Li is further supplied to the Li–doped 2212 whiskers from the calcined powder during the CAP treatment (no. 8)).

The temperature dependence of susceptibility for the whiskers CAP–treated under the experimental condition of no. 1 is shown in fig. 5–8. The volume fraction of the 2223 phase in the CAP–treated whiskers increases with increasing annealing temperature. The non–converted part of the original 2212 phase is observed in the whiskers annealed below 848°C, evident from the susceptibility signal around 75 K. The phase conversion is completed between 853 and 858°C as far as the annealing time of 150 h. When the CAP treatment is carried out at 860°C, we do not find the whiskers in the powder anymore and the whiskers are not recovered from the powder. The appropriate annealing temperature for obtaining the 2223 whiskers with the x=0.0 powder is, therefore, between 853 and 858°C. The annealing temperature should be controlled within 5 degrees to obtain the pure 2223 whiskers.

The temperature dependence of susceptibility for the whiskers CAP–treated in the x=0.1, 0.2, 0.3, 0.4, and 0.5 calcined powders is shown in figs. 5–9 – 5–13, respectively. In the case of x=0.1, it is evident from the susceptibility signal around 75 K that the unconverted 2212 phase remains in the whiskers when annealed at temperature lower than 845°C (fig. 5–9). The phase conversion is completed at temperatures 848–850°C. The appropriate annealing temperature decreases compared with the case of x=0.0. The

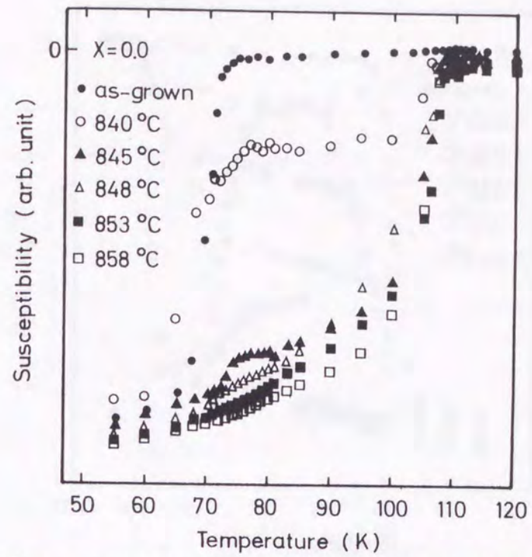

FIG. 5–8. Temperature dependence of susceptibility for the CAP–treated (x=0.0 calcined powder) whiskers at various temperatures for 150 h.

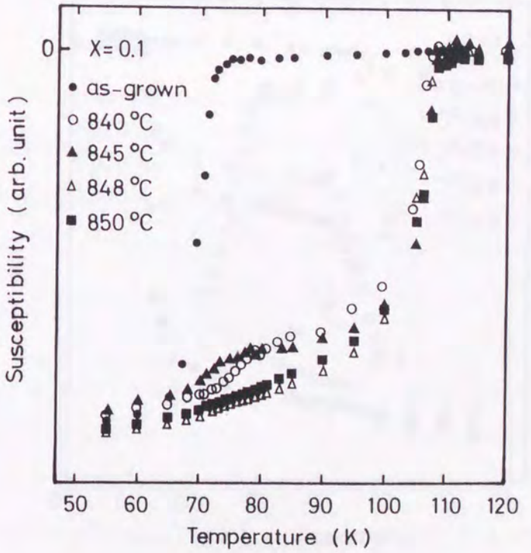

FIG. 5–9. Temperature dependence of susceptibility for the CAP–treated (x=0.1 calcined powder) whiskers at various temperatures for 150 h.

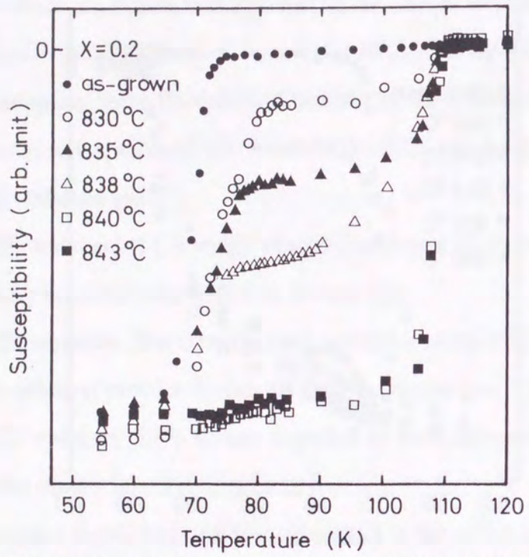

FIG. 5–10. Temperature dependence of susceptibility for the CAP–treated (x=0.2 calcined powder) whiskers at various temperatures for 150 h.

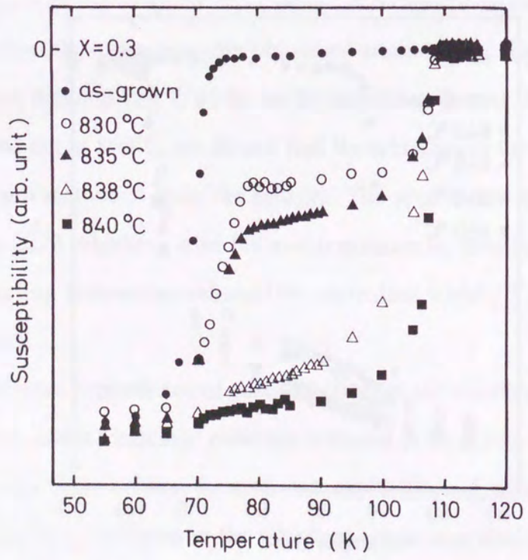

FIG. 5–11. Temperature dependence of susceptibility for the CAP–treated (x=0.3 calcined powder) whiskers at various temperatures for 150 h.

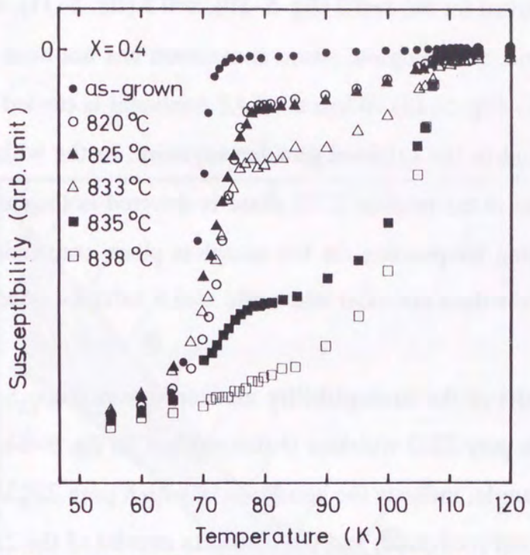

FIG. 5–12. Temperature dependence of susceptibility for the CAP–treated (x=0.4 calcined powder) whiskers at various temperatures for 150 h.

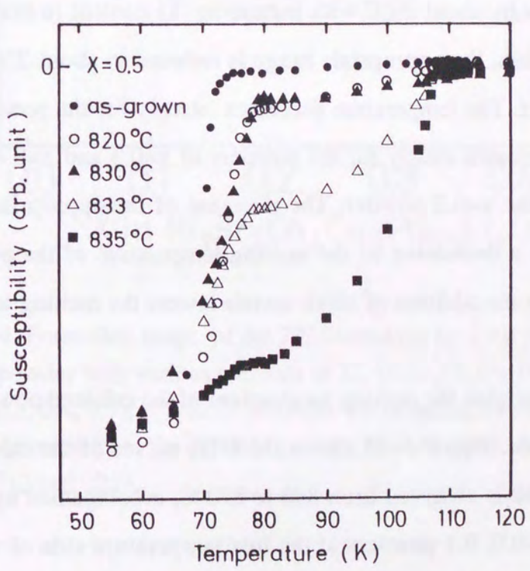

FIG. 5–13. Temperature dependence of susceptibility for the CAP–treated (x=0.5 calcined powder) whiskers at various temperatures for 150 h.

same situation is observed for the x=0.2 (fig. 5–10), x=0.3 (fig. 5–11), and x=0.4 (fig. 5–12). On the other hand, the complete phase conversion has not been observed for the x=0.5 calcined powder (fig. 5–13). When the CAP treatment is carried out at 838°C, the whiskers are not found in the calcined powder anymore. In the whiskers annealed at 835°C, a small amount of the original 2212 phase is detected in the susceptibility signal. Therefore, the annealing temperature for the complete phase conversion from the 2212 phase to the 2223 phase does not exist when the x=0.5 calcined powder is used in the CAP treatment.

From the results of the susceptibility measurements (figs. 5–8 – 5–13), the formation range of the pure 2223 whiskers is summarized in fig. 5–14. The open circle, closed circle, and triangle, indicate the condition in which pure 2223 whiskers are obtained, whiskers are not recovered, and the whiskers consist of the 2212 and the 2223 phases, respectively. The appropriate annealing temperature is between 853 and 858°C for the x=0.0 powder, indicating that the temperature allowance is within about 5°C. The temperature decreases by about 20°C with increasing Li content in the calcined powder, up to x=0.4. In addition, the appropriate range is reduced to about 2°C for the powder with a high Li content. The temperature decreases steeply for the powders of x=0.1 and x=0.2, whereas it decreases slowly for the powders of x=0.3 and x=0.4. The conversion range has a knee at the x=0.2 powder. The decrease of the appropriate temperature is thought to arise from a decreasing of the melting temperature of the powder, because it has been reported that the addition of alkali metals lowers the melting temperature in this system [37].

In order to determine the melting temperature of the calcined powder, DTA experiments have been made. Figure 5–15 shows the DTA curves of the calcined powders. A large endothermic peak is observed from 840 to 870°C, accompanied by two small peaks in the case of the X=0.0, 0.1 powders at the low temperature side of the main peak. A large peak is observed around 750°C for the x=0.4, 0.5 powders. Aota *et al.* have reported similar DTA data in conjunction with XRD patterns for the $Bi_{1.92}Pb_{0.48}Sr_2Ca_2Cu_{3.2}O_x$

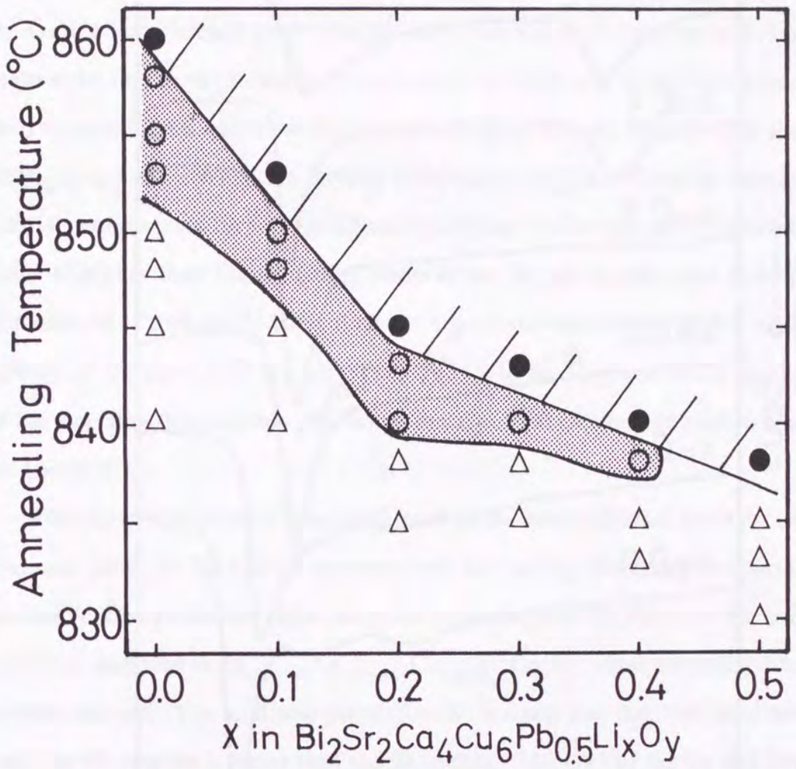

FIG. 5–14. Formation range of the 2223 whiskers by CAP method in the calcined powder with various contents of Li, $Bi_2Sr_2Ca_4Cu_6Pb_{0.5}Li_xO_y$ (x=0.0, 0.1, 0.2, 0.3, 0.4, 0.5); (○) 2223 whiskers are obtained, (●) whiskers are not recovered from the calcined powder, (Δ) obtained whiskers have two phases 2212 and 2223.

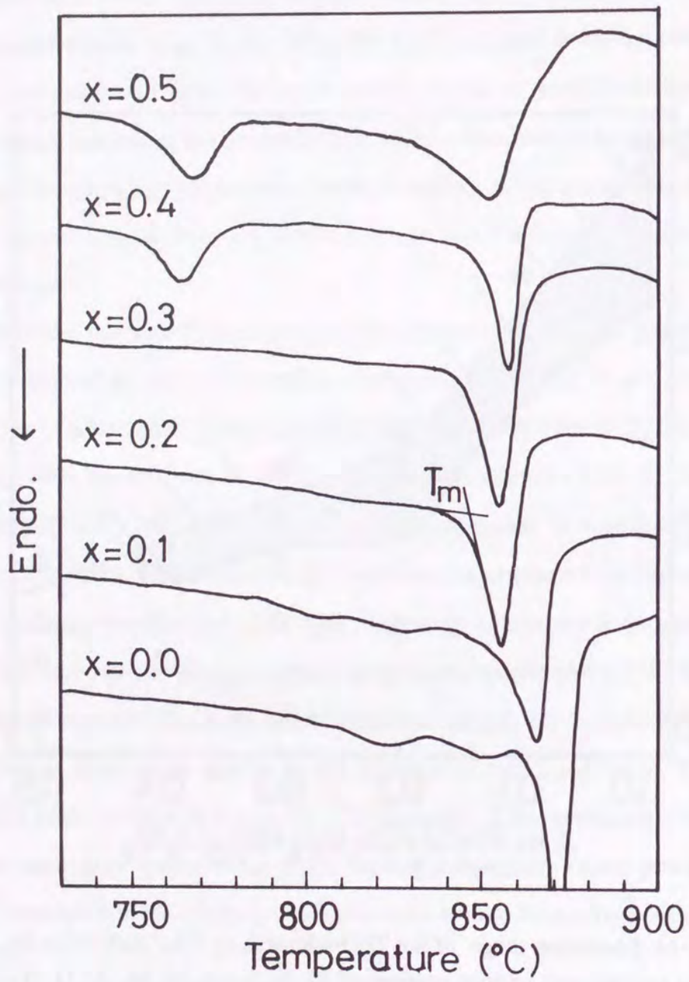

FIG. 5–15. DTA curves of the calcined powder with various Li contents x in $Bi_2Sr_2Ca_4Cu_6Pb_{0.5}Li_xO_y$. The measurement was performed in air with a heating rate of 10°C/min.

powder [28]. They have observed three endothermic peaks in the range of 840 to 880°C. Each peak is assigned to the melting of CuO, the partial melting of the 2212 phase, and the decomposition of the compound, in order of increasing temperature. The three peaks observed for the x=0.0 and the x=0.1 powders would correspond to their case. On the other hand, a endothermic peak around 750°C for the x=0.4 and the x=0.5 powders is thought to be due to the formation of a eutectic by Li_2O and Bi_2O_3 which has been reported to react each other at the temperature as low as 700°C with the ratio of Li_2O/Bi_2O_3=0.1 [38]. When the melting temperature (T_m) is defined as shown in fig. 5–15, the T_m decreases with increasing the Li content. Although the T_m defined above is about 5°C higher than the annealing temperature for giving the pure 2223 phase, the dependence of T_m on the Li content shows a good correspondence to that of the formation range of the pure 2223 whiskers (fig. 5–14). In the CAP method, it is necessary to keep the annealing temperature just below the T_m of the calcined powder to complete the phase conversion.

The phase conversion is also confirmed by the compositional analysis using EDX. The atomic ratios of Ca and Cu increase with increasing annealing temperature as the phase conversion proceeds. The composition determined by EDX for the original undoped 2212 whiskers is $Bi_{1.94\pm0.05}Sr_{1.06\pm0.06}Ca_{1.25\pm0.05}Cu_2O_x$, when normalized to 2 copper atoms/formula unit. The total amount of (Sr+Ca) is much less than the ideal stoichiometry, and the Ca content is larger than the Sr content. The sum of the Ca and Sr composition is 2.3, corresponding to the occupancy ratio of 77%. Hong *et al.* have reported the solid solution range of the 2212 compound prepared by a conventional solid–state reaction method [39]. They have indicated that the solid solution range can be represented as $(Bi_xCu_{1-x})_{4+y}(Sr_zCa_{1-z})_{3-y}O_\delta$, $0.48<x<0.57$, $0.56<z<0.80$, $0<y<0.2$. They have also summarized the solid solution range for single crystals prepared by a flux method and floating zone method which had previously reported by other investigators, and confirmed the consistency of the range for the powder samples. However, our undoped 2212 whisker is outside of their range. The (Sr+Ca) deficiency is larger than their result and

the Sr/Ca ratio of 0.85 is also out of the range to the direction of Ca-rich side. The composition of the Li-doped 2223 whiskers annealed in the x=0.2 calcined powder is $Bi_{1.82\pm0.06}Pb_{0.2\pm0.1}Sr_{1.45\pm0.08}Ca_{1.73\pm0.08}Cu_3O_y$ when normalized to 3 copper atoms/formula unit. The 2223 whiskers have a large deficiency at the alkaline earth metal site. The occupancy ratio at the site is 77% against the ideal structure, which is the same level as the case of 2212 whiskers.

The relative atomic ratio for the CAP treated whiskers is shown in fig. 5-16 as a function of annealing temperature. The composition is calculated as the sum of Bi and Pb contents is fix to two in this figure. The composition of Cu, Ca, and Sr steeply increases with increasing annealing temperature higher than 833°C for the x=0.4 powder (fig. 5-16(a)). The composition of the whiskers CAP-treated at 838°C is $(Bi_{1.84}Pb_{0.16})Sr_{1.36}Ca_{1.57}Cu_{2.82}O_y$. The content of Li in the whiskers is analyzed to be 0.06 written in the chemical formula from the measurement of atomic absorption analysis. In the case of the powder of x=0.5, although the phase conversion is not completed, the content of Cu, Ca, and Sr increases with increasing annealing temperature higher than 830°C. The composition of the whiskers CAP-treated at 835°C is $(Bi_{1.83}Pb_{0.17})Sr_{1.27}Ca_{1.47}Cu_{2.72}O_y$. The lack of Sr, Ca, and Cu content compared with the case of x=0.4 powder reflects the remaining of the original 2212 phase in the whiskers.

The T_c value of the pure 2223 whiskers has been determined by susceptibility measurement. Figure 5-17 shows the detail of the susceptibility change near T_c for the undoped 2223 whiskers (open circle) and for the Li-doped 2223 whiskers obtained by using the x=0.2 (open square) and the x=0.3 (open triangle) calcined powders. These correspond to the experimental conditions of nos. 1, 3, and 4 in table 5-3, respectively, so that the effects of Li addition through the calcined powder can be considered. The T_c values are obtained around 108 K for both the Li-doped whiskers (no. 3 and no.4). The undoped whiskers (no. 1) show a T_c value of 107.0 K, being 1.0 K lower than those for the Li-doped whiskers. This reproducible result indicates that the Li-doping is effective in raising the T_c value of the 2223 phase. Figure 5-18 shows the T_c of the 2223 whiskers

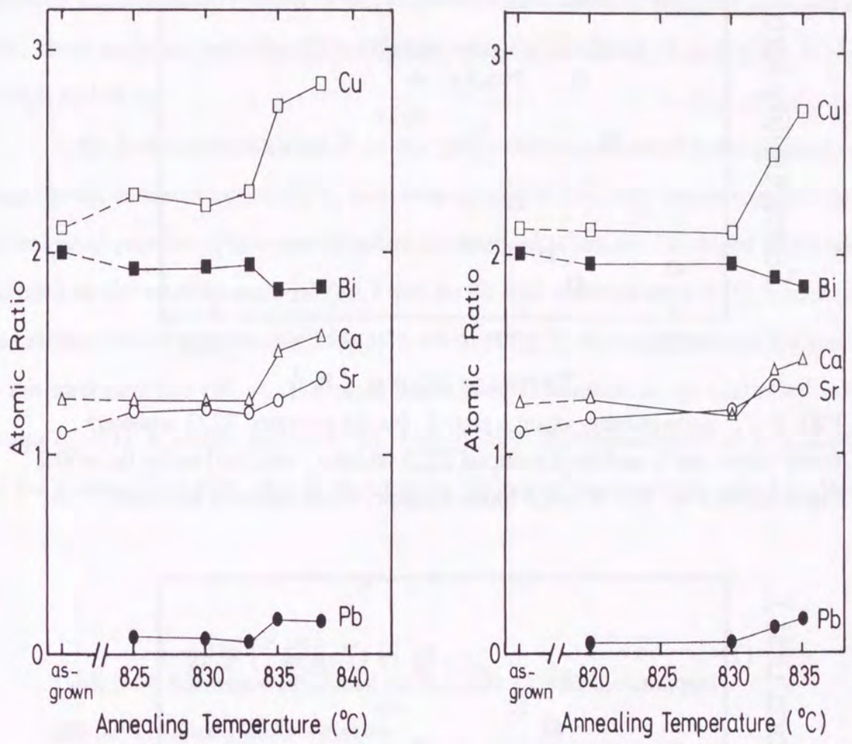

FIG. 5-16. Change of relative atomic ratio for the CAP-treated whiskers using the (a) x=0.4, (b) x=0.5 calcined powder. The ratio is calculated as the sum of Bi and Pb contents is fixed to 2.

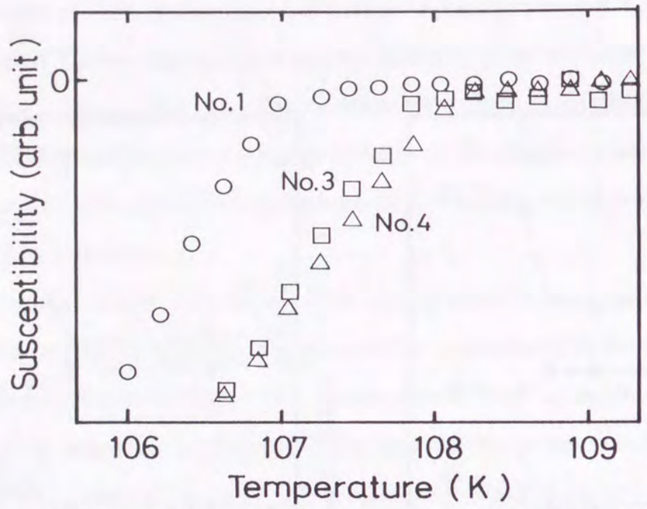

FIG. 5–17. Susceptibility change near T_c for the undoped 2223 whiskers (open circle; no.1) and the Li–doped 2223 whiskers obtained using the x=0.2 (open square; no. 3) and x=0.3 (open triangle; no.4) calcined powders.

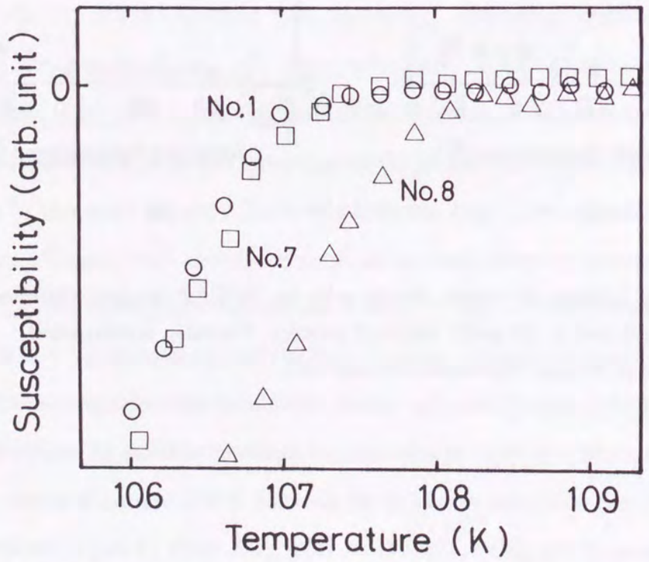

FIG. 5–18. Susceptibility change near T_c for the undoped 2223 whiskers (open circle; no.1) and the Li–doped whiskers obtained by experimental condition of no.7 (open square) and no.8 (open triangle).

obtained at the experimental conditions no.7 (open square) and no.8 (open triangle), in which the Li–doped 2212 whiskers are used as the starting material, and the T_c of the undoped 2223 whiskers (open circle; experimental condition no.1) for comparison. Of these three samples, only the 2223 whiskers with the condition of no.8 gives a T_c value as high as 108 K.

Table 5–4 summarizes the T_c of the 2223 whiskers obtained in the present experiment. In the series of nos. 1–5, T_c increases up to 108.2 K with increasing Li content in the calcined powder. The same situation is observed when the Li–doped 2212 whiskers are used as the starting material (no.7 and no.8). The enhancement of T_c is observed for the calcined powder containing Li (no.8), whereas the T_c for no.7 is almost the same level as the undoped one (no.1). The eight experimental conditions are classified into four groups (1)–(4), as described above. Of these groups, the enhancement of T_c is observed for the groups (2) and (4), that is, the cases using the calcined powder with Li. Whether

Table 5–4. Summary of critical temperature (T_c) of the undoped and the Li–doped 2223 whiskers.

No.	2212 Whiskers	Calcined Powder $Bi_2Sr_2Ca_4Cu_6Pb_{0.5}Li_xO_y$	T_c (K)
1	undoped	x=0.0	107.0
2	undoped	x=0.1	107.4
3	undoped	x=0.2	108.0
4	undoped	x=0.3	108.1
5	undoped	x=0.4	108.2
6	undoped	x=0.5	----
7	Li–doped	x=0.0	107.1
8	Li–doped	x=0.2	108.2

the starting 2212 whiskers contains Li or not, does not influence the T_c of the CAP-treated whiskers. The results of atomic absorption analysis indicate that all of the 2223 whiskers except for the no. 1 sample contain Li. Nevertheless, the whiskers of no.7 contain almost the same amount of Li as the other whiskers, but the enhancement of T_c has not been observed for this sample. This result indicates that the existence of Li in the CAP-treated 2223 whiskers does not necessarily mean for the improvement of T_c.

The resistivity of the Li-doped 2223 whisker prepared by using the x=0.2 powder is 780 μΩcm at room temperature and the zero resistance temperature is 107.5 K as shown in fig. 5-19. Critical current density (J_c) at 5 K is calculated to be $2x10^6$ A/cm^2(H=0 T), $1x10^6$ A/cm^2(H=0.5 T), $8x10^5$ A/cm^2(H=0.8 T) from M-H loop using the Bean model [40].

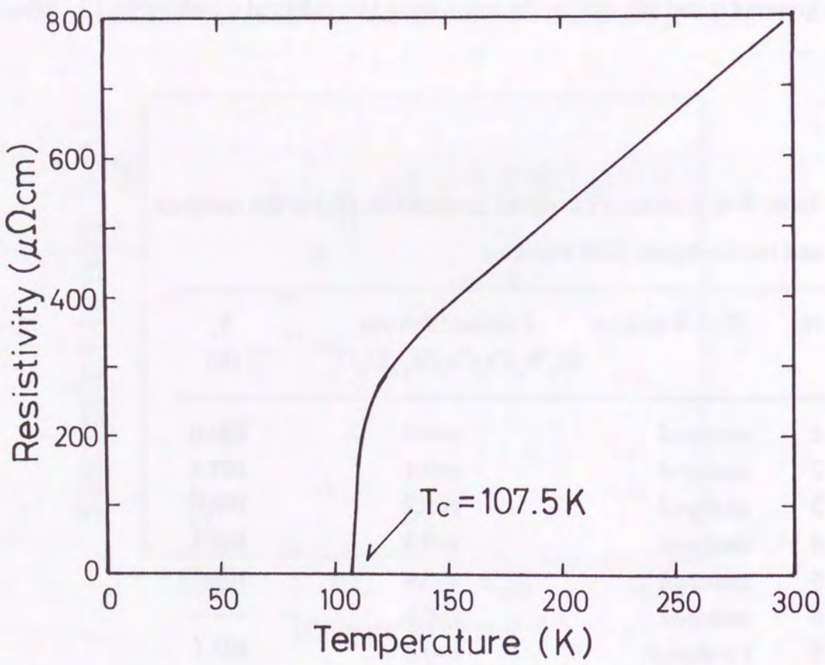

FIG. 5-19. Temperature dependence of resistivity of the Li-doped 2223 whisker prepared by using the x=0.2 powder.

In summary, the Li-doped 2223 whiskers are obtained by annealing the 2212 whiskers in a calcined powder with the composition of $Bi_2Sr_2Ca_4Cu_6Pb_{0.5}Li_xO_y$ (x=0.1, 0.2, 0.3, 0.4). They are obtained only in a very narrow temperature region, so that the annealing temperature should be controlled within 3°C. The Li-doped 2223 whiskers thus obtained have a T_c value of 108.0-108.2 K, which is reproducibly about 1 K higher than that of the undoped 2223 whiskers prepared by using the x=0.0 powder.

5–4. Mechanism of the Enhancement of T_c by Li–doping

Li–doping is effective in increasing critical temperature (T_c) of both the $Bi_2Sr_2CaCu_2O_x$ (2212) and the $Bi_2Sr_2Ca_2Cu_3O_x$ (2223) whiskers. T_c of the 2223 phase is commonly accepted to be lowered by the reduction of hole concentration, that is opposite situation to the 2212 phase. Therefore, the T_c of the Li–doped whiskers is believed to be enhanced by some mechanisms other than the optimization of the hole concentration. In order to confirm whether this mechanism is applicable to our case or not, a series of annealing experiments has been made by compulsorily reducing the oxygen content from the Li–doped and undoped 2212 whiskers under a reduced pressure. From the compositional analysis and the measurement of the *c*–axis lattice parameter on the annealed samples under the reduced pressure, the Li–doping is thought to be effective to increase the Sr/Ca ratio in the 2212 and the 2223 whiskers, resulting the enhancement of T_c for both kinds of whiskers.

Experimental

In a series of experiments to reduce the oxygen content in the 2212 whiskers, the undoped and Li–doped 2212 whiskers were annealed under a reduced pressure of $5x10^{-3}$ Torr at 200, 300, 400, 500, 600, and 700°C for 20 h. The T_c value has been evaluated from the susceptibility measurements with a superconducting quantum interference device (SQUID: Quantum Design $MPMS_2$) magnetometer in a magnetic field of 3 Oe from 5 to 120 K. The composition was determined with a Horiba EMAX–5770 energy dispersive X–ray spectroscopy (EDX) system. The Li content was determined by atomic absorption analysis.

Results and discussion

From the series of experiments in preparing the 2212 (section 5–2) and the 2223 (section 5–3) whiskers, it is revealed that the Li–doping is effective for the enhancement of T_c for both the phases. Three possible mechanisms have been proposed for the improvement of T_c by Li–doping for the 2212 phase as mentioned in section 5–1, which are optimization of hole concentration, change of cation ratio, and a more intrinsic one such as changing the electronic structure. It has been generally accepted that the optimization of hole concentration is the most probable mechanism. There are two different situations for this mechanism concerning the processing of the Li–doped 2212 compound. One is the case where the Li–doping is achieved by the electrochemical method [15,16] or the chemical reaction method by using n–butyl lithium [21,22]. Lithium ions do not substitute any cations but are believed to intercalate into the 2212 compound having a layered structure. In this case, the Li ions act as a reductant, like H^+ ions, that reduces the hole concentration. Actually, the decrease of hole concentration has been observed from the Hall effect [21,22]. The other one is more complex. Because the Li–doping is achieved during the formation of the 2212 phase, it could be proved to change the important factors affecting the hole concentration such as the oxygen content, the composition of alkaline earth metals, or the amount of deficiency. The conventional powder reaction method, the melting processing, and floating zone method belong to this case. When Li is incorporated into the Cu site as suggested by Horiuchi *et al.* [13], it would influence superconductivity through its effect on the two dimensional CuO_2 layer in which the superconductivity resides. Substituting the other metals, the Li influences on the hole concentration as to increase it. On the other hand, it has been pointed out that the substitution may give rise to a reducing effect of the oxygen content, leading to a decrease of the hole concentration [14,17]. As the hole concentration in the 2212 phase trends to be overdoped, the decrease of the oxygen content results in the enhancement of T_c.

Concerning the mechanism of the optimization of the hole concentration, our

results on the whiskers belong to the latter case. The Li–doped 2212 whiskers prepared by the glass annealing method have a T_c value of 82 K, which is 5 K higher than that of the undoped 2212 whiskers obtained by the same method [23,24]. The Li–doped 2223 whiskers also have a higher T_c value (108.2 K) than that of the undoped 2223 whiskers (107.0 K; table 5–4). The T_c of the 2223 phase is commonly accepted to be lowered by the reduction of the hole concentration [31,32], the opposite situation to the 2212 phase. If the Li–doping is supposed to act in the same manner for both the 2212 and the 2223 phases, our results seem to suggest that the mechanism of hole concentration is not applicable to our case. In order to examine whether this mechanism is applicable to our case or not, a series of annealing experiments has been made by compulsorily reducing the oxygen content from the Li–doped and dopant–free 2212 whiskers under a reduced pressure. The T_c value has been evaluated from the susceptibility measurements.

In fig. 5–20, the *c*–axis lattice parameter of the 2212 whiskers annealed at various temperature for 20 h under a reduced pressure ($5x10^{-3}$ Torr) is plotted against the annealing temperature. The X–ray diffraction (XRD) pattern does not show any other phase than the 2212 phase for the whiskers annealed below 600°C. On the other hand, the whiskers annealed at 700°C show no peak due to the 2212 phase in the XRD pattern, and their color turns to orange due to the reduction of Cu to a monovalent state, which is evident from the peaks of Cu_2O in the XRD pattern. The decomposition occurs at temperature higher than 600°C under this condition. The *c*–axis lattice parameter saturates at temperatures higher than 300°C. A long annealing (100 h) has not induced further elongation of the *c*–axis lattice parameter compared with that of 20 h, indicating that annealing for 20 h is enough to achieve an equilibrium state. For the as–grown whiskers, the *c*–axis lattice parameter of the Li–doped 2212 sample (30.71 Å) is 0.1 Å longer than that of the undoped whiskers (30.61 Å). These whiskers have a different *c*–axis lattice parameter and behave in a same manner against the annealing temperature. The *c*–axis lattice parameter of the Li–doped whiskers is always longer than that of the undoped whiskers by about 0.1 Å.

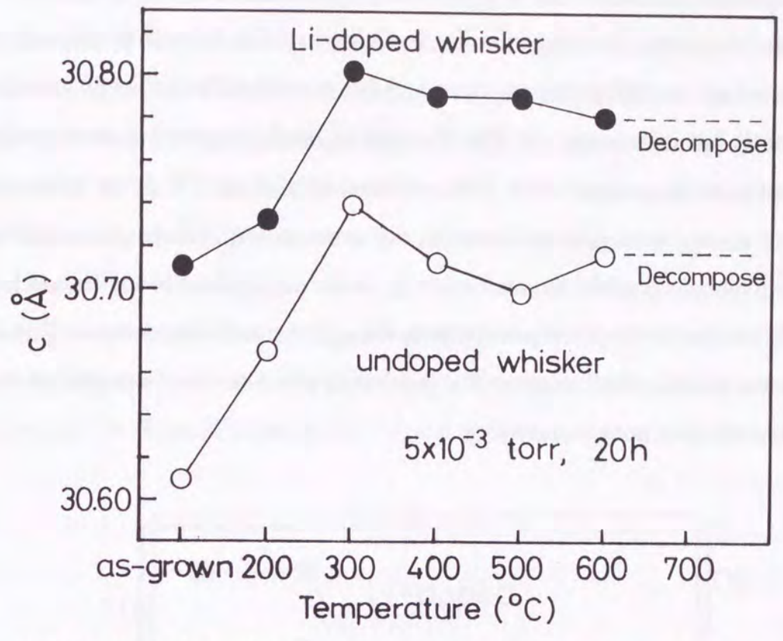

FIG. 5–20. Relationship between the *c*–axis lattice parameter and the annealing temperature under a reduced pressure ($5x10^{-3}$ Torr) for the undoped and Li–doped 2212 whiskers.

T_c data for the two kinds of samples determined from the susceptibility measurement are plotted as a function of the annealing temperature in fig. 5–21. With increasing annealing temperature, a maximum T_c is observed at 300°C for both the Li–doped (closed circle) and undoped (open circle) whiskers. The increase of T_c by this treatment is about 5–6 K as compared with the as–grown whiskers. This change corresponds to the elongation of the *c*–axis lattice parameter. However, T_c decreases to 73–75 K for the higher annealing temperature, whereas the *c*–axis lattice parameter for each sample keeps a constant value up to 600°C. This could be explained by a difference in the oxygen site desorbed during the annealing. The excess oxygen in Bi–O layer which can be one of the

origins for generating holes would be desorbed by annealing at a low annealing temperature. On the other hand, the oxygen in the Sr–O layer or Cu–O layer would start to be desorbed at a high annealing temperature, which has a small influence on the *c*–axis lattice parameter but influences T_c. The T_c value of the Li–doped whiskers is always higher than that of the undoped ones, with a difference of about 5 K. If the enhancement of T_c by Li–doping is simply attributed to the optimization of hole concentration by reducing the oxygen content, the maximum T_c of the undoped whiskers should have a value as high as that of the Li–doped whiskers through the annealing process. This is not the case in our results, which suggests that the doping effect can not be explained by the simple optimization of hole concentration.

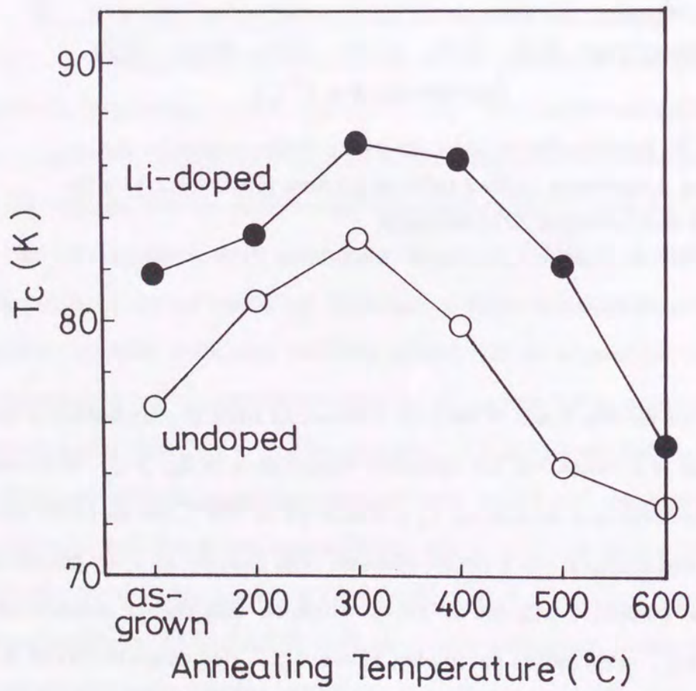

FIG. 5–21. Relationship between T_c of the 2212 phase and the annealing temperature under a reduced pressure ($5x10^{-3}$ Torr) for the undoped and Li–doped 2212 whiskers.

As the 2212 whiskers contain about 1 vol.% of the 2223 phase, the superconducting transition of the whiskers is composed of two stages in the susceptibility curve at around 105 and 80 K. Therefore, the change of T_c due to the 2223 phase in the whiskers is detectable from the susceptibility curve, although the volume fraction is rather small. Figure 5–22 shows the relationship between the T_c of the 2223 phase and the annealing temperature. T_c of the 2223 phase in the as–grown Li–doped whiskers is about 4 K higher than that of the undoped whiskers, as in the case of fig. 5–21. With increasing annealing temperature, that is, decreasing oxygen content, the T_c of the 2223 phase monotonically decreases for both the samples. This behavior is in accordance with the previous reports on the 2223 phase [41, 42] and opposite to that on the 2212 phase.

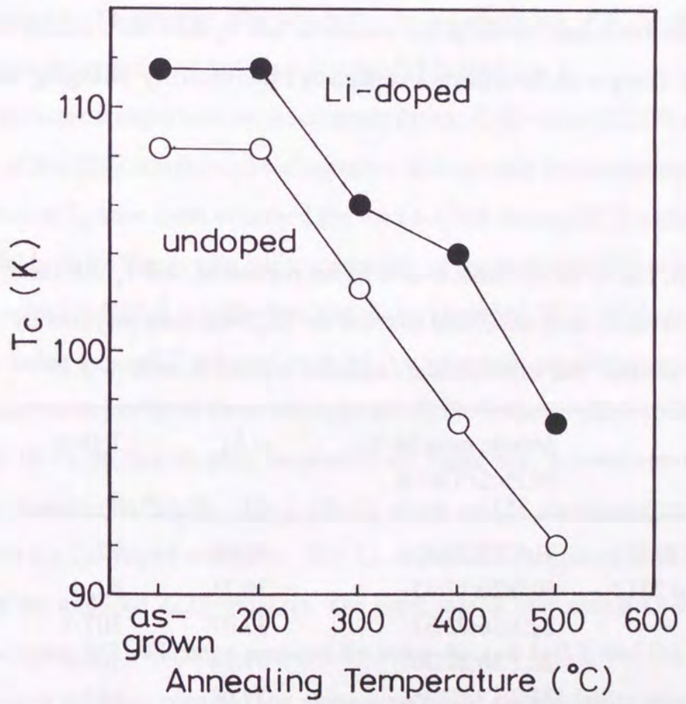

FIG. 5–22. Relationship between T_c of the 2223 phase contained in the 2212 whiskers as a minor phase and the annealing temperature under a reduced pressure ($5x10^{-3}$ Torr) for the undoped and Li–doped 2212 whiskers.

The results of the annealing experiment suggest that the mechanism of the enhancement of T_c by the Li-doping is not due to the optimization of hole concentration through the change of the oxygen content. Therefore, the cation ratio in the whiskers has been examined. The composition of the undoped and Li-doped whiskers for both the 2212 and the 2223 whiskers has been determined by EDX. Table 5-5 lists the sample, atomic ratio, *c*-axis lattice parameter, and T_c. The atomic ratios (at.%) of the undoped and Li-doped 2212 whiskers are Bi:Sr:Ca:Cu=31:17:20:32 and 30:20:17:33, respectively. These are written approximately in $Bi_2(Sr_{1-x}Ca_x)_{2.2}Cu_2O_y$ (x=0.54 for the undoped whiskers; x=0.46 for the Li-doped whiskers). Both kinds of whiskers have the same amount of deficiency at the alkaline earth metal site, whereas the ratio of Sr/Ca is different for each. The Li-doped whiskers have a larger Sr/Ca ratio than the undoped ones. The effects of the Sr/Ca ratio on the lattice parameter and T_c have been exactly examined [2, 37, 43-45]. Hong *et al*. have made a systematic experiment by changing the Sr/Ca ratio in $Bi_2(Sr_{1-x}Ca_x)_{n-1}Cu_nO_y$ (n=2, 3) and reported the relationship between Sr content and the *c*-axis lattice parameter or T_c [39]. Their result for the 2212 phase (n=2) indicates that the *c*-axis lattice parameter increases linearly with increasing Sr/Ca ratio. An increase of the Sr content by 3 at.% causes the 0.08 Å elongation in the *c*-axis lattice parameter. Their result corresponds well to our result in the 2212 whiskers. The elongation of the *c*-axis lattice parameter of the Li-doped whiskers as compared with the undoped ones (=0.1 Å) is able to be explained by the change of Sr content (3 at.%) in the 2212 whiskers. They also have found a linear relationship between T_c and the *c*-axis lattice parameter, in which the enhancement of T_c by 5 K corresponds to the elongation of the *c*-axis lattice parameter by 0.11 Å. This also corresponds well to our result in the 2212 whiskers (increase of T_c by 5 K and elongation of the *c*-axis lattice parameter of 0.1 Å are caused by Li-doping). Consequently, the enhancement of T_c by the Li-doping is attributed to the increase of Sr/Ca ratio in the 2212 whiskers.

Table 5-5. List of atomic ratio, *c*-axis lattice parameter, and T_c. All the samples of no. 1, no.3, no. 7, and no.8 are the 2223 whiskers prepared by the CAP method. The experimental condition is listed in table 5-3.

Sample	Atomic ratio (at.%) Bi:Pb:Sr:Ca:Cu	*c*(Å)	T_c(K)[a)]
undoped 2212	31:0:17:20:32	30.61	77
Li-doped 2212	30:0:20:17:33	30.71	82
No. 1	22:3:16:22:37	37.07	107.0
No. 3	22:3:18:21:36	37.14	108.0
No. 7	23:2:17:22:36	37.08	107.1
No. 8	23:2:18:21:36	37.12	108.2

[a)]Determined by susceptibility measurement.

The same comparison has been made for the CAP-treated 2223 whiskers. As in the case of the 2212 whiskers, the elongation of the *c*-axis lattice parameter and the enhancement of T_c have been observed for the Li-CAP-doped 2223 whiskers (no. 3 and no. 8 in table 5-5). The *c*-axis lattice parameter of the undoped 2223 whiskers (no. 1) is 37.07 Å, which is 0.07 Å smaller than that of the Li-doped 2223 whiskers (37.14 Å) prepared by using the x=0.2 calcined powder (experimental condition no.3 in table 5-3). The atomic ratios (at.%) of these whiskers are Bi:Pb:Sr:Ca:Cu=22:3:16:22:37 (undoped) and 22:3:18:21:36 (Li-doped), respectively. These are written approximately in a chemical formula $(Bi,Pb)_2(Sr_{1-x}Ca_x)_{3.1}Cu_3O_y$ where x=0.58 for the undoped whiskers and x=0.54 for the Li-doped whiskers. The Li-doped 2223 whiskers have a higher Sr/Ca ratio than the undoped 2223 whiskers. The same results have also been obtained for the other Li-doped 2223 whiskers prepared by using the x=0.1, 0.3, and 0.4 calcined powders. Hong *et al*. have reported the elongation of the *c*-axis lattice parameter and the enhancement of T_c with increasing Sr/Ca ratio in the 2223 phase [39]. From their results, T_c has a linear relationship with the *c*-axis lattice parameter, and the enhancement of T_c

by 1 K corresponds to the elongation of the *c*–axis lattice parameter by 0.06 Å. This is comparable to our result on the whiskers. Therefore, the enhancement of T_c observed for the 2212 and 2223 whiskers by Li–doping is consistently attributed to the increase of the Sr/Ca ratio. The Li–doping causes the increase of Sr/Ca ratio, resulting in the increase of T_c.

In the case of the 2223 whiskers prepared by using the Li–doped 2212 whiskers (experimental condition nos. 7 and 8), the same tendency has been obtained. The elongation of the *c*–axis lattice parameter and the enhancement of T_c have been achieved for the Li–CAP–doped 2223 whiskers (table 5–5, no. 8). Li is expected, because of its size, to replace Cu. Actually, the preparation of $La_2Cu_{1-x}Li_xO_{4-\delta}$ single crystals and ceramics has been reported [46]. Hoshizaki *et al*. have prepared the Li–doped 2212 single crystals with the self–flux method [26]. They have confirmed that Li substitutes for Cu in the single crystals from the results of EMPA and inductively coupled plasma (ICP) spectrometry. Therefore, in the case of the whiskers, it is thought that Li occupies the Cu–site. The 2223 whiskers of nos.1 and 7 have the same level of T_c, indicating that T_c is little affected by the existence of Li. This would be due to the amount of Li, which is too small to influence T_c. T_c depends on the final composition, especially Sr/Ca ratio, which is determined by whether Li is contained in the calcined powder used in the CAP treatment.

Here, the growth mechanism of the 2212 and 2223 whiskers is discussed concerning the increase of Sr/Ca ratio. The 2212 whiskers grow out from their root part being nourished through the liquid phase near the surface of the crystallized glass plate (section 2–3). As for the 2223 whiskers obtained by the CAP method, the phase conversion takes place in the partial melting region of the calcined powder, as described in section 4–3. On the surface of the CAP–treated whiskers, many steps with round edges are observed, indicating erosion by a liquid phase. The phase conversion from the 2212 phase to the 2223 phase would be attained by the diffusion of Ca, Cu, and Pb ions into the 2212 phase through the liquid phase generated around the whiskers during annealing. The liquid phase due to the partial melting plays an important role in the growing process for both

the whiskers. The addition of Li reduces the partial melting temperature, which is evident from the decrease of the growing temperature of the 2212 whiskers [24] and 2223 whiskers (fig. 5–14). It has been reported that the alkali element added to the Bi–system works as a flux which provides a diffusion path for each element [17]. The existence of Li would alter the composition of the liquid phase to a Sr–rich one, resulting in the increase of Sr/Ca ratio in the whiskers.

In summary, the Li–doping is effective for increasing T_c for both the 2212 and 2223 phases. The mechanism of the enhancement of T_c by Li–doping is discussed concerning the change of electronic structure, optimization of hole concentration, and change of composition. The evidence of compositional analysis, elongation of the *c*–axis lattice parameter, and the reduction of the oxygen content from the 2212 whiskers containing the 2223 phase, indicates that the increase of the Sr/Ca ratio in the whiskers is the most probable mechanism for the enhancement of T_c. The Li–doping causes the increase of the Sr/Ca ratio in the whiskers preferably by changing the composition of the liquid phase which acts an important part in the preparation process for both the 2212 and 2223 whiskers.

References

[1] J.L.Tallon, R.G.Buckley, P.W.Gilberd, M.R.Presland, I.W.M.Brown, M.E.Bowden, L.A.Christian, and R.Goguel, Nature, **333**, 153 (1988).

[2] H.Niu, N.Fukushima, and K.Ando, Jpn.J.Appl.Phys., **27**, L1442 (1988).

[3] Y.Deshimaru, T.Otani, Y.Shimizu, N.Miura, and N.Yamazoe, Jpn.J.Appl.Phys., **30**, L1798 (1991).

[4] Y.Kimishima and J.Nakao, Physica C **185–189**, 835 (1991).

[5] S.Nomura, T.Yamashita, H.Yoshino, and K.Ando, J.Am.Ceram.Soc., **74**, 2711 (1991).

[6] R.M.Fleming, S.A.Sunshine, L.F.Schneemeyer, R.B. Van Dover, R.J.Cava, P.M.Marsh, J.V.Waszczak, S.H.Glarum, and S.M.Zahurak, Physica C, **173**, 37 (1991).

[7] M.–H.Whangbo, D.B.Kang, and C.C.Torardi, Physica C, **158**, 371 (1989).

[8] C.Murayama, N.Mori, S.Yomo, H.Takagi, S.Uchida, and Y.Tokura, Nature, **339**, 293 (1989).

[9] Y.Ohta, T.Tohyama, and S.Maekawa, Physica C, **166**, 385 (1990).

[10] H.Nobumasa, K.Shimizu, and T.Kawai, Physica C, **167**, 515 (1990).

[11] C.Kuwabara and T.Nakanishi, J.Phys.Soc.Jpn., **59**, 3835 (1990).

[12] T.Kawai, T.Horiuchi, K.Mitsui, K.Ogura, S.Takagi, and S.Kawai, Physica C, **161**, 561 (1989).

[13] T.Horiuchi, T.Kawai, K.Mitsui, K.Ogura, and S.Kawai, Physica C, **168**, 309 (1990).

[14] C.Engkagul, K.Eaiprasertsak, J.Laksanaboonsong, K.Treechairusme, N.Chaichit, S.Leelaprute, N.Chiengpratoom, and I.M.Tang, Physica C, **181**, 63 (1991).

[15] P.Strobel, B.Bonnet, C.Mouuget, and B.Souletie, Physica C, **172**, 193 (1990).

[16] Y.Morikawa, K.Satoh, S.Ogawaw, K.Nakamura, H.Yamanoto, and M.Tanaka, Physica C, **185–189**, 431 (1991).

[17] S.X.Dou, H.K.Liu, W.M.Wu, W.X.Wang, and C.C.Sorrell, Physica C, **172**, 295 (1990).

[18] J.Schwartz and S.Wu, Physica C, **185–189**, 2403 (1991).

[19] G.Poullain, T.Brousse, V.Chauvel–Kobabi, J.–F.Hamet, and H.Murray, Physica C, **182**, 137 (1991).

[20] T.Horiuchi, K.Kitahama, T.Kawai, S.Kawai, S.Hontsu, K.Ogura, I.Shigaki, and Y.Kawate, Physica C, **185–189**, 629 (1991).

[21] Y.Koike, T.Okubo, A.Fujiwara, T.Noji, and Y.Saito, Solid State Commun., **79**, 501 (1991)

[22] T.Okubo, A.Fujiwara, Y.Koike, T.Noji, and Y.Saito, Physica C, **185–189**, 847 (1991).

[23] I.Matsubara H.Tanigawa, T.Ogura, H.Yamashita, M.Kinoshita, and T.Kawai, Appl.Phys.Lett., **56**, 2141 (1990).

[24] I.Matsubara, H.Tanigawa, T.Ogura, H.Yamashita, M.Kinoshita, and T.Kawai, Physica C, **167**, 503 (1990).

[25] I.Matsubara, T.Ogura, H.Yamashita, M.Kinoshita, and T.Kawai, Appl.Phys.Lett., **60**, 901 (1992).

[26] H.Hoshizaki, S.Kawabata, N.Kawahara, H.Enami, T.Shinohara, and T.Imura, J.Cryst.Growth, **121**, 53 (1992).

[27] I.Matsubara, T.Ogura, H.Yamashita, M.Kinoshita, Y.Hashimoto, and T.Kawai, Physica C, **201**, 83 (1992).

[28] K.Aota, H.Hattori, T.Hatano, K.Nakamura, and K.Ogawa, Jpn.J.Appl.Phys., **28**, L2196 (1989).

[29] J.L.Tallon, R.G.Buckley, P.W.Gilberd, M.R.Presland,I.W.M.Brown, M.E.Bowden, L.A.Christian and R.Goguel, Nature, **333**, 153 (1988).

[30] S.Miura, T.Yoshitake, T.Manako, Y.Miyasaka, N.Shohata, and T.Satoh, Appl.Phys.Lett., **55**, 1360 (1989).

[31] H.Hattori, K.Nakamura, and K.Ogawa, Jpn.J.Appl.Phys., **29**, L36 (1990).

[32] J.Zhao, M.Wu, W.Abdul-Razzaq, and M.S.Seehra, Physica C, **165**, 135 (1990).

[33] B.Ni, T.Munataka, T.Matsushita, M.Iwakuma, K.Funaki, and M.Takeo, Jpn.J.Appl.Phys., **27**, 1658 (1988).

[34] G.Deutscher and K.A.Müller, Phys.Rev.Lett., **59**, 1745 (1987).

[35] T.Hikata, T.Nishikawa, H.Mukai, K.Sato and H.Hitotsuyanagi, Jpn.J.Appl.Phys., **28**, L1204 (1989).

[36] D.Shi, M.S.Moley, J.G.Chen, M.Xu, K.Vandervoort, Y.X.Liao, A.Zangvil, J.Akujieze, and S.Segre, Appl.Phys.Lett., **55**, 699 (1989).

[37] K.Kanai, T.Kamo, and S.P.Matsuda, Jpn.J.Appl.Phys., **28**, L551 (1989).

[38] E.M.Levin and R.S.Roth, J.Res.Nat.Bur.Stand., **68**, 198 (1964).

[39] B.Hong and T.O.Mason, J.Am.Ceram.Soc., **74**, 1045 (1991).

[40] C.P.Bean, Phys.Rev.Lett., **8**, 250 (1962).

[41] T.Ishida, Jpn.J.Appl.Phys., **28**, L197 (1989).

[42] N.Miura, H.Suzuta, Y.Deshimaru, Y.Shimizu, H.Sakashita, and N.Yamazoe, Jpn.J.Appl.Phys., **28**, L1112 (1989).

[43] G.S.Grader, E.M.Gyorgy, P.K.Gallagher, H.M.O'Bryan, D.W.Johnson,Jr., S.Sunshine, S.M.Zahurak, S.Jin, and R.C.Sherwood, Phys.Rev. B, **38**, 757 (1988).

[44] A.Moto, A.Morimoto, and T.Shimizu, Jpn.J.Appl.Phys., **28**, L1144 (1989).

[45] Y.Deshimaru, T.Otani, Y.Shimizu, N.Miura, and N.Yamazoe, Jpn.J.Appl.Phy., **30**, L1798 (1991).

[46] M.A.Kastner, R.J.Birgeneau, C.Y.Chen, Y.M.Chiang, D.R.Gabbe, H.P.Jenssen, T.Junk, C.J.Peters, P.J.Picone, Tineke Thio, T.R.Thurston, and H.L.Tuller, Phys.Rev.B, **37**, 111 (1988).

Chapter 6

Summary and Conclusions

Preparation and properties of the superconducting whiskers in the Bi-system have been investigated. We have successfully developed new methods to give large and high-quality whiskers for all the $Bi_2Sr_2CuO_x$ (2201), $Bi_2Sr_2CaCu_2O_x$ (2212), and $Bi_2Sr_2Ca_2Cu_3O_x$ (2223) phases. The 2212 whiskers have been prepared by annealing a melt-quenched glass plate in a stream of O_2 gas. Each whisker with the dimensions of 2-10 μm thick, 10-500 μm wide and ~20 mm long is composed of several plate-like single crystals which are stacked in a layered structure. For the whisker growth, the glass precursor, Al addition to the glass, and a steady stream of O_2 are required. We have proposed a model for the growing mechanism of the 2212 whiskers. The 2212 whiskers are flexible and are elastically bent up to the curvature of radius of 0.2 mm corresponding to a bending strain of 0.5%. Taking advantage of this property, we have revealed the effects of bending strain on critical temperature (T_c) and critical current density (J_c). Mechanical properties such as tensile strength and elastic modulus have also been investigated using the 2212 whiskers. The 2201 whiskers have been prepared by the same method as that for the 2212 whiskers. The 2201 phase is dominant in the whiskers grown at lower annealing temperature. The growing phase (2212 or 2201 phase) of the whiskers is controllable by changing the initial composition and annealing temperature.

On the other hand, the 2223 whiskers have been prepared by conversion by annealing in powder method (CAP method). They have been obtained by annealing the 2212 whiskers in a Ca and Cu rich Bi-Sr-Ca-Cu-Pb-O calcined powder. The appropriate annealing temperature is in the partial melting region of the calcined powder, as determined by DTA analysis. The phase conversion is brought by diffusion of Ca and Cu into the 2212 whiskers from the liquid phase due to the partial melting. Anisotropy of upper critical field (H_{c2}) and coherence length has been investigated using the 2223 whiskers. The CAP method has been applied also to single crystals prepared by a flux

method, resulting in 2223 sheet crystals as large as 1 mm^2.

The substitution experiments have been made on the 2212 and the 2223 whiskers. We have confirmed that the Li–doping is effective for increasing T_c for both the 2212 and the 2223 whiskers and revealed the mechanism of the enhancement in T_c by the Li–doping.

In chapter 2, preparation and properties of 2212 whiskers have been investigated. The 2212 whiskers have been successfully prepared by annealing a melt–quenched glass plate in a stream of O_2 gas. The crystallographic orientation of the 2212 whiskers has been determined by means of X–ray diffraction, Weissenberg photograph, and polarized Raman spectra. The results show that the growing axis of the whisker is the *a*–axis, the *b*–axis lies in the well–grown plane, and the *c*–axis is perpendicular to this plane. Typically, the 2212 whiskers show two steps in the R–T curve at 105 and 76 K, and the zero resistance temperature ($T_{c,zero}$) is 74–75 K. A slight diamagnetic susceptibility is observed between 104 and 80 K corresponding to the first resistance drop. From the susceptibility curve, the volume fraction of the 2223 phase is estimated to be <1%. The 2212 whiskers contain a small amount of the 2223 phase. A maximum critical current density of $7.3x10^4$ A/cm^2 (66 K, 0 T) is obtained by a four–probe method.

There are three important factors in the growth conditions of the 2212 whiskers other than the appropriate annealing temperature and starting composition. The first is the glass precursor and the second is the presence of Al in the glass precursor; although the 2212 whiskers contain no Al, the addition of Al to the glass precursor is found to greatly enhance the whisker growth. The appropriate amount of Al in the glass precursor is around 10 at.%. The third factor is a steady stream of O_2 gas (>100 ml/min) during annealing. Using the results of microstructural and compositional analysis, a model of the growth mechanism of the 2212 whiskers is devised. The Al–added glass precursor forms the Bi–Sr–Ca–Al–O complex oxide distributed near the surface and acting as a 'rigid skeleton' to support the bottom part of the whisker which is surrounded by a thin layer of the Bi–rich phase and fits into the 'microcrucible' of the Bi–Sr–Ca–Al–O phase.

The Bi–rich phase has the same composition as the liquid phase equilibrated with the 2212 phase and melts at the annealing temperature. The whisker growth takes place through the continuous precipitation of the 2212 phase from the melt on the base end of the whisker. This model can be called as a self–supporting micro–top–seeding mechanism.

The effects of bending strain upon T_c and J_c have been studied using the Pb–doped 2212 whiskers. The whiskers can be elastically bent up to a bending strain of 0.5% without changing in T_c. This property is quite attractive for the twisting of wires in practical applications. The J_c value in a nonbending state ($6.7x10^4$ A/cm^2) is kept at the same level for the bending strain smaller than 0.2%.

Mechanical properties of the undoped and Li–doped 2212 whiskers of single crystals have been determined. Tensile strength, which is assumed to be an intrinsic strength of the compound, has been measured by pulling the whiskers in the direction of *a*–axis corresponding to the whisker axis. There are no substantial differences in the mechanical properties between the undoped and the Li–doped whiskers. The maximum tensile strength and the elastic modulus determined from the stress–strain curve are 940 MPa and 92 GPa, respectively.

In chapter 3, preparation condition and properties of 2201 whiskers have been investigated. The 2201 whiskers are grown by the same method as that for the 2212 whiskers by changing the annealing temperature and the composition of the glass precursor. The 2201 phase is dominant in the whiskers grown at lower temperature, 820 and 810°C. The growing phase (2212 or 2201 phase) of the whiskers is controllable by changing the initial composition and annealing temperature, whereas the pure 2223 whiskers have not been obtained in this method. The 2201 whiskers show no evidence of superconductivity.

In chapter 4, preparation and properties of 2223 whiskers have been investigated. We have successfully developed a new approach giving the 2223 whiskers to be called conversion by annealing in powder (CAP) method. The 2223 whiskers are obtained by

annealing 2212 whiskers in a Ca- and Cu-rich Bi-Sr-Ca-Cu-Pb-O calcined powder with retaining the outline of the form in the original crystals. The $T_{c,zero}$ value of the2223 whisker is 107 K, and there is no evidence for remaining the original 2212 phase in the whiskers from the susceptibility measurements. To prepare the pure 2223 whiskers, three temperature region should be overlapped each other, formation and the thermal stability of the 2223 phase, the region where the whiskers can be recovered from the calcined powder, and the melting temperature of the calcined powder. The phase conversion is thought to proceed as follows. A liquid phase is generated in the powder around the 2212 whiskers. It reacts with the 2212 whiskers and nucleation of the 2223 phase occurs at the interface between the liquid phase and the whiskers. By supplying Ca, Cu, and Pb ions into the whisker through the liquid phase, the 2223 phase spreads into the whiskers remaining the outline of the original crystal shape. From the kinetic study on the CAP method, the diffusion controlled two-dimensional growth with decreasing nucleation rate is found to be most provable model for the phase conversion from the 2212 to the 2223 phase. The CAP method is also applied to 2212 single crystals grown by the self-flux method, resulting 2223 sheet crystals as large as 1 mm^2 in area. The 2223 whiskers and crystals are of great importance for obtaining basic information on the physical properties of the 2223 phase.

We have studied the temperature and magnetic field dependence of J_c and the anisotropy of the H_{c2} and coherence length using the 2223 whiskers. The whisker yields a maximum J_c of $7.3x10^4$ A/cm^2 at 77 K, and higher than $1x10^4$ A/cm^2 below 96 K in a zero applied field. The 2223 whisker shows n=2 dependence in $J_c \propto (1-t)^n$ for T close to T_c where $t=T/T_c$. At 77 K, the 2223 whisker shows J_c values above $1x10^4$ A/cm^2 up to 1 T, in contrast to the 2212 whisker ($1x10^2$ A/cm^2, H=1 T) which shows the steep decrease of J_c in magnetic field above 0.2 T. The magnetoresistance for the 2223 whisker has been measured. Linear relation is obtained in H_{c2}-T curve defined at $\rho(T)/\rho_N(T)=0.5$, and according to the WHH theory and the GL relations, the coherence lengths of $\xi_{ab}(0)=29$ Å and $\xi_c(0)=0.93$ Å are obtained for the 2223 phase. The large anisotropic factor of coherence length (31) and the small $\xi_c(0)$ value indicate that the 2223 compound is expected to show strong two dimensional properties.

In chapter 5, the effects of Li-doping on the superconductivity of the 2212 and the 2223 whiskers have been investigated. We have prepared not only Li-doped 2212 whiskers but also Li-doped 2223 whiskers by the CAP method, and confirmed the enhancement of T_c for both the whiskers. The T_c values of the 2212 whiskers are enhanced with the increase of Li content in the whiskers, which can be controlled by changing the initial composition of the glass precursor. A maximum J_c of $3.4x10^4$ A/cm^2 at 77 K and $3x10^5$ A/cm^2 at 66 K in a zero magnetic field is obtained for the Li-doped whisker which shows a $T_{c,zero}$ of 82 K. The Li-doped 2223 whiskers are obtained only in a very narrow temperature region, so that the annealing temperature should be controlled within 3°C. The Li-doped 2223 whiskers thus obtained have a T_c of 108.0-108.2K, which is reproducibly about 1 K higher than that of the undoped 2223 whiskers.

We have discussed on mechanism for the enhancement of T_c by Li doping, such as the change of electronic structure, optimization of hole concentration, and change of composition. The evidences of compositional analysis, elongation of the *c*-axis lattice parameter, and the reduction of the oxygen content from the 2212 whiskers containing the small amount of 2223 phase, indicate that the increase of the Sr/Ca ratio in the whiskers is the most probable mechanism for the enhancement of T_c. The Li-doping causes the increase of the Sr/Ca ratio in the whiskers preferably by changing the composition of the liquid phase which acts an important part in the preparation process for both the 2212 and the 2223 whiskers.

List of publications

[1] Preparation of Fibrous Bi(Pb)–Sr–Ca–Cu–O Crystals and Their Superconducting Properties in a Bending State.
I.Matsubara, H.Kageyama, H.Tanigawa, T.Ogura, H.Yamashita, and T.Kawai,
Jpn.J.Appl.Phys., **28**, L1121 (1989).

[2] Preparation of Bi(Pb)–Sr–Ca–Cu–O Fibrous Crystals Containing the High–T_c Phase.
I.Matsubara, H.Tanigawa, T.Ogura, H.Yamashita, M.Kinoshita, and T.Kawai,
Jpn.J.Appl.Phys., **28**, L1358 (1989).

[3] Preparation of Superconducting Whiskers of Bi System and Their Electrical Properties.
I.Matsubara, H.Tanigawa, T.Ogura, H.Yamashita, M.Kinoshita, and T.Kawai,
Proc. 6th Japan–Korea Seminar on Ceramics, 107 (1989).

[4] Flexible Superconducting Whiskers of the Li–doped Bi–Sr–Ca–Cu Oxide.
I.Matsubara, H.Tanigawa, T.Ogura, H.Yamashita, M.Kinoshita, and T.Kawai,
Appl.Phys.Lett., **56**, 2141 (1990).

[5] Growth of Li–doped and Dopant–free Bi–Sr–Ca–Cu–O Superconducting Whiskers.
I.Matsubara, H.Tanigawa, T.Ogura, H.Yamashita, M.Kinoshita, and T.Kawai,
Physica C, **167**, 503 (1990).

[6] Preparation of Fibrous Bi(Pb)–Sr–Ca–Cu–O Crystals Containing the High–T_c Phase.
I.Matsubara, H.Tanigawa, T.Ogura, H.Yamashita, M.Kinoshita, and T.Kawai,
MRS Symposium Proceedings, **169**, 325 (1990).

[7] Preparation and Critical Current Density of $Bi_2Sr_2Ca_2Cu_3O_{10+x}$ Superconducting Whiskers.
I.Matsubara, H.Tanigawa, T.Ogura, H.Yamashita, M.Kinoshita, and T.Kawai,
Appl.Phys.Lett., **57**, 2490 (1990).

[8] Superconducting Whiskers and Crystals of the High T_c $Bi_2Sr_2Ca_2Cu_3O_{10}$ Phase.
I.Matsubara, H.Tanigawa, T.Ogura, H.Yamashita, M.Kinoshita, and T.Kawai,
Appl.Phys.Lett., **58**, 409 (1991).

[9] Raman Spectra of Bi–Sr–Ca–Cu–O Glasses.
M.Hangyo, N.Nagasaki, S.Nakashima, I.Matsubara, and H.Yamashita,
Solid State Commun., **77**, 713 (1991).

[10] Growth of Bi–Sr–Ca–Cu–O Based Superconducting Whiskers.
I.Matsubara, T.Ogura, H.Tanigawa, H.Yamashita, M.Kinoshita, and T.Kawai,
J.Cryst.Growth, **110**, 973 (1991).

[11] Preparation and Properties of the High–T_c $Bi_2Sr_2Ca_2Cu_3O_{10}$ Whiskers and Crystals.
I.Matsubara, H.Tanigawa, T.Ogura, H.Yamashita, M.Kinoshita, and T.Kawai,
Proceedings of the 3rd ISS, 785 (1991).

[12] Mechanical Properties of Bi–based Superconducting Whiskers.
I.Matsubara, Y.Hashimoto, K.Atago, H.Yamashita, M.Kinoshita, and T.Kawai,
Jpn.J.Appl.Phys., **31**, L14 (1992).

[13] Li–doped Bi Three–Layered Superconducting Whiskers.
I.Matsubara, T.Ogura, H.Yamashita, M.Kinoshita, and T.Kawai,
Appl.Phys.Lett., **60**, 901 (1992).

[14] Upper Critical Field and Anisotropy of the High–T_c $Bi_2Sr_2Ca_2Cu_3O_x$ Phase.
I.Matsubara, H.Tanigawa, T.Ogura, H.Yamashita, M.Kinoshita, and T.Kawai,
Phys.Rev.B, **45**, 7414 (1992).

[15] Effects of Li–doping on the Superconductivity of $Bi_2Sr_2Ca_2Cu_3O_{10}$ Whiskers.
I.Matsubara, T.Ogura, H.Yamashita, M.Kinoshita, and T.Kawai,
Proceedings of the 4th ISS, 225 (1992).

[16] Effects of Li doping on the Superconducting Properties of Bi–based Superconducting Whiskers.
I.Matsubara, T.Ogura, H.Yamashita, M.Kinoshita, Y.Hashimoto, and T.Kawai,
Physica C, **201**, 83 (1992).

[17] Superconductivity of Bi(Pb)–Sr–Ca–Cu–O Whiskers.
H.Jin, Y.Ge, Q.Lin, Z.Hu, C.Shi, I.Matsubara, and H.Tanigawa,
Chin.Sci.Bull., **38**, 342 (1993).

[18] Growth of Superconducting Whiskers in the Bi System.
I.Matsubara, H.Yamashita, and T.Kawai,
J.Cryst.Growth, **128**, 719 (1993).

[19] Conversion of $Bi_2Sr_2CaCu_2O_x$ Whiskers to the $Bi_2Sr_2Ca_2Cu_3O_x$ Phase by Annealing in Powder.
I.Matsubara, R.Funahashi, T.Ogura, H.Yamashita, Y.Uzawa, K.Tanizoe, and T.Kawai, Physica C, **218**, 181 (1993).

[20] Growth Mechanism of $Bi_2Sr_2CaCu_2O_x$ Superconducting Whiskers.
I.Matsubara, R.Funahashi, T.Ogura, H.Yamashita, K.Tsuru, and T.Kawai,
J.Cryst.Growth, **141**, 131 (1994).